FUNDAMENTAL CHARACTERISTICS OF THERMAL CONVECTION UNDER THE CONDITION OF COOLING PERIOD IN THE NORTHERN PART OF LAKE BIWA

MALEMBEKA FREDERICK PAUL

2011

FUNDAMENTAL CHARACTERISTICS OF THERMAL

CONVECTION UNDER THE CONDITION OF COOLING

PERIOD IN THE NORTHERN PART OF LAKE BIWA

Thesis submitted by

Malembeka Frederick Paul

to

Department of Urban Management

in partial fullfillment of the requirements

for the degree of

Doctor of Philosophy

Kyoto University

2011

To my dearest mother and late father

for all the love you gave

ACKNOWLEDGEMENTS

List of Publications

This thesis is based on the following accepted and/or published conference and journal papers :

Hosoda, T., T. Isono, and F. Malembeka (2009), Some considerations on numerical experiments of thermal convection in the northern part of Lake Biwa by means of Stochastic Model, in *Proceedings of 6th International Symposium on Turbulence, Heat and Mass Transfer, Rome, Italy*, 14-18 September 2009, pp. 893 – 896, Begell House Inc.

Hosoda, T., and F. Malembeka (2010), Generation mechanism of typical vertical distributions of dissolved oxygen in the northern part of Lake Biwa, in *Proceedings of 6th International Symposium on Environmental Hydraulics, Athens, Greece*, 23-24 June 2010, vol. 1, edited by G. Christodoulou and A. Stamou, pp. 385–390, Taylor & Francis Group.

Hosoda, T., and F. Malembeka (2011), Applicability of mean-field approximation to numerical experiments of thermal convection under the condition of Lake Biwa, *Journal of Annual Hydraulic Engineering, JSCE (Japanese Society of Civil Engineers)*, vol 55, pp 1477 – 1482 (In Japanese).

Hosoda, T., and F. Malembeka (2011), Applicability of a Stochastic Model to Thermal Convection Simulation under Conditions of Cooling Period in Lake Biwa, Paper submitted in *7th International Symposium on Stratified Flows, Rome, Italy*, August 22 - 26, 2011, (Accepted).

Malembeka, F and T. Hosoda, (2011), Numerical Experiments of Thermal Convection Near Lake's Shores During Cooling Period: Case Study Of Lake Biwa, Paper submitted in *The 13th International Summer Symposium, JSCE (Japanese Society of Civil Engineers)*, August 26, 2011, (Accepted)

TABLE OF CONTENTS

LIST OF FIGURES

Figure

LIST OF TABLES

ABSTRACT

Lakes' waters undergo natural changes during different climatic seasons. Biological, chemical as well as physical changes are interconnected to each other in various ways, making it difficult the study of the isolated component in the ecosystem. Climate of the lake's surroundings is the important agent for lakes behavioral changes, and recent outcry of global warming and climate change is a concern to wellbeing of many lakes. The increase in air temperature due to global warming creates new thermal stratification patterns which could vitally be connected to extended periods of anoxia at lakes bottom depths by altering the natural phenomena of seasonal cycles of thermal stratification and destratification (*Carr and Neary*, 2008).

This thesis was confined in studying the cooling process of the lake, in particular, the characteristics of lake involving cyclic summer thermal influx and eventual cooling, with northern part of Japanese lake, Lake Biwa as a case study. A one-dimensional hydrodynamic model which simulates long-term water quality variables is first discussed. The model predict hydrodynamic turbulent distribution alongside appreciable qualitative performance in estimation of some of the water quality indices, as reported in two different cases studies (*Hosoda and Hosomi* (2004) and *Jacimovic et al.* (2011)). Based on the estimates of dissolved oxygen components from the 1-D hydrodynamic model, a simple 1-D dissolved oxygen model was proposed in DO modelling. Two distinct distributions were reproduced; the stable and monotonously decreasing distribution, and the intermediate distribution characterized with a sharp drop (local minimum) around the thermocline.

The model showed the significance of limited diffusion around the thermocline in stability of DO distributions.

3-D numerical model was used for further the study of elements of lake's cooling mechanism, including fluid particles interaction and influence of water surface cooling rate to fluid particles. A vertical movement was observed to be the main driving force of properties exchange between interacting fluid particles. Based on forests dynamics by *Kubo et al.* (1996) and neighborhood interaction from 3-D numerical model, a stochastic model was proposed to describe the thermal convection process by considering the results of mechanistic numerical model of physical laws. Growth rate of cold cells behaved in similar manner corresponding to water surface cooling rate in the 3-D numerical model in prediction of densities. The two models were comparable as well in inhibition of scale-free property between clusters of cold sites and their sizes by showing power law property. Further work was suggested in refining the stochastic model in the future.

Numerical experiments of thermal convection near lake around the shore showed potentially the density currents could be produced in the lake's flow near the shores, with water particles from the surface moving downwards along the slope to the lower depths also cooled water from the surface falling into lower depths. These two mechanism created internal waves along the thermal interface causing rapid change of properties as observed from simulated temperature time series taken near lake's bed. Such phenomena from simulated results were qualitatively similar to observed data from Lake Biwa. In general, it can be concluded that flow induced by density currents could be responsible for temperature and DO profiles which are observable in Lake Biwa. Further work was recommended in ascertaining lake flow under these geometrical conditions.

Introduction

1.1 Background

Understanding nature has been intimately an important reason for scientific inquiry through ages. Models are incepted to produce a closely prototype of the natural process and in the process they give an insight of the underlying mechanism. The crucial trait of productive modelling is to offer a close background mechanism of the natural or artificial phenomena for practical use. However in some occasions the use of the model can not be scaled in terms of engineering value per se. The gained insight of the model might give a new way of understanding nature, and fruits from the approach can later be translated and realized into pragmatic use. In this thesis, various subtopics are discussed about the mechanics of lakes in conjunction with effects of climate change on some of water qualities indicators during cooling period after summer thermal heating. Lakes are important components as sources of freshwaters alongside other surface sources and groundwater. Proper management and eventual monitoring of lakes requires scientists to be able to predict their behaviors in the contemporary challenges related to climate changes threats.

1.2 Case Study and Research's Motives

Climate change and its consequential effect, the global warming, is amongst the most contemporary challenges faced by modern science and humanity as a whole. Climate
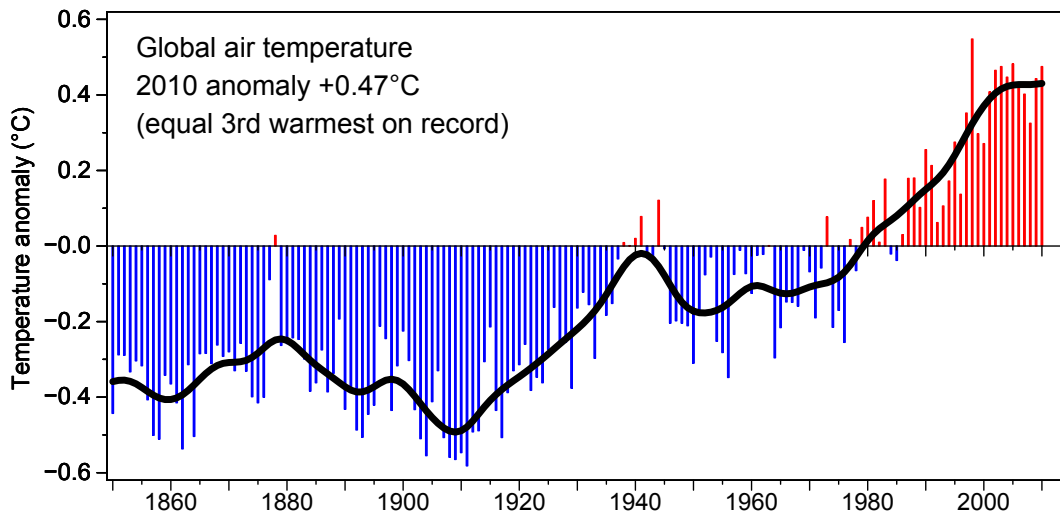
Figure 1.1: Global air temperature anomalies (Source: CRI and Met. Office - UK)

change is believed to be behind most recently woes to humankind propagated by droughts and floods. In context of agricultural losses the food security of many nations is now in jeopardy, parallel to skewed prices of food and other agricultural products which are dearly needed by various sectors. These conditions could be also a recipe for poverty and social unrest. *Climatic Research Unit* and the *UK Meteorological Office Hadley Centre* compiled a time series of temperature anomaly from as early as 1850 to 2010 (Figure 1.1) [1]. The records show that on average, the global temperatures departures from the mean are on a rise in recent decades. The atmospheric temperature is recorded to increase by approximately 0.5 ^0C *per year*.

There is an overt linkage between lake's behavior and climate change, as the former is highly affected by the latter. Lakes can be considered as *sentinels* of climate change, as they respond to changes in the input variables, derived in both, their localities as well as in their respective catchments (*Adrian et al.*, 2009). Response variables in the lake, such as changes in water level, water temperature and dissolved organic carbon can be used to indicate the effect of climate change. Such response variables are easy to be recorded, though some other variables related to climate change might not be measured straight-forwardly.

Increase in air temperature has a significant effect towards lake ecology. The rise in temperature affect lake mixing cycles and cause fast turnovers, the condition in the lake

---

[1]Image and CSV data available at http://www.cru.uea.ac.uk/cru/info/warming/

whereby the thermal stratification breaks early and as a result, a period of anoxia in the bottom vicinities becomes elongated, and hence threatening the lives of aquatic organisms in those deep waters which depends on dissolved oxygen for their survival.

Lake Biwa is the largest lake in Japan, located in Shiga Prefecture. It has a total surface area of 680 km and 27.5×10^9 m^3 total storage with 104 m as maximum depth. The lake is a source of Seta River which is important source of water for the nearby civilization. The lake is also a *UNESCO's Ramsar site* for its value and diversity in world's heritage. Urbanization of most cities is related to more water demands and potential exposure to pollution. Climate change and global warming in the other hand threatens the lake's ecosystem due to increase in air temperature and as a results the dynamics of lake's mixing are altered. One of the direct effect of these changes is the elongation of low dissolved oxygen period at lake's bottom.

Various researchers have been working in related problems of global warming, lake mixing and how the water properties are affected. As pointed-out that lake might be sentinels of climatic changes, study by *Yoshimizu et al.* (2010) confirmed that Lake Biwa mixing and eventual waters' properties in deeper locations are susceptible to year-to-year changes in meteorological inputs.

Figure [1.2] shows the observed dissolved oxygen (DO) data taken at the northern part of Lake Biwa by Lake Biwa Research Institute (LBRI) at a sampling location with 94 m depth of water column. The figure shows the data taken at 1 m and 10 m from the lake's bed from a period between October 2002 and March 2003. In the period between October 2002 and Early days of January 2003, DO values are spiraling mainly below 5 mg/l, which is alarming value to aquatic life survival if been sustained for a long time. At this time of the year the lake is being thermally cooled following strong heat wave during summer period of July - September.

In this thesis, selected topics regarding thermal convection in thermally stratified lakes are discussed. Ecological facet of hydrodynamics is studied, with behavior of the lake mixing during cooling period being of particular importance in conjunction with influence of climate change. A part which describe the link between statistical model and physical
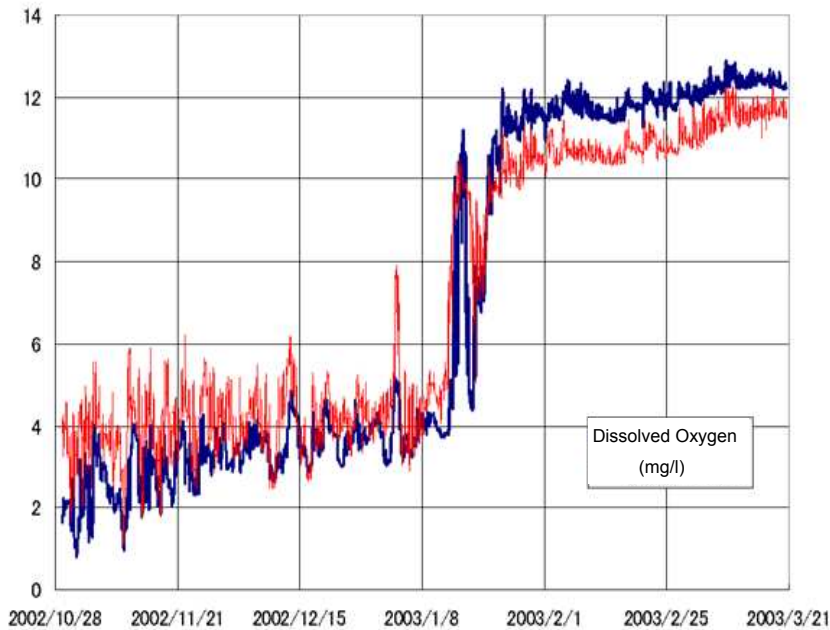
Figure 1.2: DO data from Lake Biwa. Data are taken at 1 *m* (shown in blue) and 10 *m* (shown in red) above the bed at location with depth 94 *m*.(*Source: LBRI*)

model is also discussed, in attempt to show new possibility of understanding thermal convection process.

1.3 Thesis' Layout

Chapter [II] covers lake's water quality modelling from 1-D models. The formulation involving long-term simulation of water quality and hydrodynamics variables is firstly described, and the results from the model were used in mathematical formulation of a simple 1-D dissolved model.

In chapter [III], the 3-D model in which Navier-Stokes equations are solved numerically is described. The model is applied in study of influence of surface processes on a thermally cooling lake. The spatial analysis is described from the results of the numerical model. The model is also used in the study of influence of neighborhood cell's interaction from a thermal stratified lake, a study which is a basis a stochastic model introduced later-on in chapter [IV] for consideration of thermal convection in lakes.

In chapter [IV] a stochastic model is described in consideration of the numerical ex-

periments of the thermally cooling late as described in chapter [III]. The model is used to consider some aspects of the thermal convection process in the lake. Modified mean-field theory and paired approximations of the Stochastic model are described. Spatial analysis of the results from the Monte-Carlo Simulation of the stochastic model is done in gaining the insight involving the sinking cells. Properties such as densities and clusters are studied in relation with model parameters and also in conjunction with results from the 3-D numerical model.

In chapter [V], a 3-D model described in chapter [III] is used in simulation of the flow near the lake shores in a thermally stratified lake. Simulated temperature and velocity fields are compared from typical observations. The model setup allows study of the influence of the physical features to the flow to be conducted.

Chapter [VI] summarizes the contents of this thesis. Methods applied are highlighted with their contribution towards the subjects they deal with, are presented. To sum up the study, few points are pointed-out in the end for future work.

2

Generation Mechanism of Vertical DO Distributions with Local Minimum

2.1 Background

Climate change and Global Warming have been identified by several researchers as a new threat to water resources on earth. (*Carr and Neary* (2008)). Prediction of effects of climate change to water bodies is important in management and monitoring of water resources necessary for viability of human civilization and existence. Lakes are important sources of freshwaters, alongside other surface and subsurface sources. Lake's water quality modelling by 1-dimensional modelling is sufficient in occasion when the use of multi-spatial dimension modelling is inadequate due to complexity in model's closure, parameter estimation and(or) computational overhead. 1-D models in most cases are not subjected to parsimonious limitations usually imposed on their multi-dimensional counterparts. Several models in prediction of stratified water bodies exist in literature, the works of *Hamilton and Schladow* (1997), *Bell et al.* (2006) are few examples.

In this chapter 1-D model for prediction of dissolved oxygen generation in lakes is described. 1-D hydrodynamic model applied by *Hosoda and Hosomi* (2004) gave a qualitative estimation of components of DO generation. Using the distribution of these components, a simple 1-D model is proposed for dissolved oxygen generation.

2.2　1 -D Longterm Water Quality Simulation

2.2.1　General

Completely unidirectional flows in lakes are uncharacteristic and impractical, but it could be agreed that application of 1-D modeling can be suitable on some of occasions whereas the use of complex and (sometimes) parsimonious higher dimensional models is cumbersome and unproductive. 1-D water quality model formulation proposed in modelling water quality and hydrodynamics properties of Lake Biwa by
Hosoda and Hosomi (2004) is presented. The results of this model are useful in understanding the hydrodynamic variables distribution in a water column. Knowledge on distribution of dissolved oxygen's components such as diffusion coefficient, consumption and production terms are important in the study introduced in the next section (§2.3) in pages [16 - 28], whereby a different approach is used in study of typical dissolved oxygen distributions.

2.2.2　Mathematical Formulation

The mathematical formulation can be subdivided into two stages; the first stage is the prediction of hydrodynamic conditions such as turbulent diffusion terms and temperature profiles accorded to environmental inputs such as cloud cover, wind speed as well as surroundings' air temperature. The second part of the formulation covers modelling of water quality variables such as chlorophyll-a in phytoplankton, carbon in zooplankton, organic and inorganic nitrogen, organic and inorganic phosphorus as well as dissolved oxygen.

Momentum conservation was modelled using equation [2.1]:

$$\frac{\partial U}{\partial t} = \frac{-1}{\rho}\frac{\partial P}{\partial z} + \frac{\partial}{\partial z}(\nu\frac{\partial U}{\partial z} - \overline{u'v'}) \tag{2.1}$$

where,

U　is the horizontal velocity

P　is the pressure

Table 2.1: $k - \varepsilon$ model's constants

Parameter	Value
c_{ε_1}	1.44
c_{ε_2}	1.92
c_{ε_3}	0.00
σ_k	1.00
σ_ε	1.30
c_μ	0.09

ν is the dynamic molecular viscosity, and

$-\overline{\rho u'v'}$ is Reynolds stress

ρ is the reference water density , and

z is the vertical coordinate

Turbulence terms were modelled using standard $k - \varepsilon$ model as shown in equation [2.2]:

$$\frac{\partial k}{\partial t} = -\overline{u'v'}\frac{\partial U}{\partial z} - \varepsilon + \frac{\partial}{\partial z}[(\frac{D_{mz}}{\sigma_k} + \nu)\frac{\partial k}{\partial z}] + \frac{g}{\rho}D_{Tz}\frac{\partial \rho}{\partial z} \tag{2.2a}$$

$$\frac{\partial \varepsilon}{\partial t} = -c_{\varepsilon_1}\frac{\varepsilon}{k}\overline{u'v'}\frac{\partial U}{\partial z} - c_{\varepsilon_2}\frac{\varepsilon^2}{k} + \frac{\partial}{\partial z}[(\frac{D_{mz}}{\sigma_\varepsilon} + \nu)\frac{\partial \varepsilon}{\partial z}] + c_{\varepsilon_3}\frac{g}{\rho}\frac{\varepsilon}{k}D_{Tz}\frac{\partial \rho}{\partial z} \tag{2.2b}$$

$$-\overline{u'v'} = D_{mz}\frac{\partial U}{\partial z} \tag{2.2c}$$

where :

k is turbulent kinetic energy

ε is turbulent energy dissipation

D_{mz} is turbulent eddy viscosity, and

g is acceleration due to gravitational pull

The constants used in the $k - \varepsilon$ equations are shown in table [2.1].

Following heat balancing in the water column, temperature scalar transport was modelled by equation [2.3].

$$\frac{\partial T}{\partial t} = \frac{1}{\rho C_p}\frac{\partial Q_z}{\partial z} + \frac{\partial}{\partial z}(D_{Tz}\frac{\partial T}{\partial z}) \tag{2.3}$$

where :

T is the temperature

t is time

C_p is specific heat

Qz is heat flux , and

D_{Tz} is turbulent diffusion coefficient

With regard to effect of density stratification in the lake, the eddy viscosity, D_{mz} and diffusion coefficient, D_{Tz} were evaluated by equations [2.4] and [2.7], respectively.

$$D_{mz} = c_\mu f_b \frac{k^2}{\varepsilon} \tag{2.4}$$

where:

$$f_b = \frac{1}{1+0.2B} \tag{2.5}$$

and:

$$B = \frac{g}{\rho_o}(\frac{k}{\varepsilon})^2\frac{\partial \rho}{\partial z} \tag{2.6}$$

$$D_{Tz} = \frac{1}{P_{rt0}}\frac{1}{1+0.24B}D_{mz} \tag{2.7}$$

where:

$$P_{rt0} = 1/1.6 \tag{2.8}$$

Additional mixing due to internal and surface waves is taken care of by adding the coefficient, D_{EX} to D_{Tz}.

$$D_{EX} = C_{EX}(k_s)^{0.5} l_s exp(-d_{dump} \frac{z_s - z}{l_s}) \qquad (2.9)$$

where:

l_s is the mixing length scale ($= 0.5m$),

C_{EX} is an empirical constant ($= 0.2$), and

d_{dump} is an empirical constant ($= 0.1$)

Numerical solution of the momentum equation uses surface condition as per equations [2.10], [2.11] and [2.12] below:

$$(\nu + D_{mz}) = u_{*s}^2 \qquad (2.10)$$

$$k_s = \frac{u_{*s}^2}{c_\mu^{1/2}} \qquad (2.11)$$

$$\varepsilon_s = \frac{c_\mu^{3/4} k_s^{3/2}}{0.4\Delta z_s} \qquad (2.12)$$

where:

u_{*s} is the friction velocity at the water surface induced by wind, and

Δz_s is a half of spatial mesh size for the finite difference scheme.

Heat exchange at the water surface is computed following equation [2.13].

$$D_{Tz} \frac{\partial T}{\partial z} = \frac{Q_0}{\rho_a C_p} (z = z_s) \qquad (2.13)$$

where:

Q_0 is the heat absorbed at the water surface into water column per unit area and time

Q_0 is evaluated by equation [2.14]

$$Q_0 = \beta Q_s - (Q_e + Q_c + Q_{rw} + Q_a) \tag{2.14}$$

where:

Q_s is net solar radiation $= (1 - A_r)Q_{SO}$,

Q_{S0} is solar radiation,

A_r is albedo $(= 0.06)$,

Q_e is evaporation heat flux,

Q_c is sensible heat flux,

Q_{rw} is water surface radiation heat flux,

Q_a is net atmospheric radiation heat flux

β is the ratio of absorbed to net incoming radiation $(= 0.5)$

The terms in equation [2.14] are evaluated by using known empirical formulae. The variable Q_z in heat equation (equation 2.3) is computed using equation [] below:

$$Q_z = (1 - \beta)Q_s \, exp(-\kappa(z_s - z)), \ \kappa = \kappa_0 + \kappa_p P \tag{2.15}$$

where:

κ_0 is attenuation coefficient $(= 0.2)$,

κ_P is dispersion coefficient due to phytoplankton $(= 0.001)$,

P is chlorophyll-a in phytoplankton

In simulation of effect of natural convection occuring between early autumn and winter when density at elevation z_c is less than the average density from z_c to a water surface, the temperatures of a layer over z_c are replaced with constant value, T_{ave} calculated by equation [2.16].
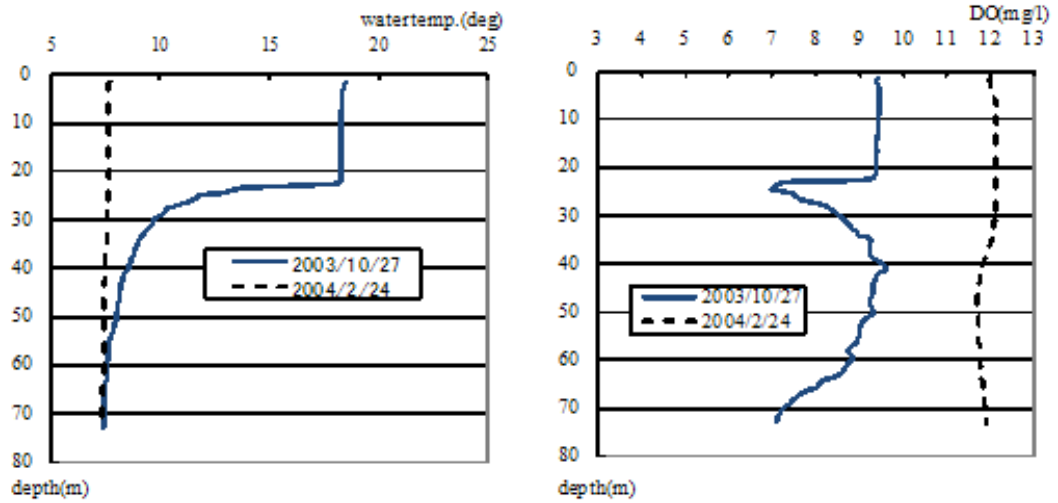
Figure 2.1: Dissolved oxygen and temperature data from northern part of Lake Biwa

$$\int_{zc}^{zs} T\,dz = (z_s - z_c)T_{ave} \tag{2.16}$$

Details of the used water quality sub-models are included in Appendix.

2.2.3   Results

In general, 1-D hydrodynamic model with water quality routines reproduced results which qualitatively reflected the observed temperature and dissolved oxygen profiles and other water quality indices as recorded in northern part of Lake Biwa.

2.2.3.1   Temperature and Dissolved Oxygen Profiles

Figure [2.1] shows the observed data of dissolved oxygen and corresponding temperature profiles from *LBRI* as cited by *Hosoda and Hosomi* (2004). Temperature profile reveal thermal layers formed after period of relative intense heating of summer. The corresponding dissolved oxygen distribution reveal a *local minimum* at depth near or around the thermocline. This type of DO distribution was reported to occur during autumn and summer periods in Lake Biwa. Similar dissolved oxygen distribution with a minimum value were reported in works of other authors such as *Jacimovic et al.* (2011) and *Elçi* (2008).

From the 1-D hydrodynamic model, simulated temperature distribution at different
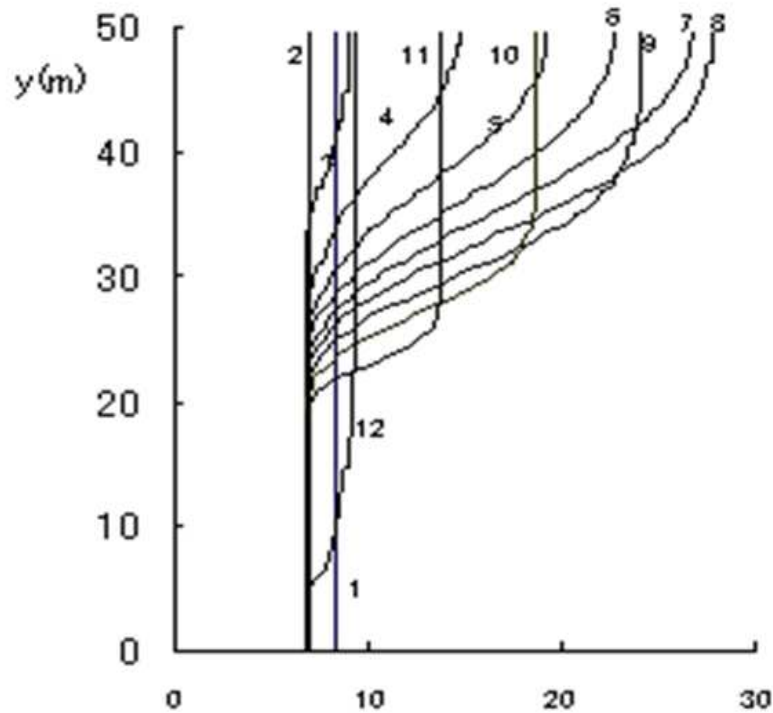
Figure 2.2: Simulated monthly temperature profiles (in ^0C) from 1-D hydrodynamic model. Respective months are shown as numbers 1 to 12.

months are shown in figure [2.2] in page 14. The temperature difference between upper and lower layers grows larger after the month of January towards September in which maximum difference is attained after summer heating. In the month of September onwards until January, the lake is cooled and the temperature difference is reduced. The simulated results closely follows the typical observed monthly temperature data from year 1998, shown in figure [2.3].

The model qualitatively reproduced the distribution of dissolved oxygen as well, as comprehensively shown in figure [2.4] in page 15. The DO distribution with minimum part is qualitatively shown during the month of November while the other distribution showing a uniform distribution is predicted to occur in the month of February. The corresponding simulated temperature profiles are included in the figure, to show the existence of thermal layers during these two important DO distributions.
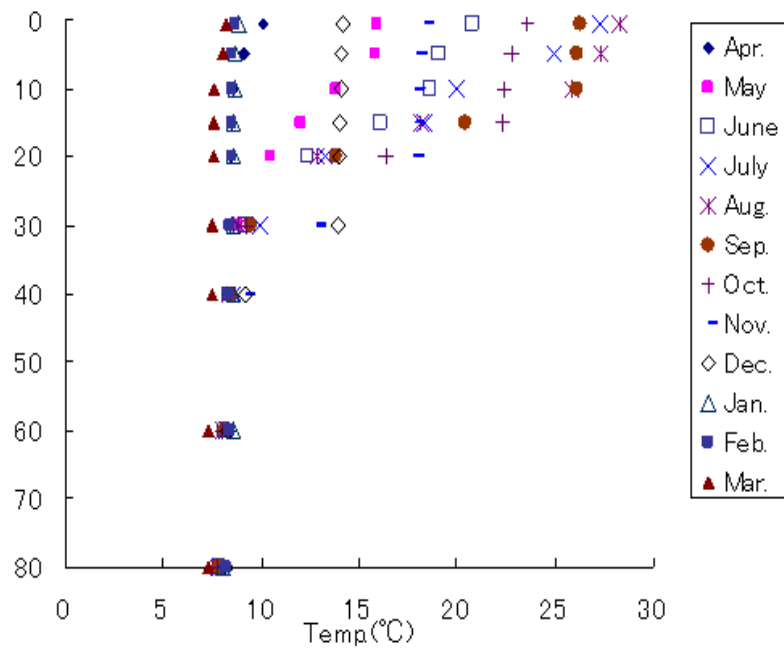
Figure 2.3: Observed monthly temperature profile from northern part of Lake Biwa taken in year 1998 (Source: LBRI)
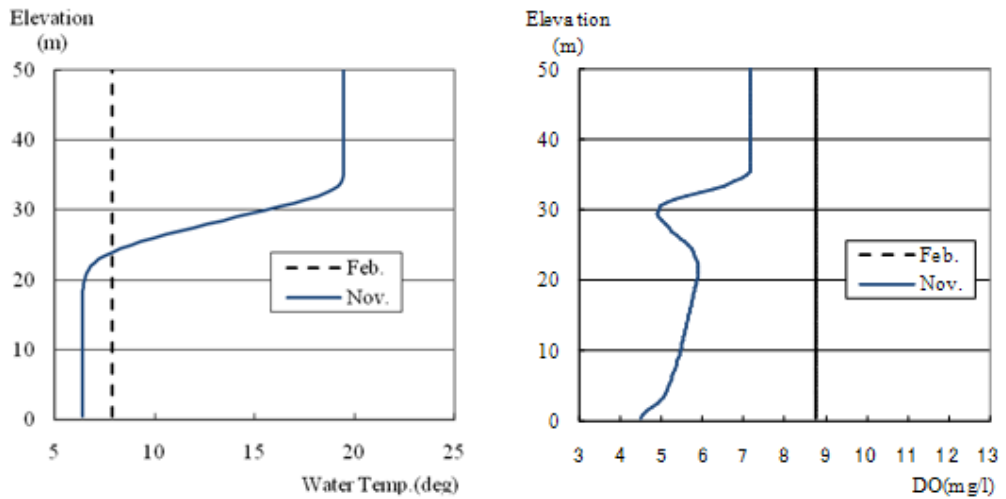
Figure 2.4: Modelled results of the dissolved oxygen and temperature profiles
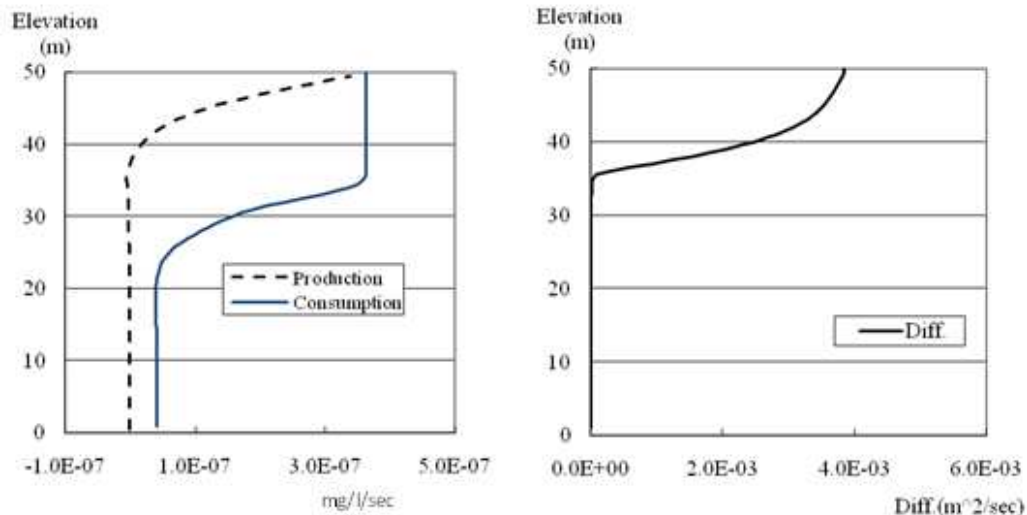
Figure 2.5: Estimated distributions of terms composing DO dynamics

2.2.3.2 Other water quality indices

From 1-D hydrodynamic model the distributions of the dissolved oxygen's compo-
nents responsible for production, consumption and diffusion were also estimated, and the
results are summarized in figure [2.5]. All three components have higher values near the
water surface. In natural waters production of oxygen through photosynthesis is highly
supported near the water surface due to the fact that the sunlight needed can reach the
waters for few centimeters in adequate amounts and also the presence of algae and plants
responsible for carrying-out the conversion is guaranteed. Presence of organisms near the
water surface equally suggests the depiction of higher DO consumption near the surface.

The estimated monthly distributions of chlorophyll-a in phytoplankton are shown in
figure [2.6].

2.3 Generation Mechanism of Vertical DO Distributions with Local Minimum

Following the estimated distributions of consumption and generation terms and diffu-
sive coefficient responsible for dynamics of dissolved oxygen from the 1-D hydrodynamic
model with water quality extensions, a simple 1-D model for estimation of dissolved oxy-
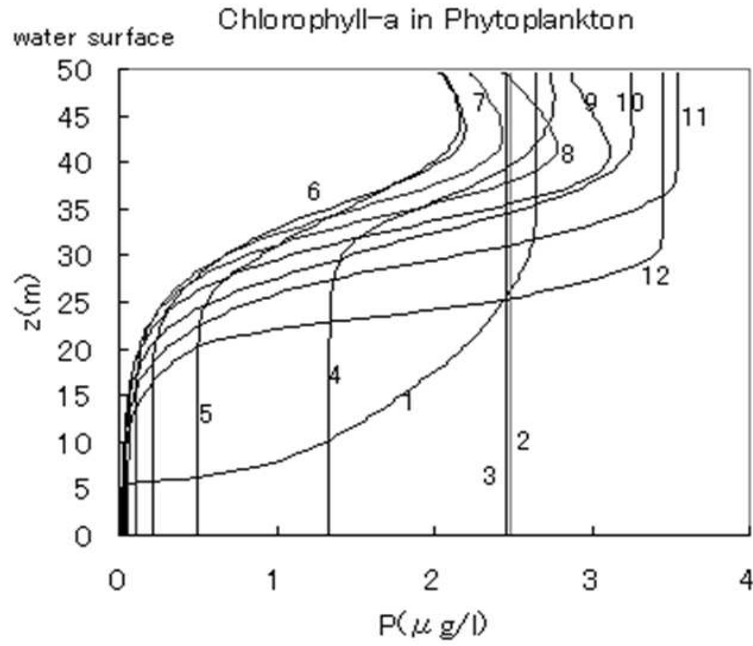
Figure 2.6: Simulated monthly distribution of chlorophyll-a in phytoplankton

gen is formulated. In this model, prediction of DO distribution is considered under unsteady conditions, allowing variation of DO to occur with depth and time.

2.3.1 Model Formulation

Dissolved oxygen (DO) prediction follows dynamics by transport equation [2.17] below.

$$\frac{\partial DO}{\partial t} = D\frac{\partial^2 DO}{\partial z^2} + P - C \tag{2.17}$$

where,

DO is the dissolved oxygen concentration,

$P\ and\ C$ are production and consumption terms respectively, and

D is the diffusion coefficient.

Table 2.2: Parameters for Unsteady-state DO Model

Parameter	Value
Φ_p	5×10^{-3}
Φ_{cu}	$[1 \ or \ 5] \times 10^{-6}$
Φ_{cl}	1×10^{-7}
D_u	2×10^{-1}
D_l	2×10^{-5}
γ_b	1×10^{-3}
β_s	1×10^{-3}
Φ_{cmax}	1×10^{-2}

The following boundary conditions are applied at the water surface (equation [2.18]) and bottom (equation [2.19]) of the lake to ensure model's closure:

$$D\frac{\partial DO}{\partial z} = \frac{\beta_s(DO_{sat} - DO)}{\Delta z} \tag{2.18}$$

$$(D\frac{\partial DO}{\partial z})_{bottom} = \gamma_b \tag{2.19}$$

Four try-outs were completed with changes made to the distribution of the diffusion coefficient in the entire water column and/or the consumption term distribution. In all these cases,we present schematic diagrams showing the distributions of DO's components in the water column. The assumed distributions for DO components; *Consumption* and *Generation* terms are represented in green and red lines, respectively, while the *Diffusion* coefficient is shown in blue.

In all the cases the values of z_o, z_a, z_b, z_c, z_d, z_e and z_s were maintained at $0 \ m$, $25 \ m$, $30 \ m$, $35 \ m$, $40 \ m$, $45 \ m$ and $50 \ m$, respectively.

The values of the parameters used in the simulation are shown in Table [2.2]. The units of quantities Φ_p,Φ_{cu} and Φ_{cl} are in $(mg/l/sec)$, while quantities D_u and D_l are in (m^2/sec). γ_b is expressed in $(mg/l).(m/s)$.

Figure 2.7: Schematic representation of the distribution of diffusion coefficient, generation and consumption terms (Case I)

2.3.2 Diffusion Coefficient and Consumption term - Case I

In this proposed arrangement the distribution of the diffusion coefficient is allowed to increase linearly from D_l to D_u in the depth segment CD; while on top and bottom of this particular segment the values are kept constant at D_u and D_l, respectively. The production term increases linearly from 0 to Φ_p in the depth segment DE while it was kept constant with values 0 and Φ_p in depths segments OD and ES respectively. The distribution of consumption term was maintained at constants values of Φ_{cl} and Φ_{cu} at depth segments OA and CS, respectively; while it was linearly increasing from Φ_{cl} to Φ_{cu} in the depth segment AC. Figure [2.7] is a schematic diagram representing this arrangement.

Figure [2.8] in page [21] shows the results from Case I. At $\Phi_{cu} = 5 \times 10^{-6}$ the consumption DO overpowers DO production and as the result local minimum value is evident at depth near thermocline. Allowing further simulation time for this case, show that the

shape of the distribution in water column is unchanged with the minimum value continue to get smaller and smaller (larger magnitudes with negative values). With $\Phi_{cu} = 1 \times 10^{-6}$ the DO distribution is constantly decreasing with some sign of saddle points. After around 720 *days* simulation time, the shape of the distribution is hardly changed.

2.3.3 Diffusion Coefficient and Consumption term - Case II

In this proposed arrangement of terms, the distribution of the diffusion coefficient is allowed to increase linearly from D_l to D_u in the depth segment BC; while on top and bottom of this particular segment the diffusion coefficient is kept constant at values D_u and D_l, respectively. The variation of consumption and production terms with respect to depth are kept unchanged to those already presented under *Case I* in § [2.3.2] above. Figure [2.9] is a schematic diagram of this arrangement.

Figure [2.10] in page [23] show the simulated DO distribution of this arrangement. At $\Phi_{cu} = 5 \times 10^{-6}$ the distribution with local minimum can not be observed distinctively with the distribution showing tendency of *saddling* at depth near the thermocline. The shape of the distribution is almost not changed after 600 *hours*. At $\Phi_{cu} = 1 \times 10^{-6}$ the shape of DO distribution is decreasing monotonously. After about 600 *hours* of simulation time, the changes in shape of distribution is halted without formation of distinct local minimum.

2.3.4 Diffusion Coefficient and Consumption term - Case III

In this arrangement, diffusion coefficient increases linearly with depth from the value D_l to D_u in the depth segment AC. At the top and bottom of this segment, the diffusion term is given constant values of D_u and D_l, respectively. The variation of consumption and production terms with respect to depth are kept unchanged to those already presented under *Case I* above. This arrangement is represented conceptually by figure [2.11].

Figure [2.12] in page [25] shows the simulated DO distribution from this arrangement. When $\Phi_{cu} = 5 \times 10^{-6}$ the DO distribution is decreasing from top to bottom layer and the shape is not changed much after first 150 *hours*. Similar distribution can be observed for simulation with $\Phi_{cu} = 1 \times 10^{-6}$.
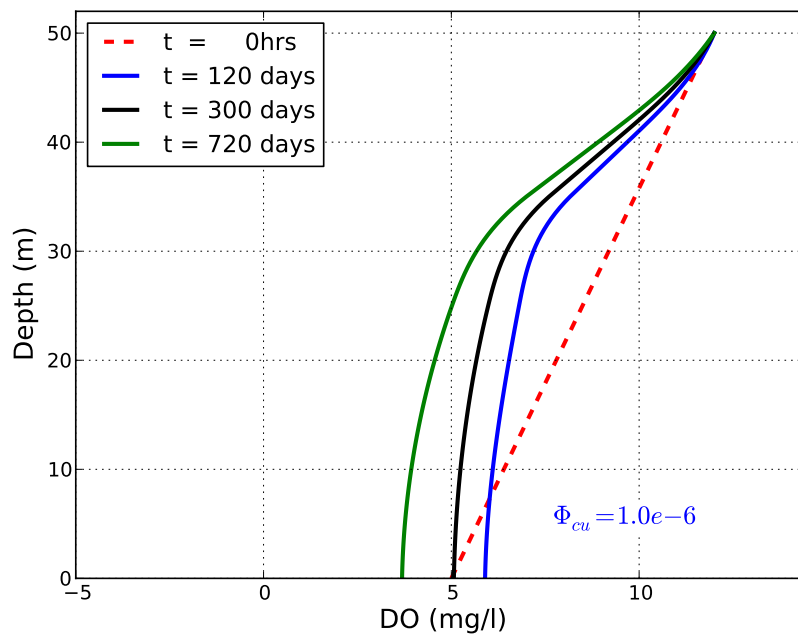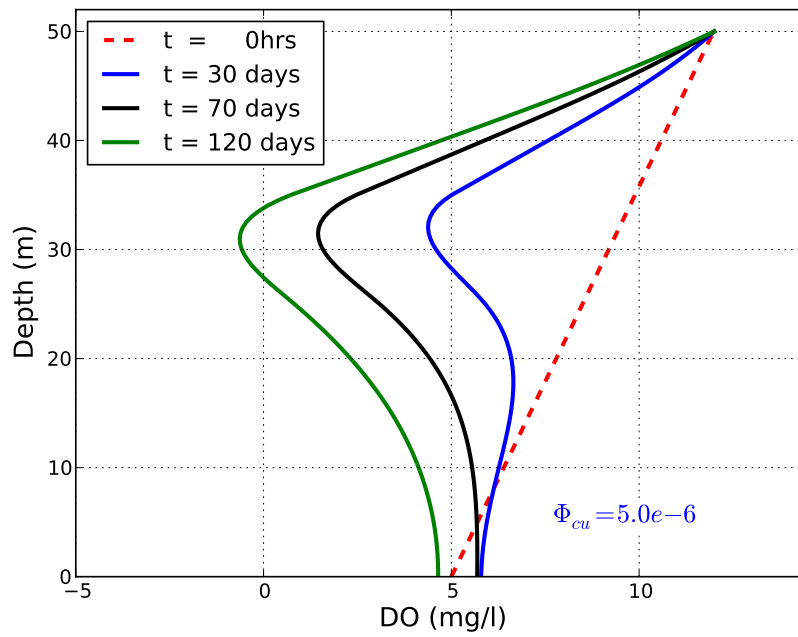
Figure 2.8: Simulated DO distribution - Case I
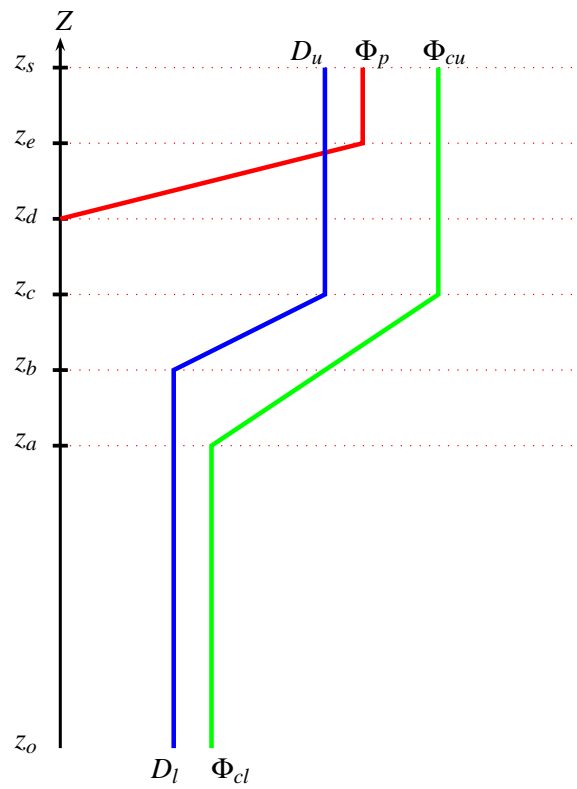
Figure 2.9: Schematic representation of the distribution of diffusion coefficient, generation and consumption terms (Case II)
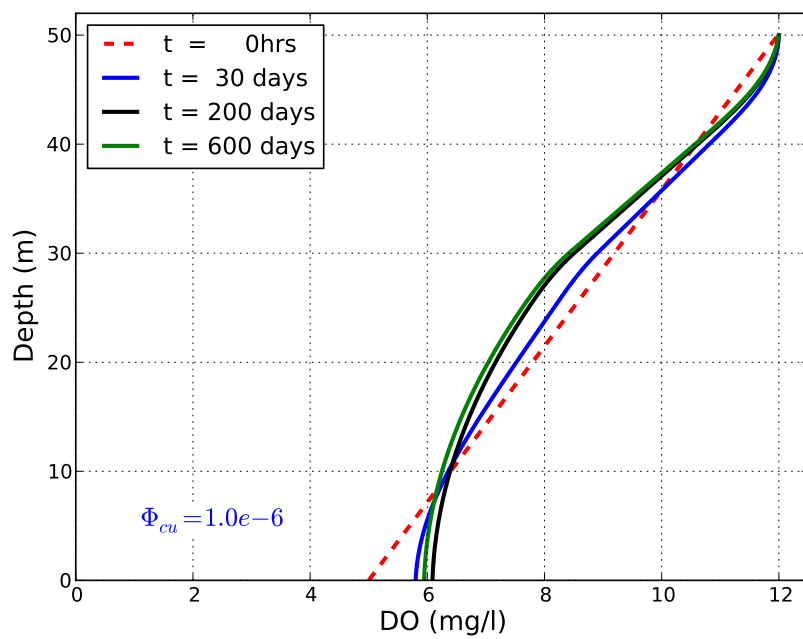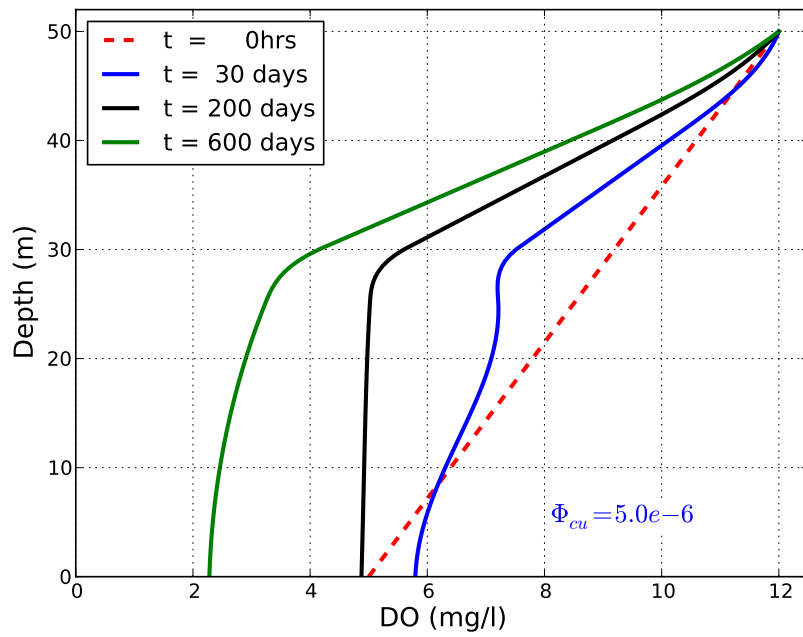
Figure 2.10: Simulated DO distribution - Case II
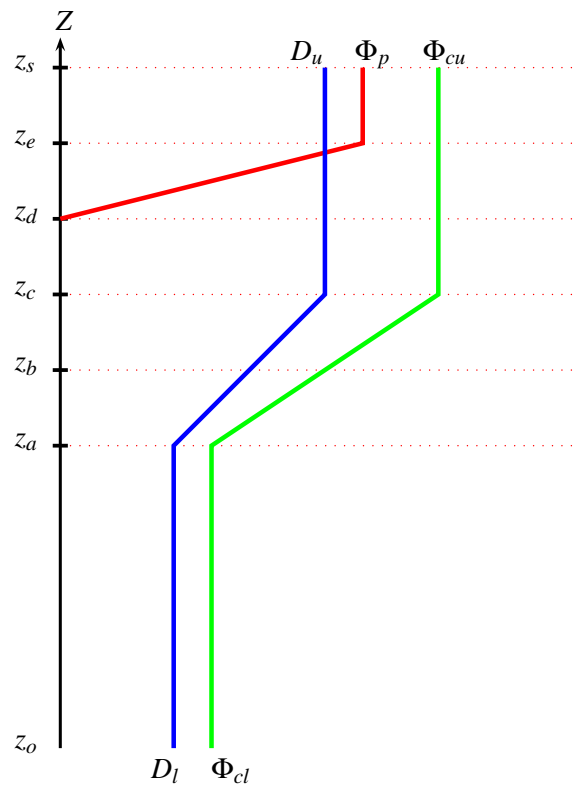
Figure 2.11: Schematic representation of the distribution of diffusion coefficient, generation and consumption terms (Case III)

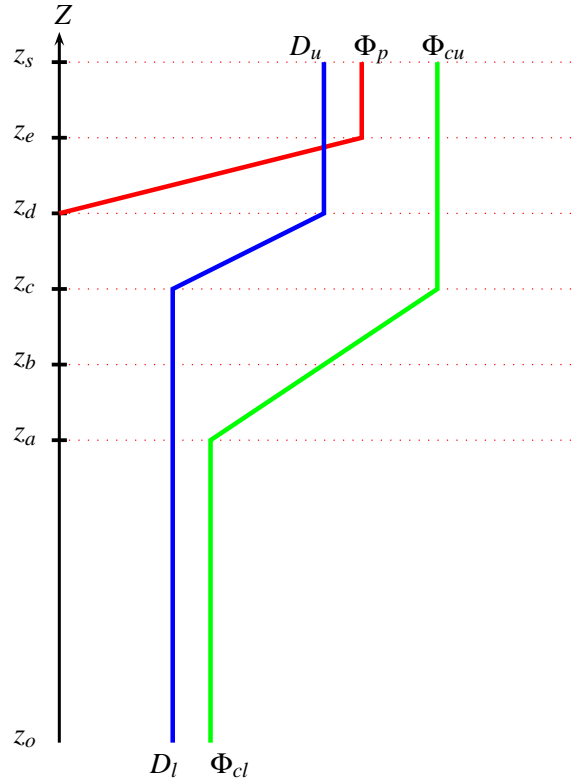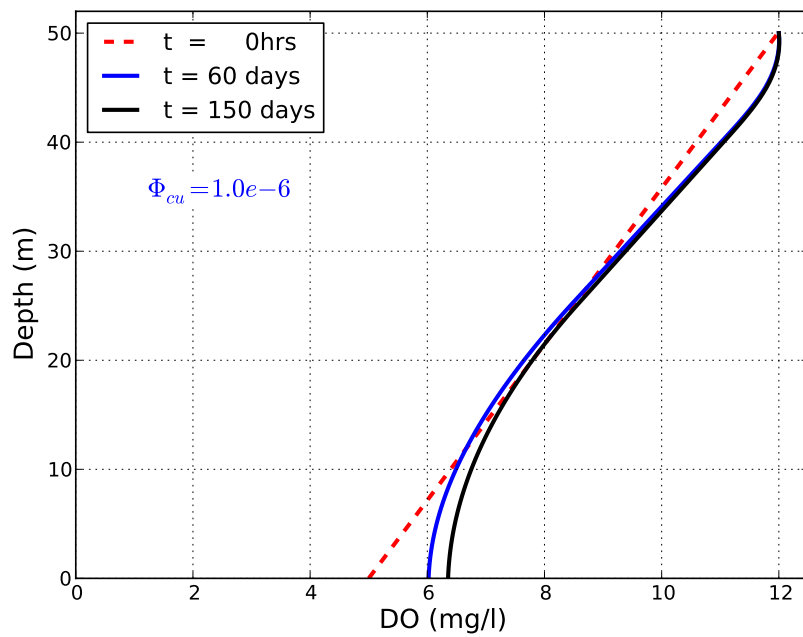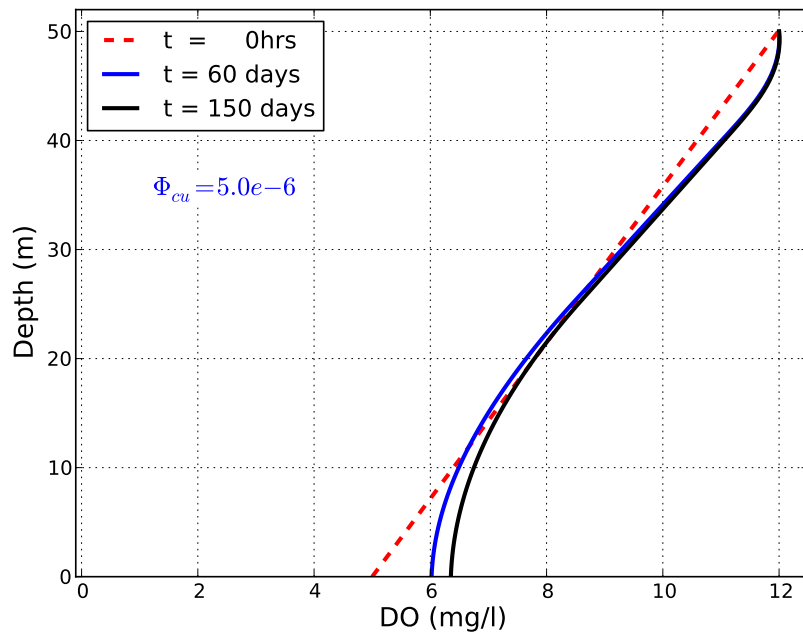Figure 2.12: Simulated DO distribution - Case III
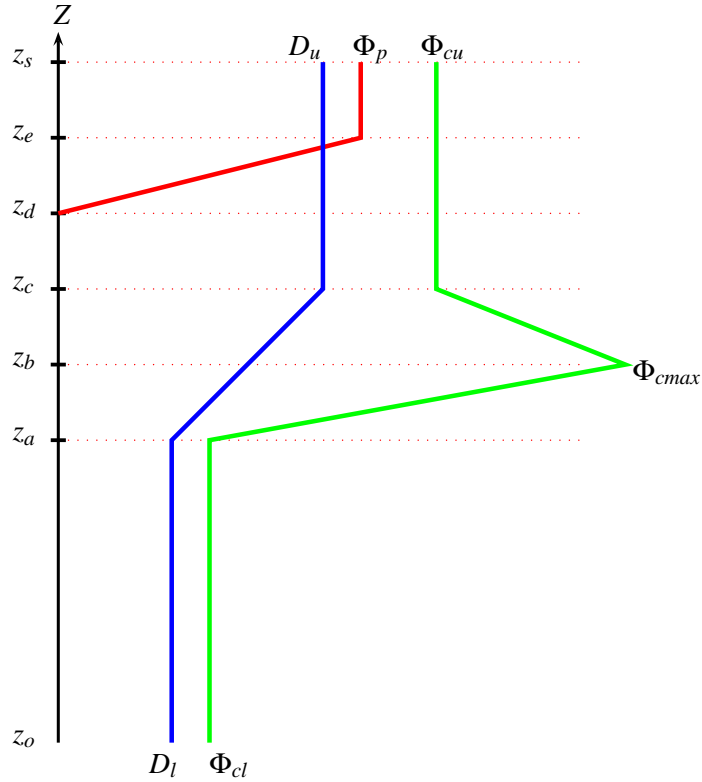
Figure 2.13: Schematic representation of the distribution of diffusion coefficient, generation and consumption terms (Case IV)

2.3.5 Diffusion Coefficient and Consumption term - Case IV

In this arrangement the distributions of diffusion coefficient and production term are similar to those in case III, described in subsection [2.3.4] above. The consumption term distribution increases from Φ_{cl} towards Φ_{cmax} in the depth segment AB, and decreases from Φ_{cmax} to Φ_{cu} in depth segment BC. The constants distribution values of Φ_{cu} and Φ_{cl} are maintained in the depth segments CS and OA respectively. Figure [2.11] is the schematic representation of terms for this case.

Figure [2.14] in page [27] shows the simulated DO distribution from Case IV. The local minimum part can be clearly seen with much sharper changes around the thermocline during early times of the simulation. The magnitude of the local minimum grows boundlessly with simulation time but the changes at the thermocline being much smoother. This trend could be observed for both $\Phi_{cu} = 1 \times 10^{-6}$ and 5×10^{-6} numerical experiments.
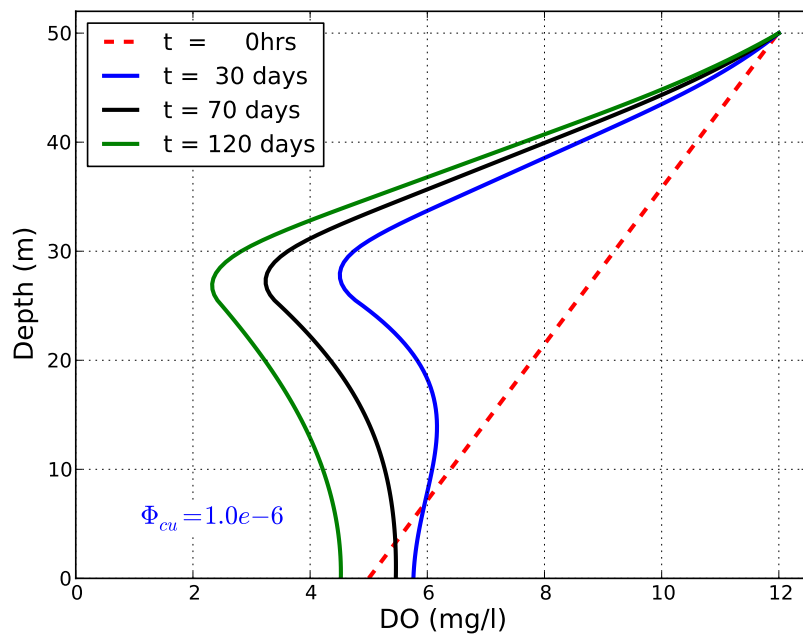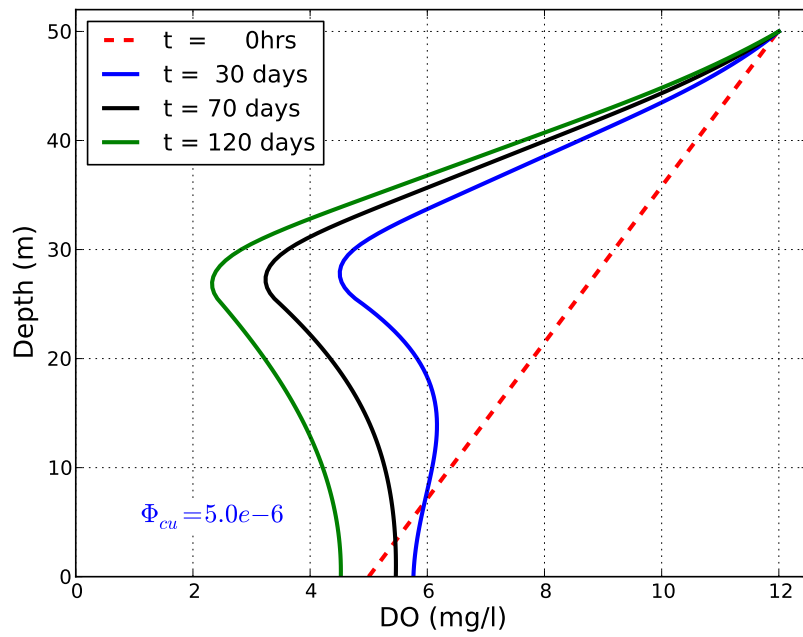
Figure 2.14: Simulated DO distribution - Case IV

In natural lakes, DO is abundant in upper layer in contact with the air. DO is produced at the layer near the water surface from photosynthesis process, whereby aquatic plants and algae consume carbondioxide in presence of sunlight and water to make their food while releasing oxygen as a by-product. Oxygen from the atmosphere may also diffuse into water phase to add into DO supply. The waters vertical mixing facilitate downward movement into lower depths which are poor in DO. The distribution of DO with depth is partly dependent on vertical movement of water and hence in general larger concentrations are expected at the upper layer and decreasing with depth.

From the model described by the four cases it can be concluded that in general, the simulated distributions of DO suggest existence of two kind of distributions. In the first type of distribution, the DO decreases from the water surface towards the lake's bottom monotonously. In this distribution, DO is produced at the surface and diffuse at lower depths towards the lake's bed. The DO flux is one directional from the surface towards the bottom layer. The second type of DO distribution show DO decreasing up to certain depth near the thermocline and further decrease with depth at smaller rates. In this type of distribution, thermocline has a minimum DO concentration, (or hollow) and it is hypothesized that it is caused by the fact that waters in the layer are characterized by small DO diffusion. In this distribution, DO flux occur from both top and bottom layers to thermocline where the local minimum is located. Similar distributions were also obtained in an unsteady DO generation model by *Hosoda and Malembeka* (2010), results which suggested existence of these two types of DO distribution are possible.

It can be noted that the model uses a fixed flux ($D\frac{\partial DO}{\partial z}$ at the lake's bed as a boundary condition, which is not realistic

2.4 Summary

In this chapter, a 1-D model based on formulation by *Hosoda and Hosomi* (2004) was described in long-term simulation of the water quality indices in Lake Biwa. The model involved estimation of hydrodynamic variables as well as estimation of the water quality indicators such as dissolved oxygen and water temperature and others. The results from

the 1-D hydrodynamic model qualitatively matched well with the observed water quality indicators from Lake Biwa.

Based on estimated distributions of consumption and production terms as well as the diffusion coefficient, a simple 1-D dissolved oxygen generation model was proposed in simulation of typical dissolved oxygen distributions. Four formulations were experimented based on the combinational arrangement of diffusion coefficient and consumption and production terms in a water column.

Overall, the model predicted the two expected distributions likely to be found in natural lake; the DO concentration with monotonously decreasing distributiion from the water surface to the lake's bed and the second distribution with a local minimum part around the thermocline. From this model it could be noted that magnitudes of diffusion and consumption terms near the thermocline are important in prediction of the extent of the formulation of the distribution of local minima. When the consumption was reduced the stable monotonous DO distribution is favored, in contrary to occurrence of local minimum when it was increased. For more DO to diffuse from the surface, the DO with minimum part could be broken by applying mechanical or biological means to supply DO around the thermocline.

In general, the 1-D hydrodynamic model could be refined by revisiting the food-web dynamics by phytoplankton. A more detailed 1-D DO generation model could also be proposed.

III
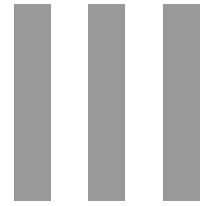
Numerical Experiments of Thermal Convection under the Conditions of Cooling Period

3.1 Background

Lakes as part of aqua-ecosystem, are open to influence from climatic and weather changes. Air temperature, wind conditions, humidity and sunlight are among major climatic factors which affect the behavior of the lake. Air forms an interface with the water surface and exchange of properties are expected at the transitional zone separating the two media, including gaseous exchanges.

Air might diffuse into the water, the process which is temperature-dependent. Water particles from the lake might also escape from the water surface into the air through evaporation. Wind action causes stir of waters and some of the air might be trapped in action and get dissolved into the water phase.

Although, lakes trophism is related to fill-out of nutrients at rates not matched by the lake's natural consumption processes, formation of temperature strata is likely to further fuel and intensify the problem. There is a direct link between climatic changes which alter the natural ecosystem to the detrimental processes in the lake such as eutrophication and lake aging.

Thermal cooling mechanism in a lake is of particular interest after a high heat influx during summer period. Thermal strata occurring after this period hinder the vertical mixing of waters due to a stratification barrier formed between the top and bottom layers. Discontinuity of flow due to the barrier is a natural phenomenon, but several researches have shown a link between raise in air temperatures due to global warming and the elongation of anoxia period in the deep lake's waters *Carr and Neary* (2008).

This chapter describes the flow simulation of thermally stratified lake using 3-D numerical model. Influence of surface processes to lake's properties was studied. The chapter also contain study of influence of neighborhood configuration in the cooling process. The input of this part is encompassed in the next chapter in which thermal convection is investigated using Stochastic model. Statistical analysis based on both numerical and stochastic models is crucial input in comparability of the two approaches in explaining thermal convection in a lake.

3.2 Scope

Fundamental characteristics of lake's cooling process are modeled by using 3-D numerical model. The aspects of numerical model are first introduced from literature, with brief inclusion of the related theoretical assumptions, equations, solution's algorithm, initial and boundary conditions as well as the related details of the computational domain.

The 3-D model is firstly applied to study the effects of climate change conditions which influence the lake from the water surface down to the entire water column. Disturbances caused by changes in the water surface are lumped into one parameter, the water surface cooling rate. Simulations are therefore done by setting up the numerical model under different conditions of water surface cooling rate, Q_{00}. Characteristics of the flow done under these conditions is then studied and summarized.

Spatial analysis involving the falling (or sinking) portions formed within the computational domain is later on made, in which the results from 3-D scenarios with differing water surface cooling rates are analyzed. The parameters, criterion and terms for the spatial analysis were introduced and the relation of flow properties with information from

spatial analysis is summarized.

The model is finally applied to study the interaction of water particles in a thermally cooling lake. Five configurations were designed to study the falling pattern of the cooling water entity under different neighborhood temperature conditions. Interaction of a falling water entity with its neighboring cells is expected to differ between configurations, the effect brought about with density-variation. The interaction of site and its neighbors is a basis of stochastic approach to thermal convection, discussed in the next chapter.

The chapter is then concluded by brief comprehension to summarize the main concepts contained in this particular topic.

3.3 Model Description

3.3.1 General

The adapted model which is described herein was intended to reproduce the important features of the cooling lake which some of them could easily be seen from observed field records or in controlled flows under artificial environment.

Modelling of fluid flow often incorporates some important elements such as law of conservation of mass (continuity equation), Newton's second law of motion (momentum equation), first law of thermodynamics (energy equation), constitutive law(s) describing the properties of the fluid as well as appropriate boundary and initial conditions of the flow. In the next subsections we introduce the most important components of the model necessary for proper and suitable modelling in consideration of a thermally cooling lake.

3.3.2 Conservation Laws

In an isolated physical system, properties of fluid do not change as the system evolves. The three conservation laws are of interest in this consideration, which involve conservation equations for quantities such as mass, momentum and energy.

Conservation of mass of fluid particles contained in the computational domain is taken care of by continuity equation, ie. equation [3.1].

$$\frac{\partial}{\partial x}u + \frac{\partial}{\partial y}v + \frac{\partial}{\partial z}w = 0 \tag{3.1}$$

The conservation of momentum of the fluid particles is represented by equation [3.2].

$$\frac{\partial u}{\partial t} + u\frac{\partial u}{\partial x} + v\frac{\partial u}{\partial y} + w\frac{\partial u}{\partial z} = -\frac{1}{\rho}\frac{\partial p}{\partial x} + \nu\left(\frac{\partial^2 u}{\partial x^2} + \frac{\partial^2 u}{\partial y^2} + \frac{\partial^2 u}{\partial z^2}\right) \tag{3.2a}$$

$$\frac{\partial v}{\partial t} + u\frac{\partial v}{\partial x} + v\frac{\partial v}{\partial y} + w\frac{\partial v}{\partial z} = -g - \frac{1}{\rho}\frac{\partial p}{\partial y} + \nu\left(\frac{\partial^2 v}{\partial x^2} + \frac{\partial^2 v}{\partial y^2} + \frac{\partial^2 v}{\partial z^2}\right) \tag{3.2b}$$

$$\frac{\partial w}{\partial t} + u\frac{\partial w}{\partial x} + v\frac{\partial w}{\partial y} + w\frac{\partial w}{\partial z} = -\frac{1}{\rho}\frac{\partial p}{\partial z} + \nu\left(\frac{\partial^2 w}{\partial x^2} + \frac{\partial^2 w}{\partial y^2} + \frac{\partial^2 w}{\partial z^2}\right) \tag{3.2c}$$

In addition, heat transfer equation is represented by temperature transport equation,

$$\frac{\partial T}{\partial t} + u\frac{\partial T}{\partial x} + v\frac{\partial T}{\partial y} + w\frac{\partial T}{\partial z} = \lambda\left(\frac{\partial^2 T}{\partial x^2} + \frac{\partial^2 T}{\partial y^2} + \frac{\partial^2 T}{\partial z^2}\right) \tag{3.3}$$

Reference density representing water particles at each cell were computed depending on temperature information (eqn. [3.4]), after the temperature was updated from transport equation. Standard information from literature was used for this particular interpolation.

$$\rho = \rho(T) \tag{3.4}$$

3.3.3 Computational Domain

The fluid flow described in this chapter was computed under Cartesian coordinates. Computational domain has had a shape of cuboid. Total number of cell in each of all three Cartesian coordinate systems was maintained at 40.

An *a priori assumption* of *continuum hypothesis* was applied for the fluid impounded within the declared computational domain, consequently, implying that some fluid's properties could be modeled by assuming that water molecules are continuous substances and occupy the whole domain, leaving neither cracks nor voids. Furthermore, the assumption means that the bulk fluid can be divided into infinitesimally small elements whose properties are same as the bulk fluid.
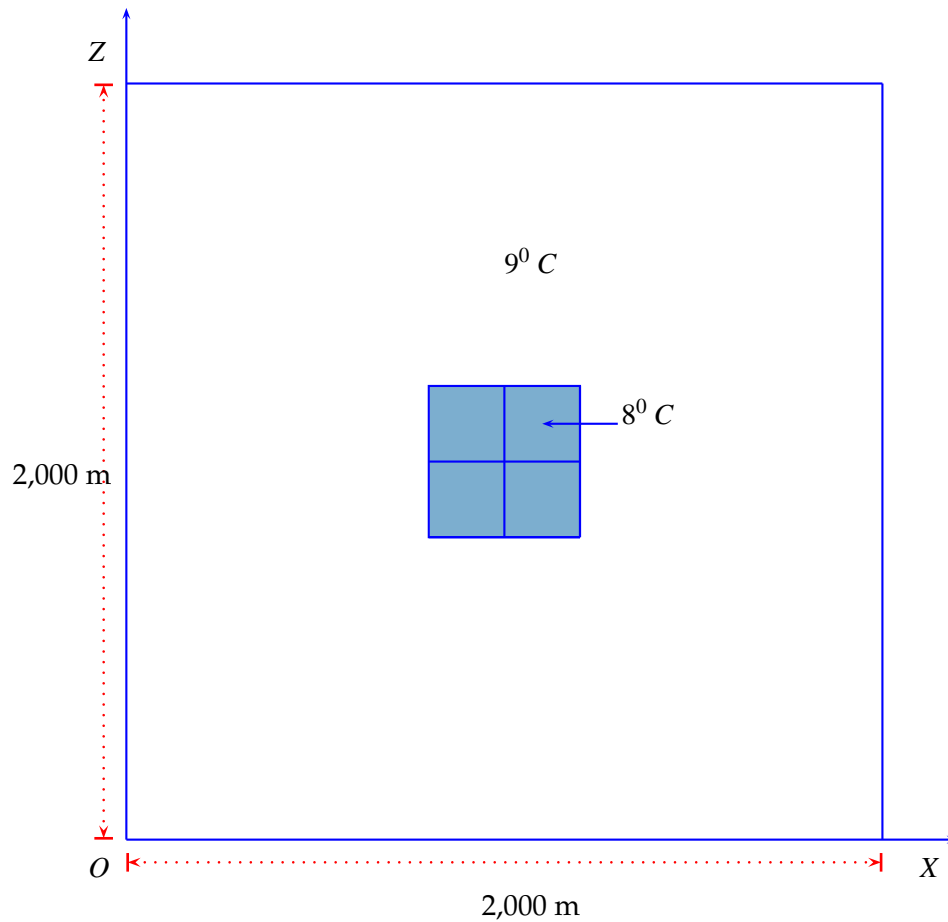
Figure 3.1: Plan view of computational domain and initial temperature condition at the water surface

Figures [3.1] and [3.2] show the plan and side views of the domain, with the temperature initial conditions. The initial water temperature distributions in the vertical direction are 9 ^0C for $20m < y \leq 80m$ and 7 ^0C elsewhere along the domain, where y is the elevation referenced from the bottom.

Some of the cells near the surface (6 × 6 cells in plan view extending from the air-water interface by 5 cells in vertical direction) are introduced to create a disturbance necessary to commence the flow. The artificial disturbance is created as these cells with colder temperature (8 ^0C) than those beneath, instigate density-gradient between cells forcing the flow to occur.
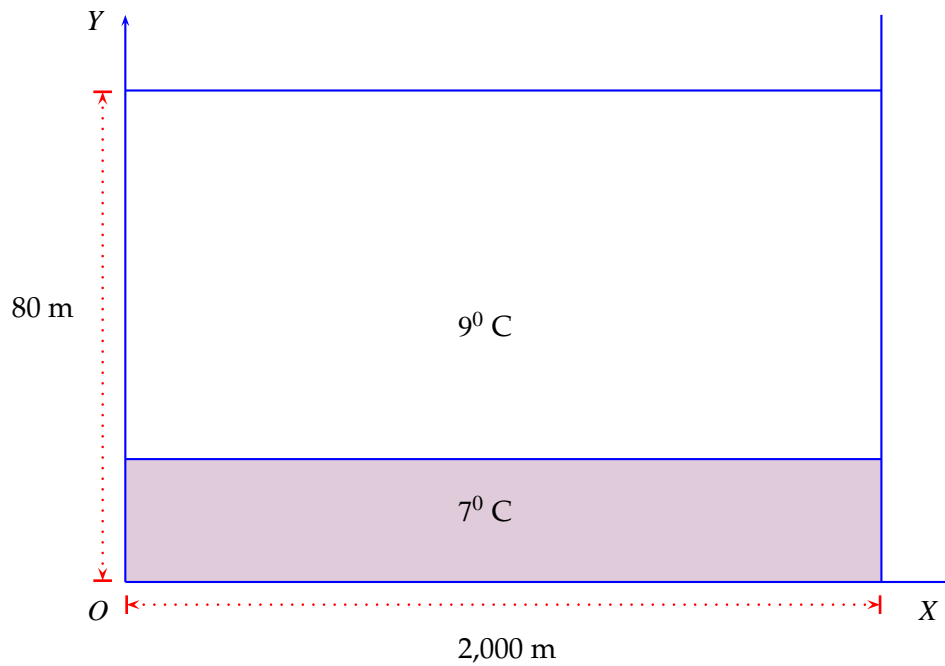
Figure 3.2: Side view of computational domain and initial temperature condition

3.3.4 Mesh and Variables Arrangement

Staggered variables' arrangement is used to define flow variables such as velocity field and temperature and pressure scalars . In staggered arrangement, shown in figure [3.3], scalar quantities such as pressure and temperature are defined at the centre of the cell computational cube while velocity components are defined at the faces of the cube surrounding the scalar points. Flow variables arranged in staggered grid system are usually necessary to produce physically correct pressure fields (*Morinishi et al.*, 1998).

3.3.5 Assumptions and Conditions

Modeling of a natural process is at best an idealization. The oversimplification imposed within the modeling or simulation setup can be tolerated when the main features of the natural process are still adequately predicted by the model. The advantage ripped from model's oversimplification should break even with intended purpose(s) of the model. The trade-off between the two determines if the assumptions are tolerable to extent of proving that the model is suitable or not.

In the solution of our numerical simulation we assume:
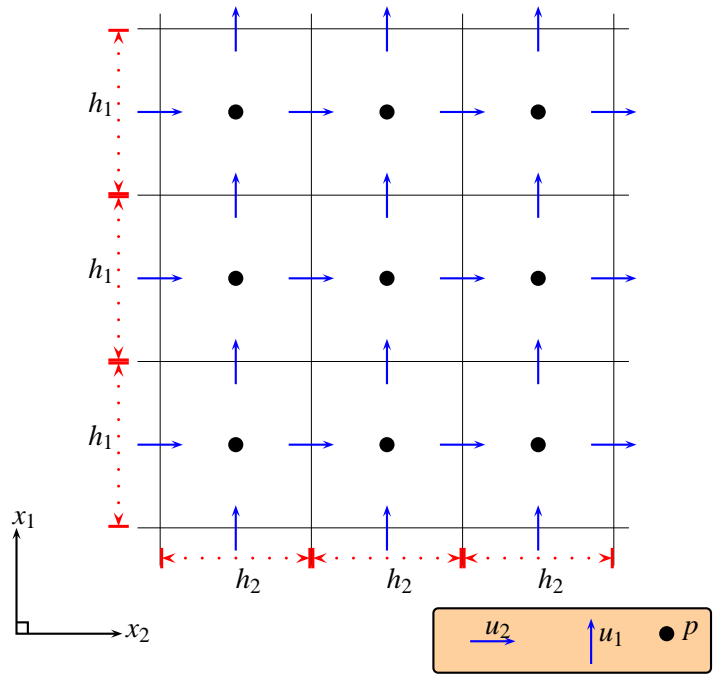
Figure 3.3: Staggered grid system in uniform Cartesian coordinates

Uniform initial temperature conditions : Temperature of the fluid are initialized as shown in figures [3.1] and [3.2] in pages [35] and [36], respectively. The portion of low temperature is included to provoke flow through disturbance which is caused by temperature difference and eventual density gradient. The initial thermal layers used in the simulation are assumed to reflect thermal strata, the condition expected on the onset of cooling period after summer period.

Fully one-phased flow : Water confined within the computational domain is assumed to be a one-phased liquid water, with negligible amount of other impurities such that their physical and chemical properties are safely negligible in the numerical setup.

Fluid incompressibility: As shown in momentum and continuity equations (equations [3.1] & [3.2] in page [34]), the flow is assumed to be incompressible.i.e the flow particles have low Mach number and modelling of turbulent terms is ignored.

3.3.6 Numerical Solution's Algorithm

Numerical solution involving a set of partial differential equations(PDEs) describing a natural process is cumbersome when there are variables which appear in more than one equation in that particular set of PDEs. Coupling of those variables appearing in more than PDE highlights the need for special attention when designing the solution of such system of PDEs. In computational fluid dynamics, algorithm formulation is important research interest alongside turbulent flows and mesh-generation.

Marker and Cell method aliased, **MAC** method (*Harlow and Welch*, 1966) is among the early work pioneered in the field of computational fluid dynamics. *Highly Simplified Mark and Cell* aliased **HS-MAC** method (*Hirt and Cook*, 1972) follows the spirit initiated by MAC authors. HS-MAC release some of the CPU overhead in the most expensive stage of the algorithm, the solution of Poisson equation. Solution of Poisson equation is necessary in obtaining the divergent-free velocity field from pressure scalar variable. HS-MAC is chosen to be used in this thesis. The convective terms found in both momentum as well as temperature transport equations are modelled using QUICK scheme (*Leonard*, 1979). Time integration in time-stepping the propagation of the simulation follows the second order Adam-Bashforth scheme.

Following adaption of staggered grid system, the definition of the momentum equation is defined at velocity points while the continuity equation is defined at pressure points. The discretization of PDEs is done following *finite volume discretization*.

Further background description of some of the elements discussed regarding the setup for this numerical model can be found in detailed manner abundantly in most of the existing fundamental literature of the subject such as *Ferziger and Peric* (2002), *Kundu and Cohen* (2002), *Anderson,* (1995) etc.

3.4 Effects of Surface Process and Spatial Analysis

In § [3.3] 3-D numerical formulation was introduced. Investigation of the effects of surface process to a thermally cooling lake is now done by considering different scenarios at the water surface of the lake. Change of conditions at the water surface are decided to

Table 3.1: Simulation cases with different water surface cooling rates, Q_{00}

Case	Q_{00} ($cal\ cm^{-2}\ sec^{-1} \times 10^4$)
SM_{010}	10
SM_{025}	25
SM_{050}	50
SM_{075}	75
SM_{100}	100
SM_{150}	150

be lumped within coefficient of water surface cooling rate (Q_{00}). A total of six cases are considered, and for simplicity and convenience in referencing they are shown in table [3.1] with denotation.

3.4.1 Simulated Features

3.4.1.1 Temperature Profile

After a relative heavy heat influx in the summer, lake is subjected to potential thermal layers. The topmost layer, also termed as *epilimnion* have water of higher temperatures and extensively mixed. Temperature in this layer is uniformly distributed. The bottom layer, *hypolimnion*, has lower temperatures and less mixed waters.

Figure [2.2] in page [14] in Chapter [II] is an example of temperature profile from Lake Biwa showing monthly temperature profiles in January-December period, the important period from the data is the period after summer heating around August-September and its eventual thermal cooling. The data are taken from year 1998 by *LBRI*, (*Hosoda and Hosomi*, 2004). After the summer, temperature layers are clearly observable.

The 3-D numerical model was able to simulate the temporal distribution of the temperature profile. Figure [3.4] show temperature profile at different simulation times. The results were plotted from SM_{050} showing decreasing temperature difference between upper and lower layers as time went on.
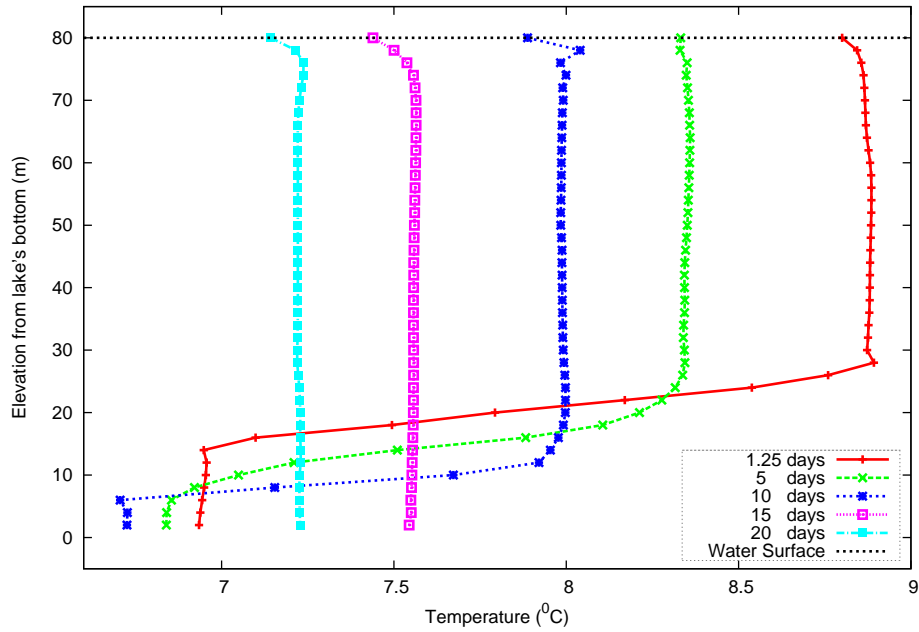
Figure 3.4: Simulated temperature profiles during cooling Process from SM_{050}

3.4.1.2 Velocity Field

Simulated fluid flow represented well the cooling process by showing the most important elemental concept of vertical movement, which is a result of density-gradient and earth's gravitational pull. Density-gradient is caused by temperature difference between adjacent cells in the computational domain. Low density cells with relatively higher temperature are lighter and therefore likely to be replaced by those cells whose density is higher because of possessing lower temperature. This transition is the key movement in a natural lake undergoing thermal cooling, whereby topmost cells are cooled and become heavier and then 'fall down' and their position taken by other cells whose temperatures are higher and lighter in weight in order to complete conservation of mass, ultimately the process results into uniform temperature in the entire water column.

Figures [3.5] and [3.7] in pages [42] and [44], show the side view and plan view of the simulation progress, respectively, from SM_{050}. The plotted data are taken after 5 and 7.5 days of simulation time. The cross-section representing the side view was taken from the mid-cross-section (dividing the computational domain into two parts along *axis Z-Z*)

, while the plan view were taken at depth 12m from the water surface cutting the vertical *axis Y-Y*. In general, temperature profile decreases as the time progressed as the lake is losing heat at the surface. Both plan and side views showed the decreasing of temperature ranges of lake's waters. Vertical movement of particles is self-evident as shown Fig. [3.6] with the velocity fields especially in the side view of the same simulations but with temperature scale reduced to show the falling water bodies in the upper layer.

Difference of flow properties between theoretical scenarios as a function of coefficient of water surface cooling rate (Q_{00}) is investigated. Data from six simulation cases were compared. As expected, the larger value of Q_{00} means the water surface will be cooled faster compared with cases with smaller values. Figures [3.8] and [3.9] show the plan and side views of the data from SM_{050} and SM_{100} taken after 5 days of simulation time. The example evidently represented by these two figures show that although the data were from same point in simulation time, the larger the magnitude of Q_{00} the cooler the waters will be as reflected with temperature profiles.

Investigation of flow properties with respect to depth were done by comparing flow properties at planes located at different depths. Figure [3.10] in page [47] is a plot of data from SM_{150} taken after $7.5days$ simulation time showing velocity and temperature fields from two layers located $12m$ and $40m$ (mid-depth) from the water surface. Water temperature range slightly differs between the two layers while the distribution of velocity field looks comparable indicating that the flow in two layers is not significantly different.

Satellite image showing the temperature map of the region around Lake Biwa is shown in figure [3.11]. The spatial color differences confirm water particles in the lake have non-uniform properties. Temperature differences is bound to cause non-uniformity in density in fluid particles. The image suggests that within the lake there is fluid motion due to this density gradient, as a results in some location cooled waters sink and are replaced with hotter waters as the lake undergoes thermal cooling. Similar temperature map can be seen from maps of simulated results taken at different layers, some of which are included in this chapter.
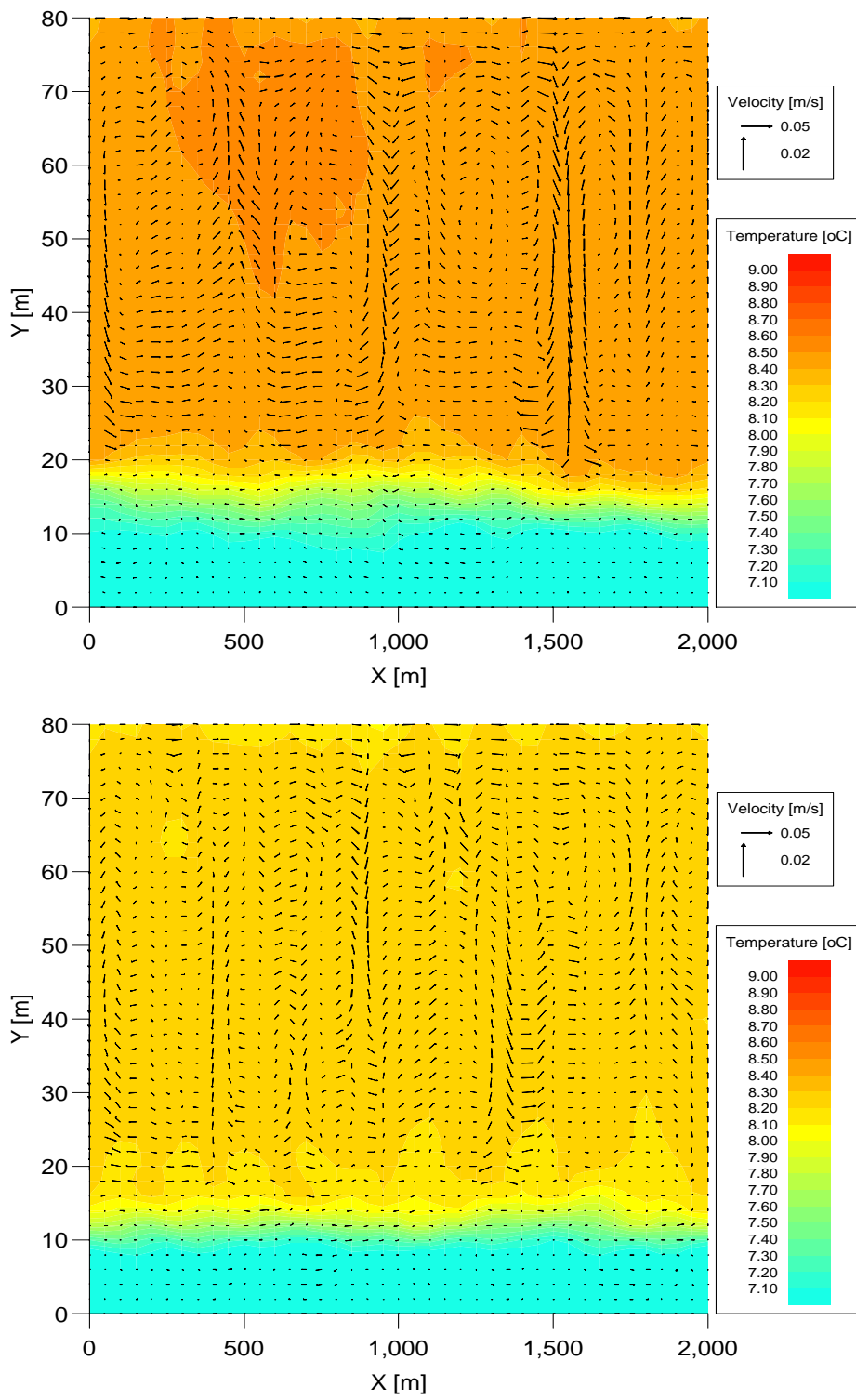
Figure 3.5: Side view of simulated flow from SM_{050}. The sub-figures were taken after 5 days (top) and 7.5 days (bottom) simulation time.
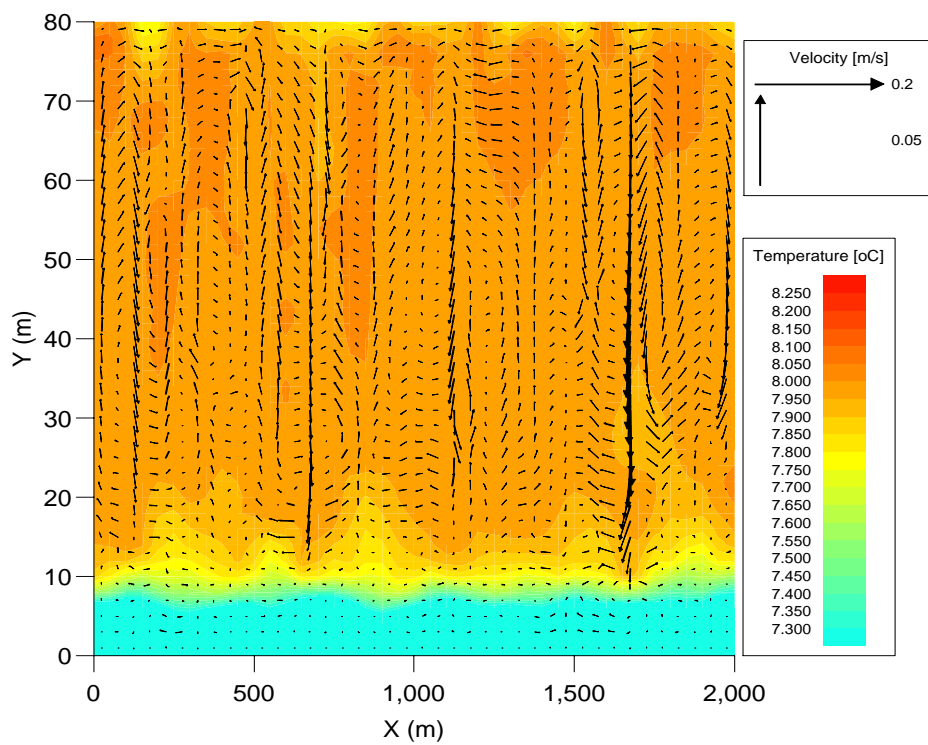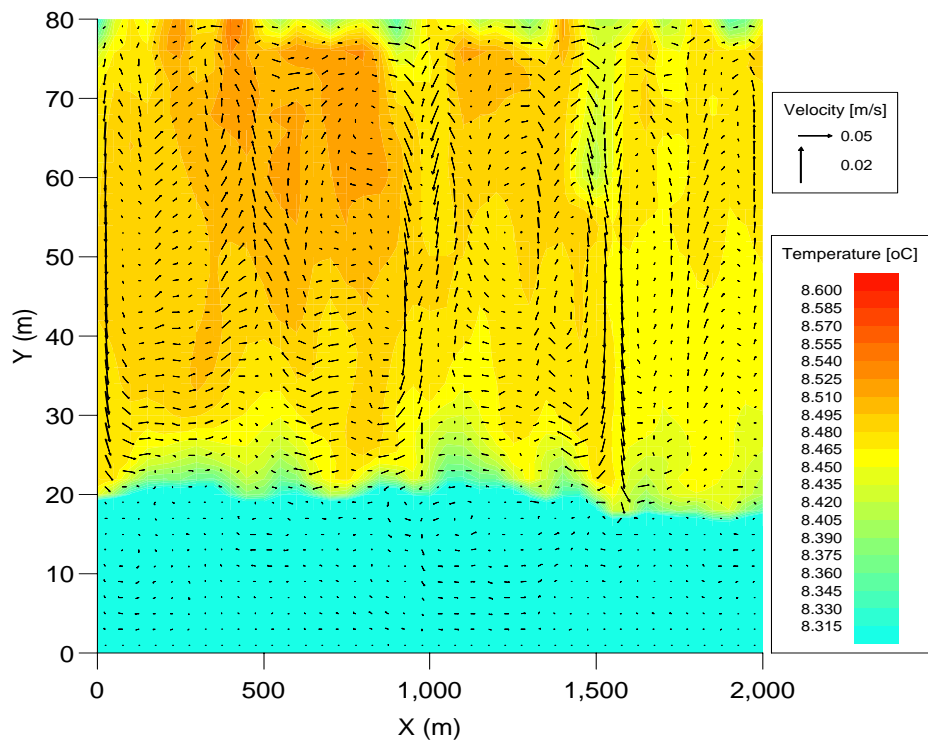
Figure 3.6: Falling cooled waters as shown from side views of simulated flow from SM_{050}(top) and SM_{050} (bottom). The sub-figures were taken after 5 days (top) simulation time.
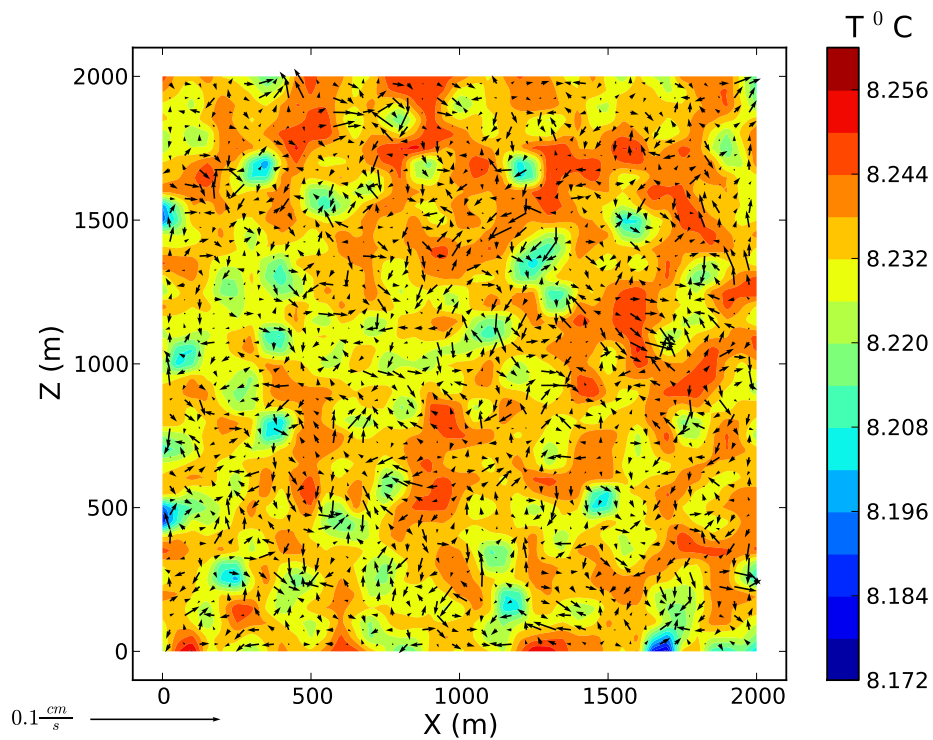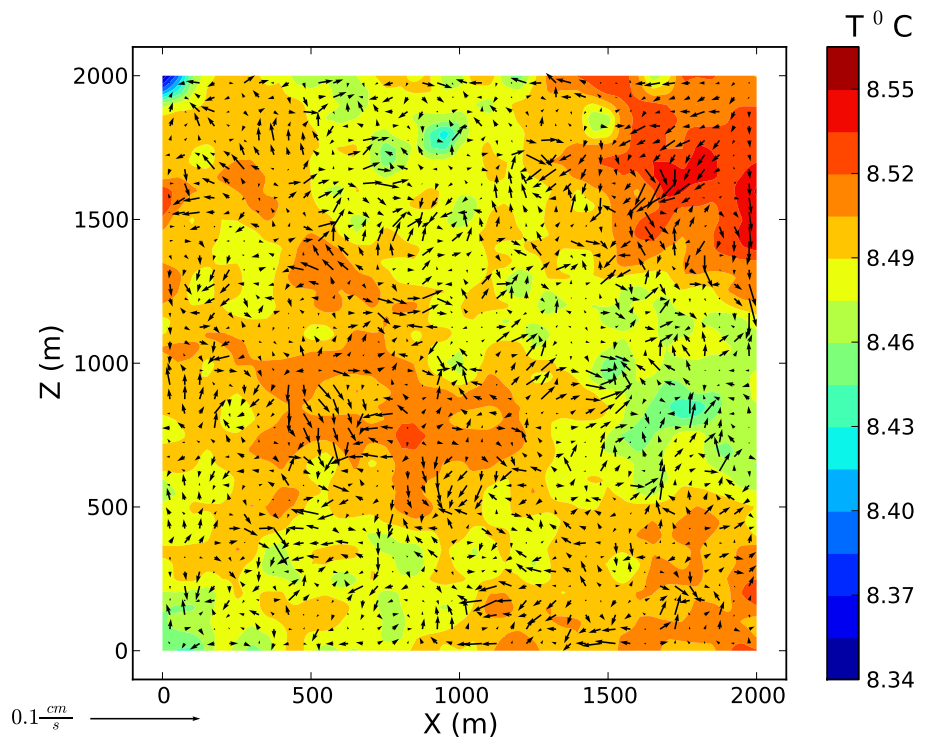
Figure 3.7: Plan view of simulated flow from SM_{050}. The sub-figures were taken after 5 days (top) and 7.5 days (bottom) simulation time.
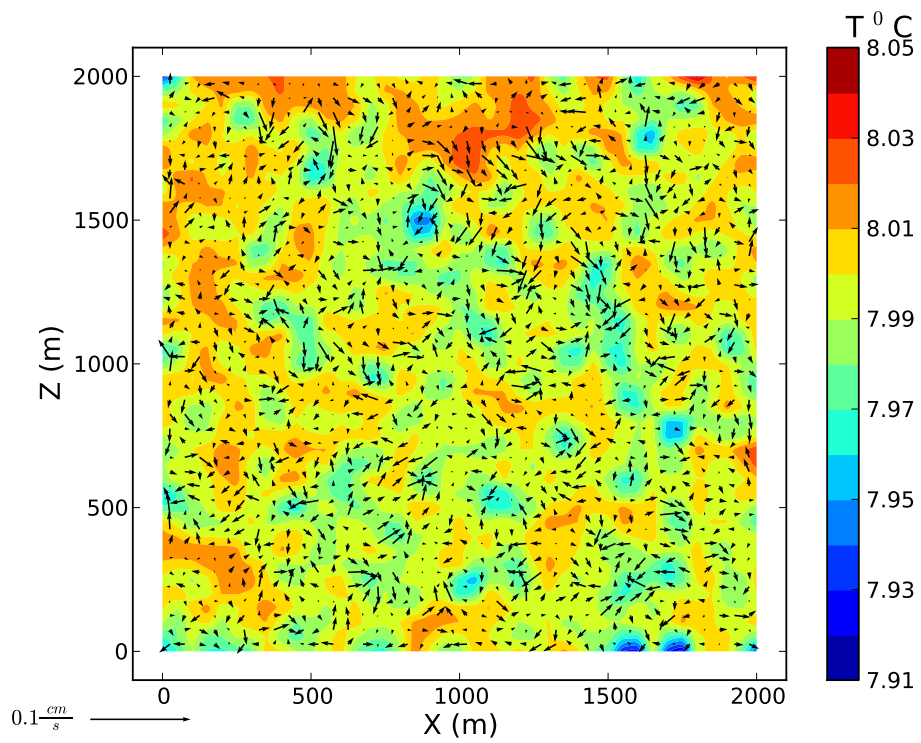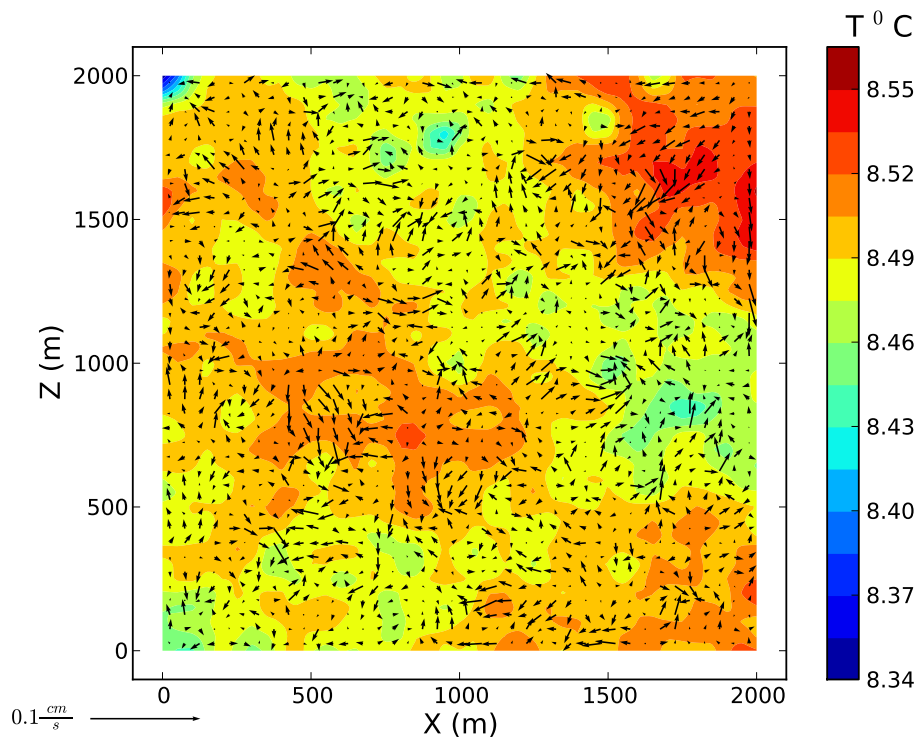
Figure 3.8: Plan view of simulated flow after 5 days simulation time. The sub-figures were taken from SM_{050} (top) and SM_{100} (bottom)
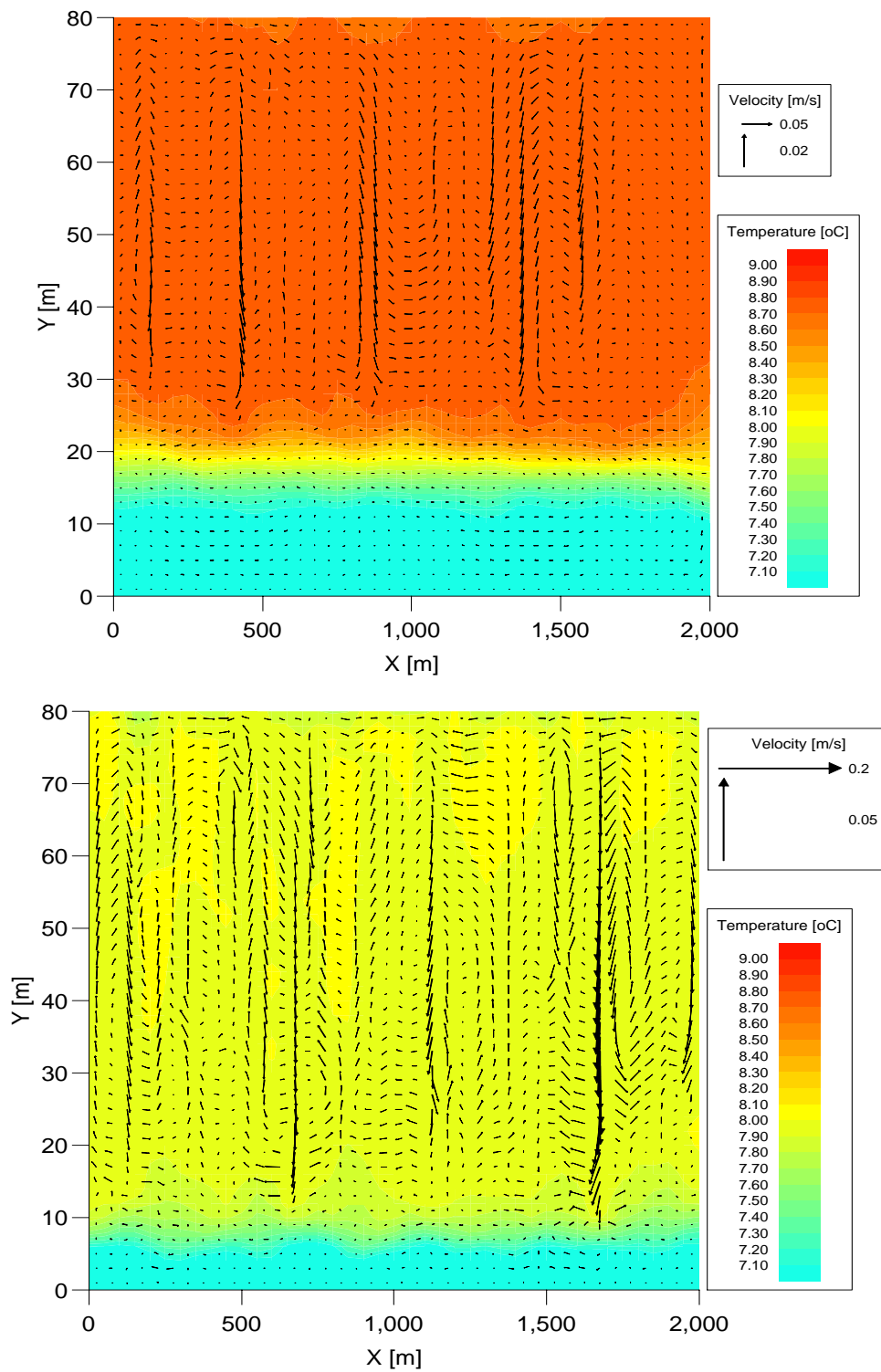
Figure 3.9: Side view of simulated flow after 5 days simulation time. The sub-figures were taken from SM_{050} (top) and SM_{100} (bottom)
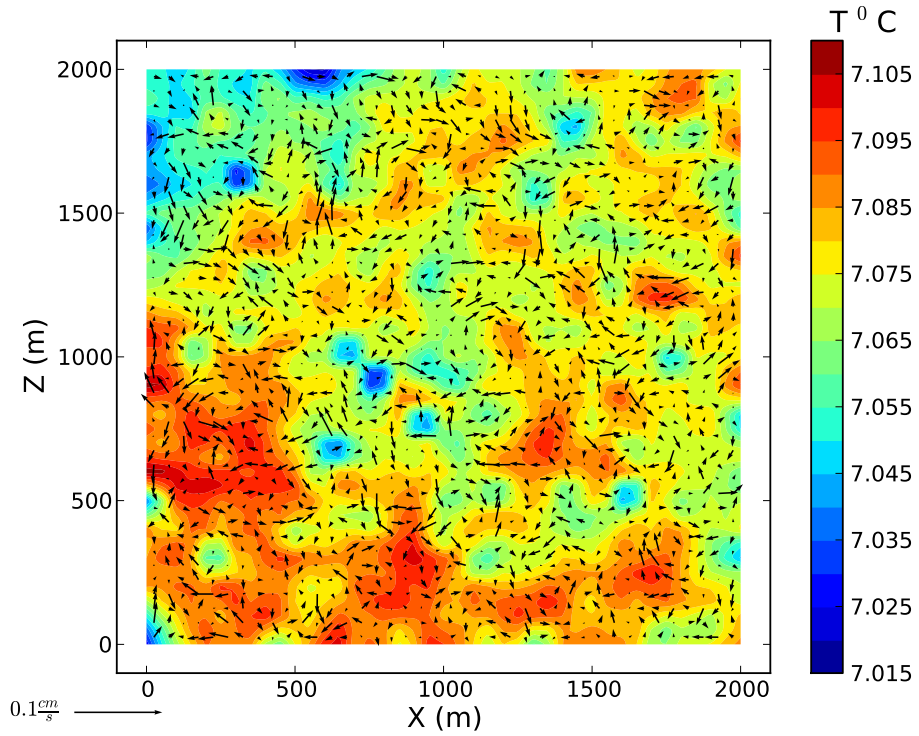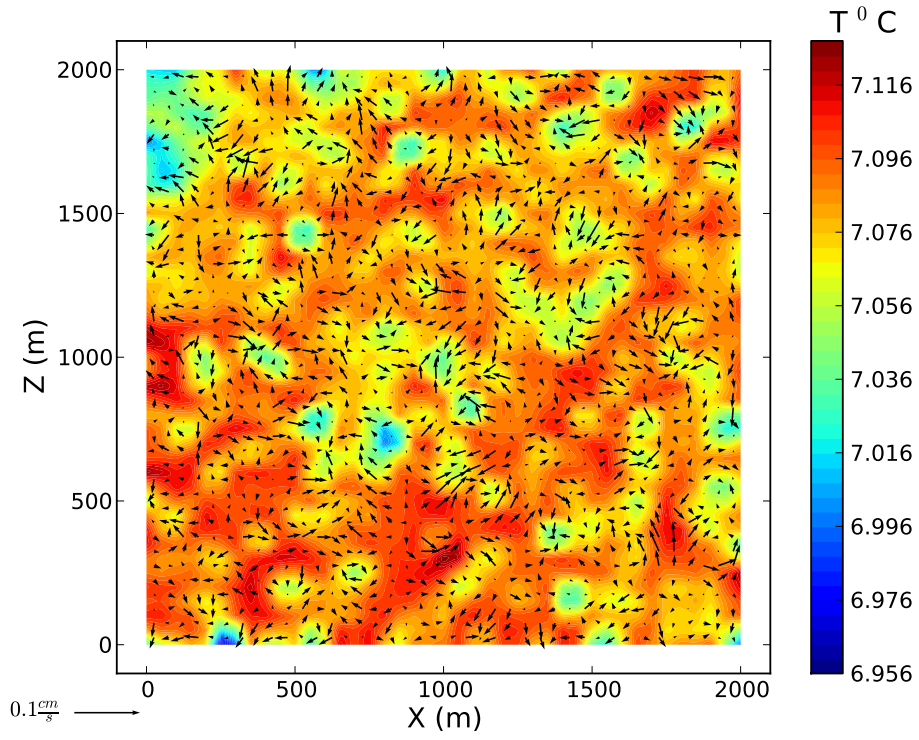
Figure 3.10: Plan view of simulated flow after 7.5 days simulation time from SM_{150}. The sub-figures were taken from $y = 12\ m$ (top) and $y = 40\ m$ (bottom)
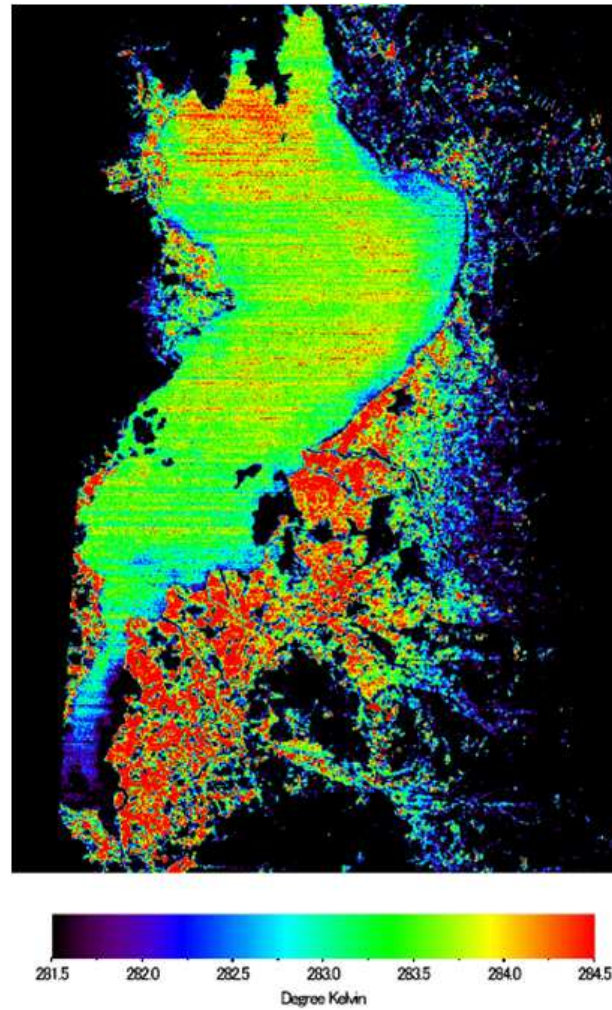
Figure 3.11: Satellite image showing water surface temperature at 10:53, January 9, 2004 in Lake Biwa. (Source: Prof. Masayuki Tamura, Kyoto Univ.)

3.4.2 Spatial Analysis

3.4.2.1 General

Spatial analysis of a system is done for results obtained from the 3-D numerical model in determination of relation between the statistical properties formulated from the cell's properties and other important flow variables which are directly linked in describing the process (in this context, the thermal cooling in lake). To identify the spatial properties, a **surface** for analysis in the horizontal plane needs to be chosen. In this regard we conducted analysis on two planes located at depth located 12 m and 40 m from the water surface in

order to study thermal convection process in various layers.

Two types of cells, $C_{i,j}$ are identified to be the only occupants of such surfaces, **cold** sites (or *cells*; these two terms will be used interchangeably throughout this thesis) and **non-cold** (or *hot*) sites. The two terms are loosely used in this context, rather as conceptual postulation that cold cells have high chance to sink downwards and the opposite expected to happen to the hot cells, both due to density gradient.

Vertical velocity component, $v_{i,j,k}$, is used on deciding the categorization of the **states** (or **spins**) of the sites. Spins are denoted as $S_{i,j}$ and spins values of "1" and "0" are used to denote states of hot and cold sites, respectively. We denote cell's discriminatory criterion on $v_{i,j,k}$ as Ω in decision on spin type, as mathematically shown in equation [3.5]. Ω uses positive-down convection.

$$S_{i,j} = \begin{cases} 0 & \text{if } v_{i,j,k} + \Omega \leq 0 \text{ ;} \\ 1 & \textit{Otherwise.} \end{cases} \qquad (3.5)$$

Figure [3.12] shows a typical example of a surface used for analysis, obtained from SM_{050} at $\Omega = 0$ *mm/s* and 5 *mm/s* after 5 *days* simulation time. The surface was chosen at depth 40*m* from the water surface. Cold sites are shown with *black squares* while hot sites are shown as *white squares*, in a domain of *40 × 40* cells. Smaller values of discriminator allow more cells to be categorized as cold sites, that is, equaling or surpassing the criterion, while the higher value of the discriminator does the opposite.

Sites neighborhood is defined following Neumann's neighborhood definition. In the definition, neighbors of site $C_{i,j}$ are counted on the nearby sites only when they share a boundary and are adjacent to each it. Sites located diagonally and beyond are not part of the neighborhood. Figure [3.13] demonstrates the Neumann's neighborhood definition. Furthermore, definition of cold sites' clusters were done considering those cells interconnected to each other following Neumann's neighborhood definition.
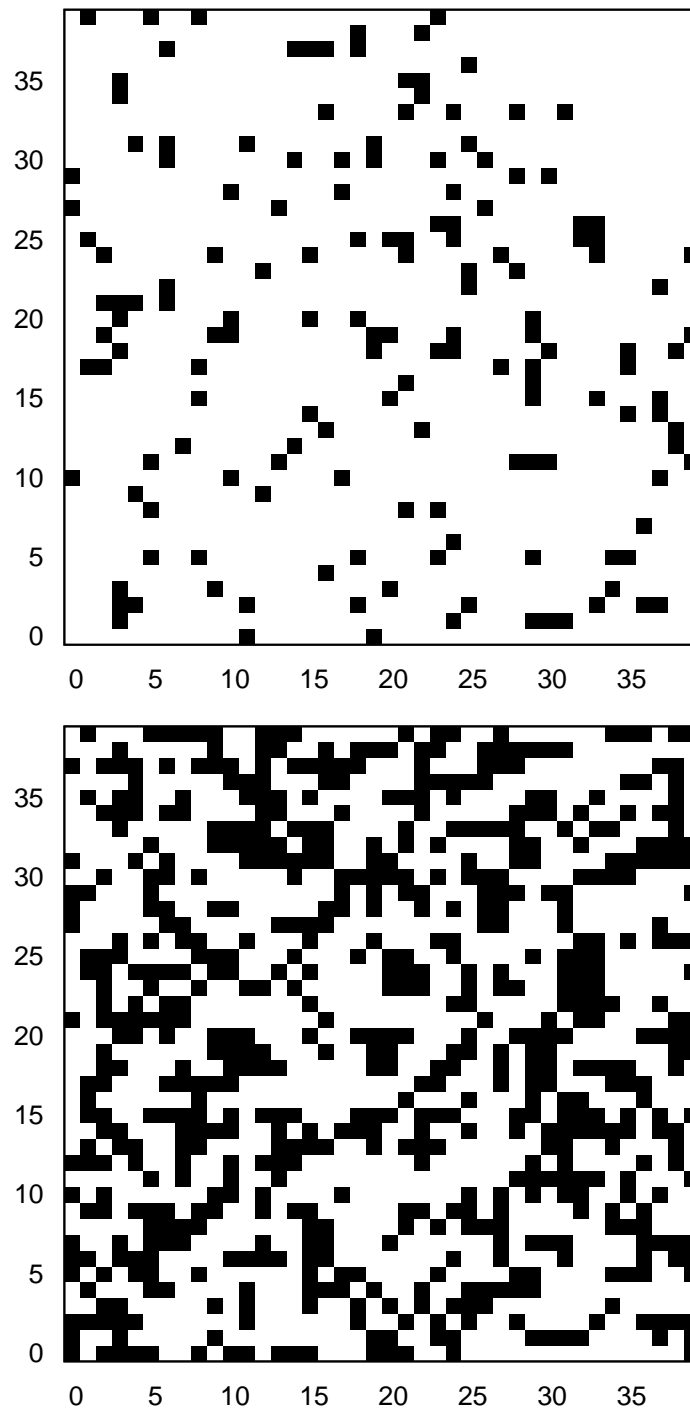
Figure 3.12: Example of a typical surface for spatial analysis of cold sites. The surface assumes two kinds of spins; cold sites marked as black squares and hot sites marked as white squares. The results are taken from SM_{050} at $t = 5days$ at horizontal surface located at mid-depth ($y = 40m$) with $\Omega = 5$ mm/s (top) and 0 mm/s (bottom).
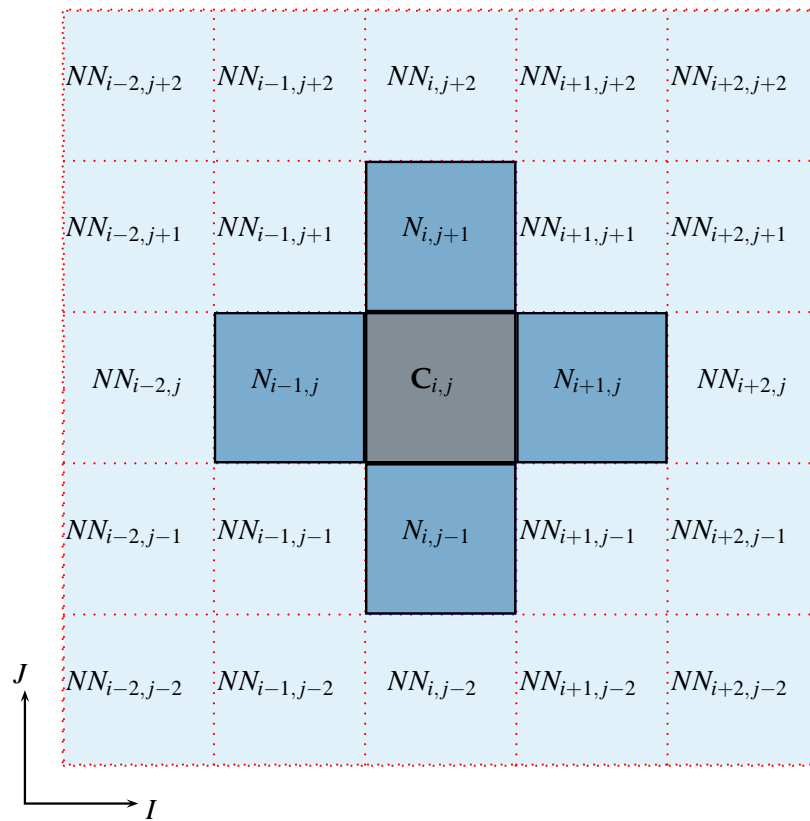
Figure 3.13: Neumann's neighborhood definition for site $C_{i,j}$. Neighbors are indicated as N and non-neighbors as NN
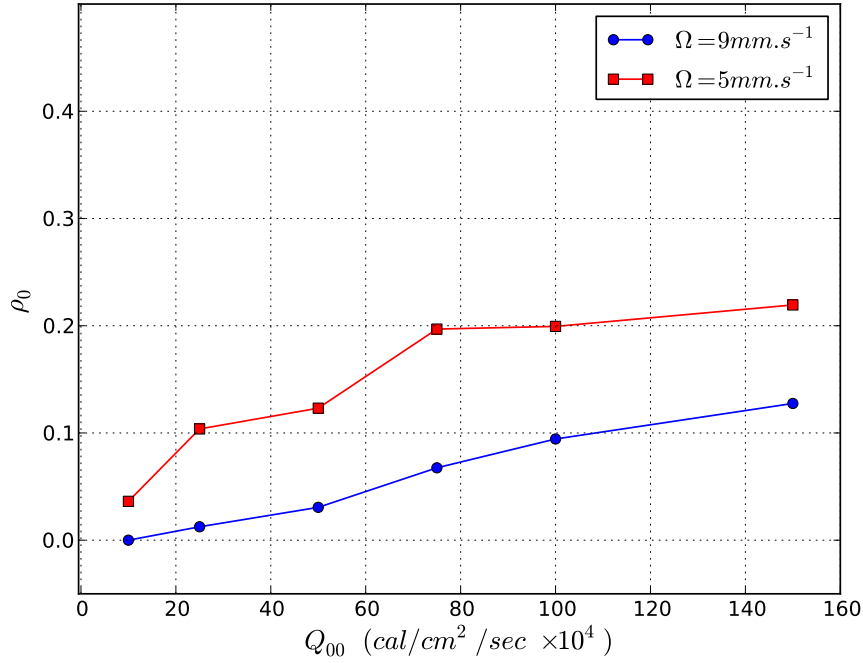
Figure 3.14: Typical variation of ρ_0 with Q_{00}. The figure is from surface at depth $12m$ from the water surface after $5\ days$ simulation time.

3.4.2.2 Densities

Two types of density are identified. The global density of sinking or cold sites, denoted as ρ_O is the ratio of number of cold spins found in a surface to total number of cells in that given surface. On other hand local density of cold sites, denoted as $q_{0/0}$ is computed by aggregating all pairs of cold sites in the surface from the portion of ρ_0.

In general, from simulated results it can be concluded that the global density grow proportionally with the magnitude of water surface cooling rate. The larger magnitudes of discriminator limit a number of cells into categorization of sinking sites and as a result, the values of ρ_0 are larger when smaller values of discriminator are used. Figure [3.14] show the variation of global densities with water surface cooling rate.

The values of global densities taken from two different layers have shown slight differences. The values taken from a layer located $12m$ deep from the water surface were not consistently greater than those taken at a mi-depth layer. The differences were not significantly large when larger values of Ω were used. Figure [3.15] show the variation of ρ_0 with
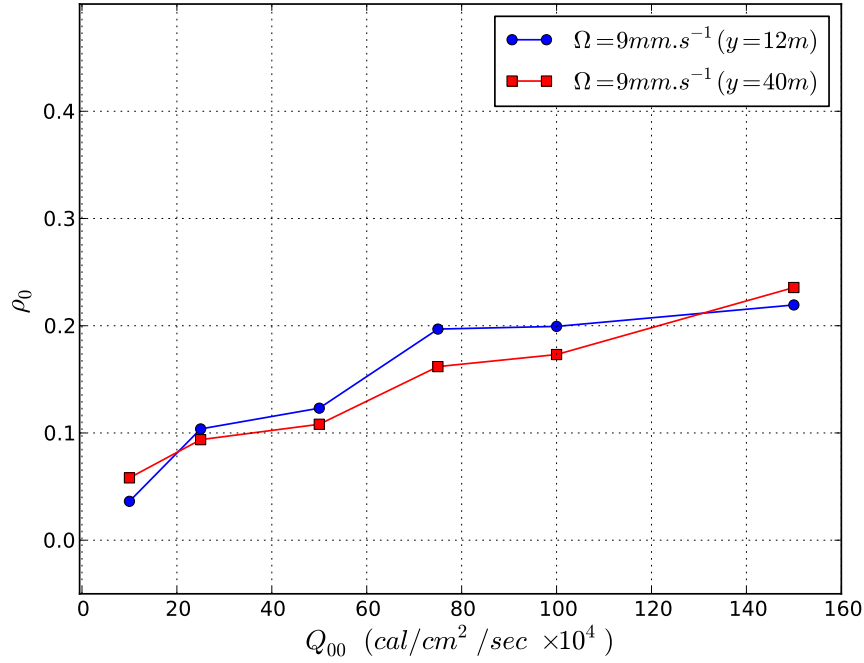
Figure 3.15: Comparison of variation of ρ_0 with Q_{00} at different depths. The data are taken after $5 days$ simulation time and y is referenced from water surface.

Q_{00} taken after 5 *days* of simulation time.

Variation of local densities with cooling rates was similar to their global densities counterparts, whereby $q_{0/0}$ increases as the value of Q_{00} increases, as shown in figure [3.16].

When comparison was made between local and global densities of the cold sites, the two densities differed, with ρ_0 consistently being larger than $q_{0/0}$, as shown in figure [3.17] with data computed from a layer located 12*m* deep from water surface after 5 days simulation time.

The variation of the local density with water surface cooling rate at different depths is shown in figure [3.18].

In general, the global and local densities of cold sites increased when the value of water surface cooling rate was increased. The variation of global and local densities from data taken at different depths did not show any conclusive variation. Global density was observed to be consistently greater than local density for the tested cases. The growth curve of global and local density with water surface cooling rate show that the increment de-
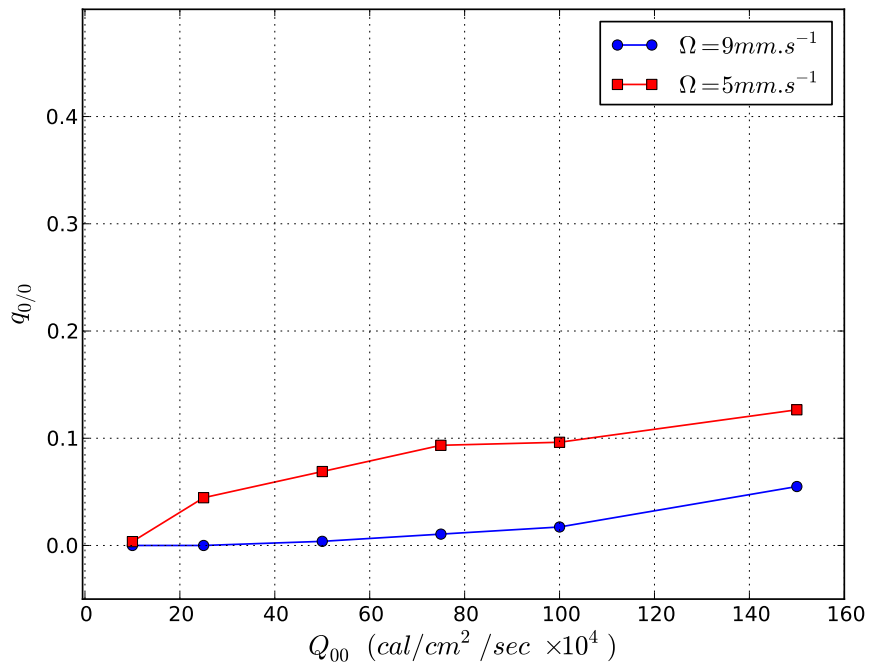
Figure 3.16: Comparison of variation of $q_{0/0}$ with Q_{00} at depth $12m$ from the water surface after 5 days simulation time.
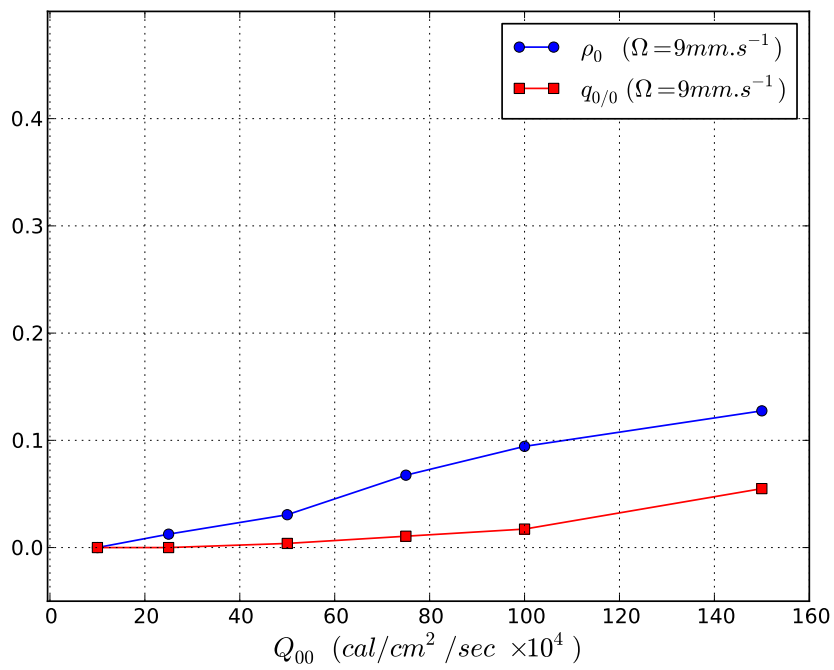
Figure 3.17: Comparison of $q_{0/0}$ and ρ_0 with Q_{00} at $y = 12m$ from the water surface after 5 days simulation time.
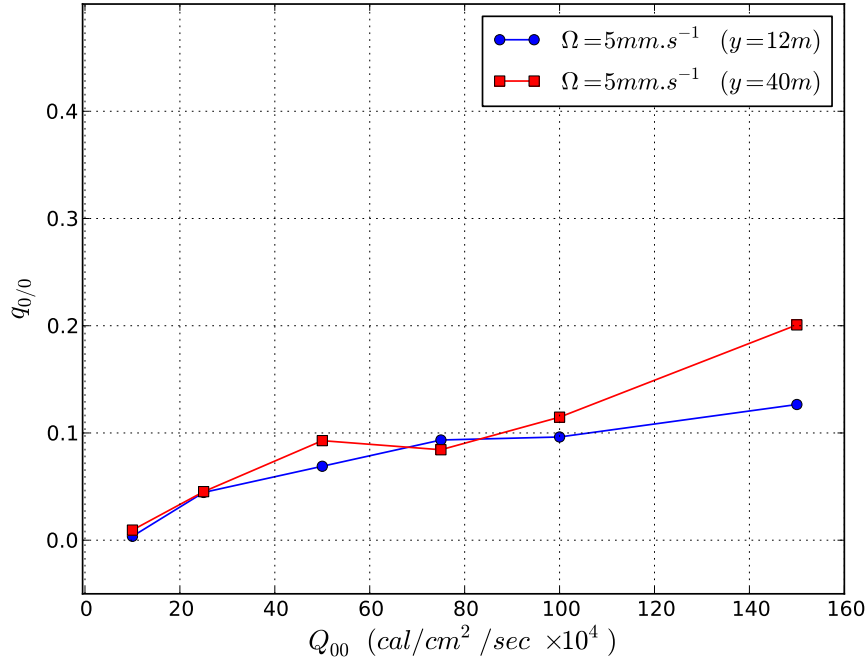
Figure 3.18: Comparison of variation of $q_{0/0}$ with Q_{00} at different depths. y is referenced from water surface.

clines as the value of water surface cooling rate increases, suggesting that at infinitively large value of Q_{00} the value of ρ_0 and $q_{0/0}$ might achieve an *asymptotic limit*.

3.4.2.3 Clusters

Clusters are combination of individual sites which are joined together in a manner pointed-out under Neumann definition of neighborhood. In order to compare properties of clusters from different surfaces, we introduced averaged cluster size for a given surface. The parameter was used in comparison between different surfaces by consistently maintaining the value of discriminator (Ω).

For a given particular surface, averaged cluster size, χ, is defined as the ratio of sum of product of size of all clusters confined in the surface and their number of occurrence to the total number of clusters in that surface. That is,

$$\chi = \frac{\sum_{all} \Psi \pi}{N} \tag{3.6}$$

where,

Ψ is the size of the cluster,

π is the number of occurrence of a cluster of a given size, and

N is the total number of clusters in a given surface.

Figure [3.19] show the values of χ as the a function of water surface cooling rates, taken at $12m$ depth surfaces. As clearly seen, at $\Omega = 0$ mm/s the values of χ are higher than other remaining cases of higher values of Ω. At $\Omega = 5$ mm/s and $\Omega = 9$ mm/s there is a minute increment of χ with Q_{00}, the increase which is hardly noticeable in contrast with $\Omega = 0$ mm/s where not distinct trend is observable. Comparison of χ from *mid-depth* and $y = 12$ m data shows that there is smaller difference but with inconsistent trend of data from the two depths.

3.4.2.4 Relation between Cluster Sizes and frequencies

Clusters formed by cold sites are focal points in this analysis. Their sizes with their respective number of occurrences are analyzed in conjunction with simulation progression, changes in water surface processes (properties lumped on Q_{00}) as well as the depth of the plane of analysis. Relation between cluster sizes and their respective frequencies is of interest in knowing their relation to the thermal cooling process. The information obtained from the analysis could link the results of the numerical model with some behavior of non-linear dynamic systems.

The results of the analysis reveal the relation between cluster sizes and their corresponding number of occurrences is *exponential*. The inclusion of more data is dependent of the value of discriminant used in delineating the spins in a given surface. With small values of discriminants, more cells qualify the criterion and pass to be categorized as cold or sinking sites. The larger number of cells from small values of discriminants means more number of clusters or/and larger sizes of clusters. Figure [3.20] demonstrates these trends from an example taken from SM_{150} after 3 days and 18 hours simulation time. A spectrum
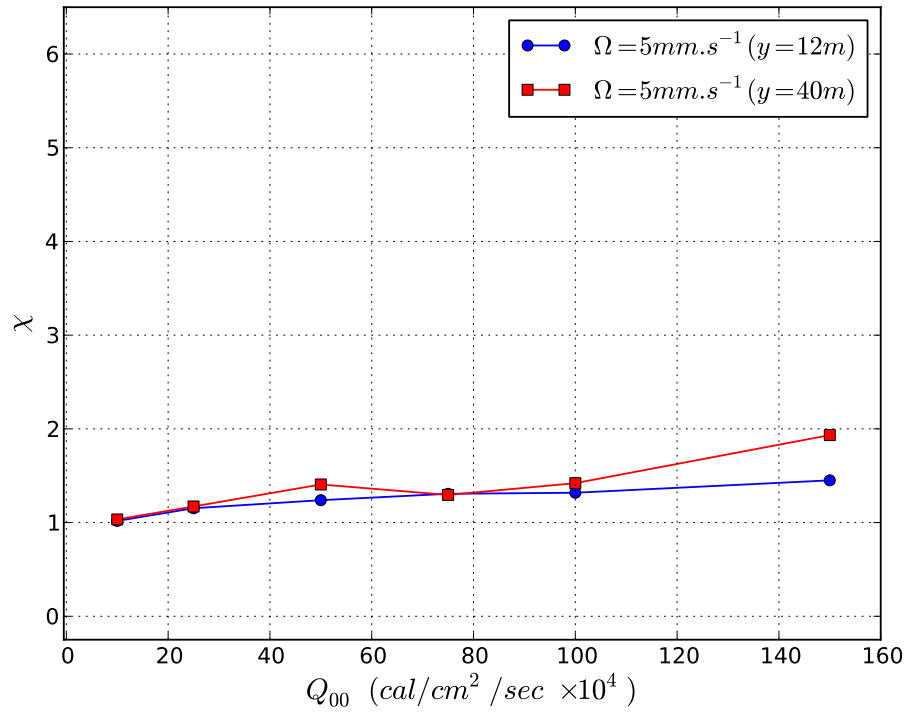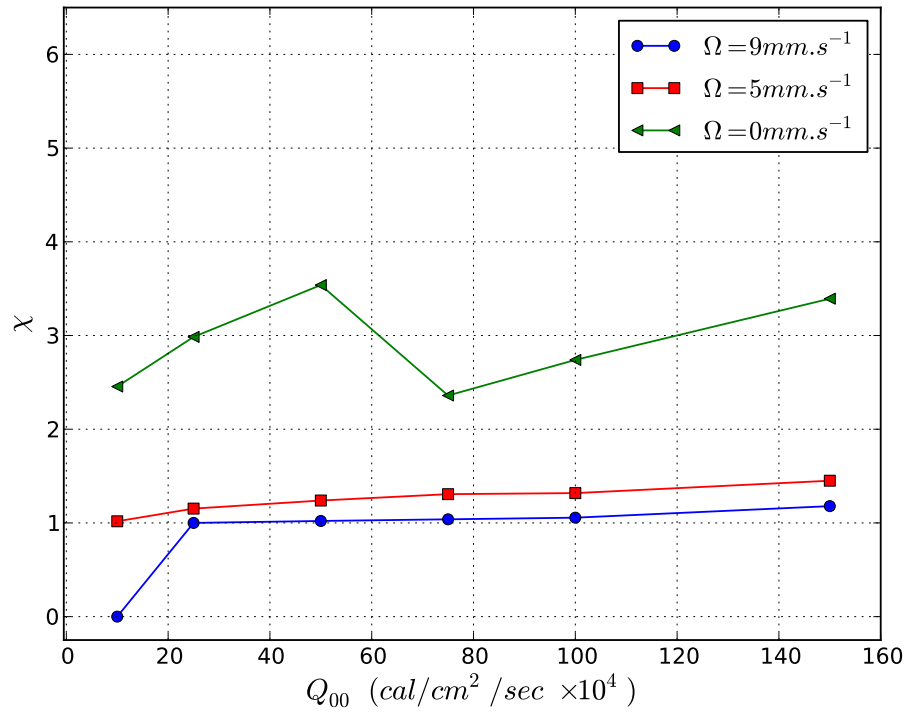
Figure 3.19: Averaged cluster size relation with Q_{00}. Sub-figure on the top shows general relation at $\Omega = 5$ *and* $9mm/s$. The bottom sub-figure show variation at depth 12 *and* 40*m* from the water surface. Data are taken after 5 *days* simulation time
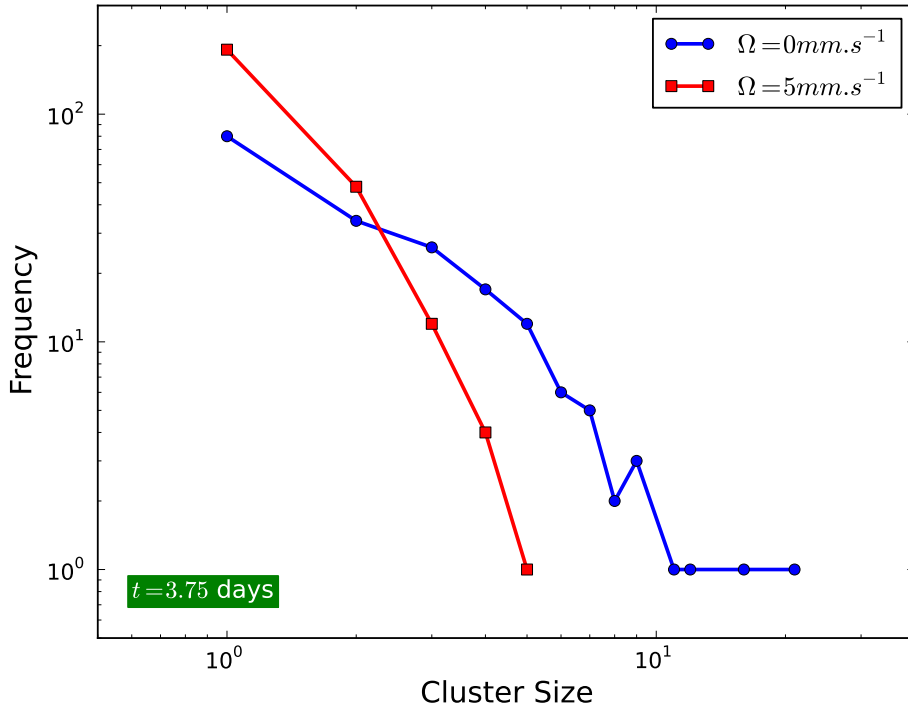
Figure 3.20: Typical example of log-log plot showing cluster size relation with frequency. Power law property is evident. The figure shows data from mid-depth ($y = 40m$) taken from SM_{150} at $t = 3.75$ *days*. Spectrum of cluster sizes is relatively increased at smaller value of Ω than at larger ones as more cells qualifies into a 'cold' category.

of cluster sizes can be observed when $\Omega = 0mm/s$, while in general small sized clusters have a higher number of occurrence.

From figure [3.20], the relation of cluster sizes and their number of occurrence suggests a power law relation. Further investigation of this relation was done by considering cluster size distribution from several surfaces differing in discriminant criterion (Ω), simulation times as well as the depth of the surface for analysis. Power law regression model was applied (equation [3.7]) and the regression coefficients were computed from minimization of *Chi-squared* distribution. Coefficient of determination was used to indicate how close the regression model was to the cluster sizes data from the 3-D numerical model results.

$$\Psi = \alpha\Pi^{-\beta} \tag{3.7}$$

Table 3.2: Power law regression of 3-D model's clusters ($z = 12m$, $\Omega = 0mm/s$)

Case IDs	β		R^2		Simulation time (days)
	$y = 12m$	$y = 40m$	$y = 12m$	$y = 40m$	
SM_{010}	1.877	1.390	0.985	0.979	
SM_{025}	0.893	0.691	0.939	0.816	
SM_{050}	1.271	1.097	0.979	0.981	
SM_{075}	1.730	1.725	0.998	0.984	3.75
SM_{100}	1.237	1.227	0.973	0.975	
SM_{150}	1.664	1.720	0.995	0.954	
SM_{010}	1.748	1.321	0.995	0.979	
SM_{025}	1.480	1.410	0.983	0.957	
SM_{050}	1.300	0.984	0.989	0.859	
SM_{075}	1.436	1.539	0.983	0.986	5
SM_{100}	1.637	1.622	0.993	0.994	
SM_{150}	1.516	1.334	0.980	0.961	
SM_{010}	1.633	1.308	0.970	0.991	
SM_{025}	1.758	1.619	0.989	0.974	
SM_{050}	1.613	1.820	0.988	0.977	
SM_{075}	1.713	1.635	0.986	0.984	7.5
SM_{100}	1.429	1.202	0.973	0.988	
SM_{150}	1.525	1.146	0.981	0.971	

Table [3.2] shows the important information related to the power law regression model. The results show a strong correlation between cluster sizes and power of their respective frequencies. When the discriminant of $\Omega = 0mm/s$ was used, large values of coefficient of determination, R^2 of above 0.90 were observed in all the cases considered. The majority of the powers were in the range of above 1.0. Minimum and maximum values of β were about 0.7 and 1.8 respectively.

In general, it can be said that the power law relation were observed for different sizes of clusters of cold sites with their respective number of occurrences and the results indicates that the formation of clusters of cold sites during a cooling process in a thermally stratified lake, displays a *scale- free property*.

3.5 Neighborhood Interaction

3.5.1 General

In a physical system composed of interacting particles, properties associated to a cell
is partly a function of nature and configuration of its surrounding particles. Influence of
neighborhood to a site in the system has been studied and proven in other natural science
disciplines. In the context of forest gap- recovery dynamics, data from real forests reported
by several ecologists and biologists has shown a relation in which the dynamics of a non-
gaps site is influenced by the states of its neighbors; that is, if a canopy site (site occupied
by vegetation) is surrounded with a number of gap sites (sites which do not have vegeta-
tion cover), the chance for it to undergo transition and become a gap site is proportional
to the number of gaps in its neighborhood. The similar neighborhood effect can be drawn
into attention considering dynamics of fire spreading in forests. Based on this relation, the
stochastic model proposed by *Kubo et al.* (1996) (discussed in the next chapter) was based
upon it. In this section we emulate this concept by setting a theoretical analogy to study the
effect of neighborhood on a site, in this context with respect to a cold site entity, in a ther-
mally stratified lake. The relation showing the dynamics of a cold site with dependence
on states and configurations of its neighbors is the basis of the stochastic model which is
proposed in the next chapter to consider the thermal convection mechanism in a lake.

3.5.2 Setup Description

Behavior of a cold site entity subject to temperature conditions of its neighboring sites is
investigated. Five test cases were studied using 3-D numerical model (already described
in §[3.3] above). A cold site entity is composed of a square with a total of nine cells or
sites. In vertical direction it extends to include a total of five cells from water surface
downwards. This entity was then surrounded with five different temperature conditions
in its neighborhood to define the patterns of our interest. In each of the five cases a cold
site is surrounded with neighboring sites differing in states and patterns. These scenarios
are presented schematically in figure [3.21]. Case *(d)* has two identical patterns, while cases
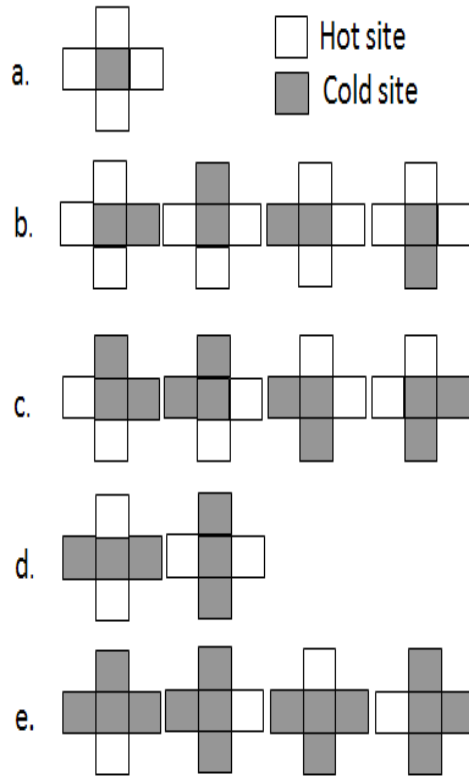
Figure 3.21: Patterns showing neighborhood conditions of the cold site

(b), *(c)* and *(e)* have four identical patterns each and therefore one representative pattern from each of these cases adequately represents the dynamics in that particular case. In both cases *(c)* and *(d)*, a cold site entity is surrounded with two hot neighboring sites, but in study of the neighborhood effect on a cold site entity, these two cases are treated differently due to their differing configuration.

Cuboid computational domain was assumed. Uniform grids were used to define Cartesian spatial dimensions. Each spatial coordinate contained a total of 40 cells. Vertical dimension had total depth of $80\,m$ and a squarely planar surface of $2Km \times 2Km$ was assumed. Total simulation time of 5,000 seconds proved to be sufficient to study the dynamics of the sinking cold water entity for all of the cases considered as it reached lowest parts of the computational domain.

3.5.3 Results

The cold water entity possessing lower temperature have higher density compared to its surrounding cells and as a result is expected to undergo a vertically downward movement. Figure [3.22] from Case A shows the side view of the simulated flow with a cold water entity sinking further and further as time progresses, while at the same time diffusing and losing heat hence becoming visibly smaller and smaller in size.

The results of the 3-D numerical model revealed that in the course of simulation the position of centroid cold sites in patterns differed from one another; ones with higher number of hot sites were generally observed to be in deeper positions as simulation progressed in comparison with the remaining patterns with less number of hot sites in their neighborhood. Figure [3.23] shows the side-view of all the five cases at simulation times $t = 1250 \, sec$ and $t = 2500 \, sec$. Result from at $t = 2500 \, sec$ shows cases *(a)* and *(b)* reveal the centroid of the cold site is further deeper compared with remaining cases, with case *(d)* close-by.

The results sums up the analogous nature to dynamics of forests, and we can conclude that a cold site will be heavily influenced by the its neighbors of opposite states and be likely to undergo sinking when it has higher number of neighboring sites of the opposite states. The cold site by undergoing downward movement it can be assumed as transiting into new state and become a hot site.

3.6 Summary

As any other other natural process found in the nature, lake cooling process and its occurrence is complex and uncertain in understanding. In this chapter we have shown that we can reproduce some of the natural features, such as variation of temperature profile as well as velocity fields occuring in a lake during thermal convection period by means of 3-D numerical model. The idealized lake of cuboidal computational domain, using mass, heat and momentum conservation laws solved numerically in Cartesian coordinates proved enough to reproduce these two features. The assumption of constant water surface cooling rate was used while the numerical solution of Navier-Stokes equation did not consider the turbulent terms.
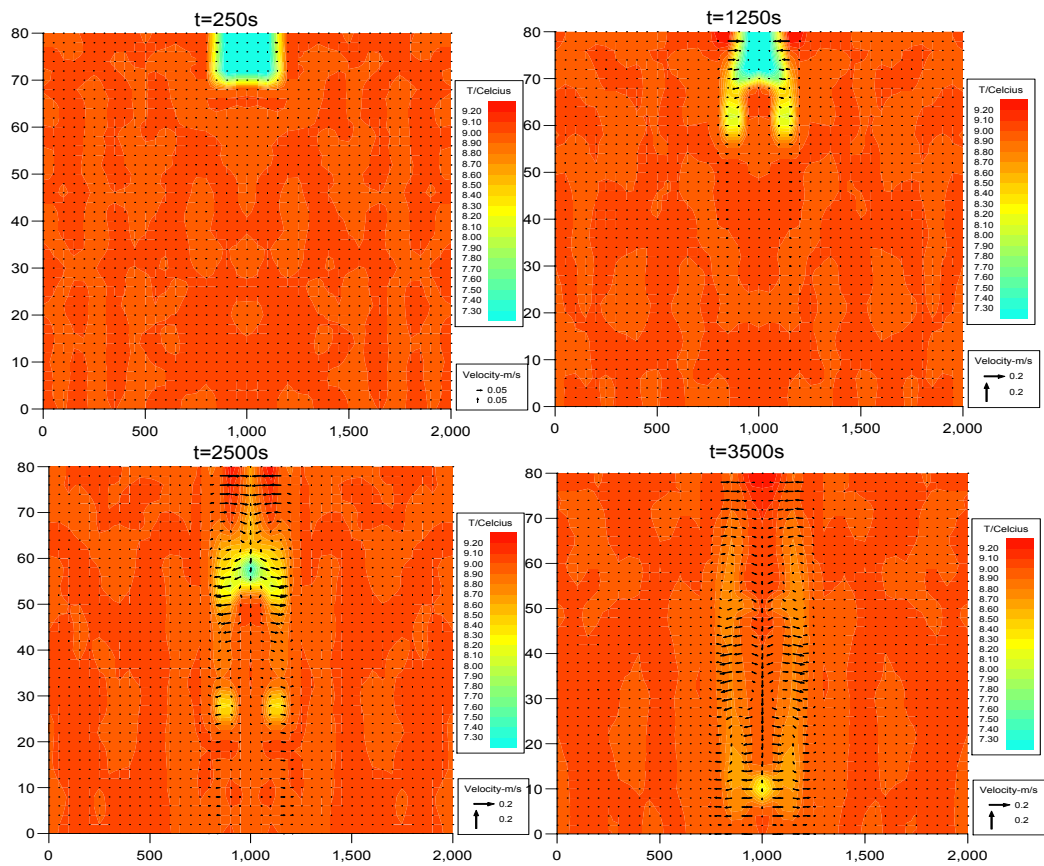
Figure 3.22: Side view showing progress of cold site from *pattern A*
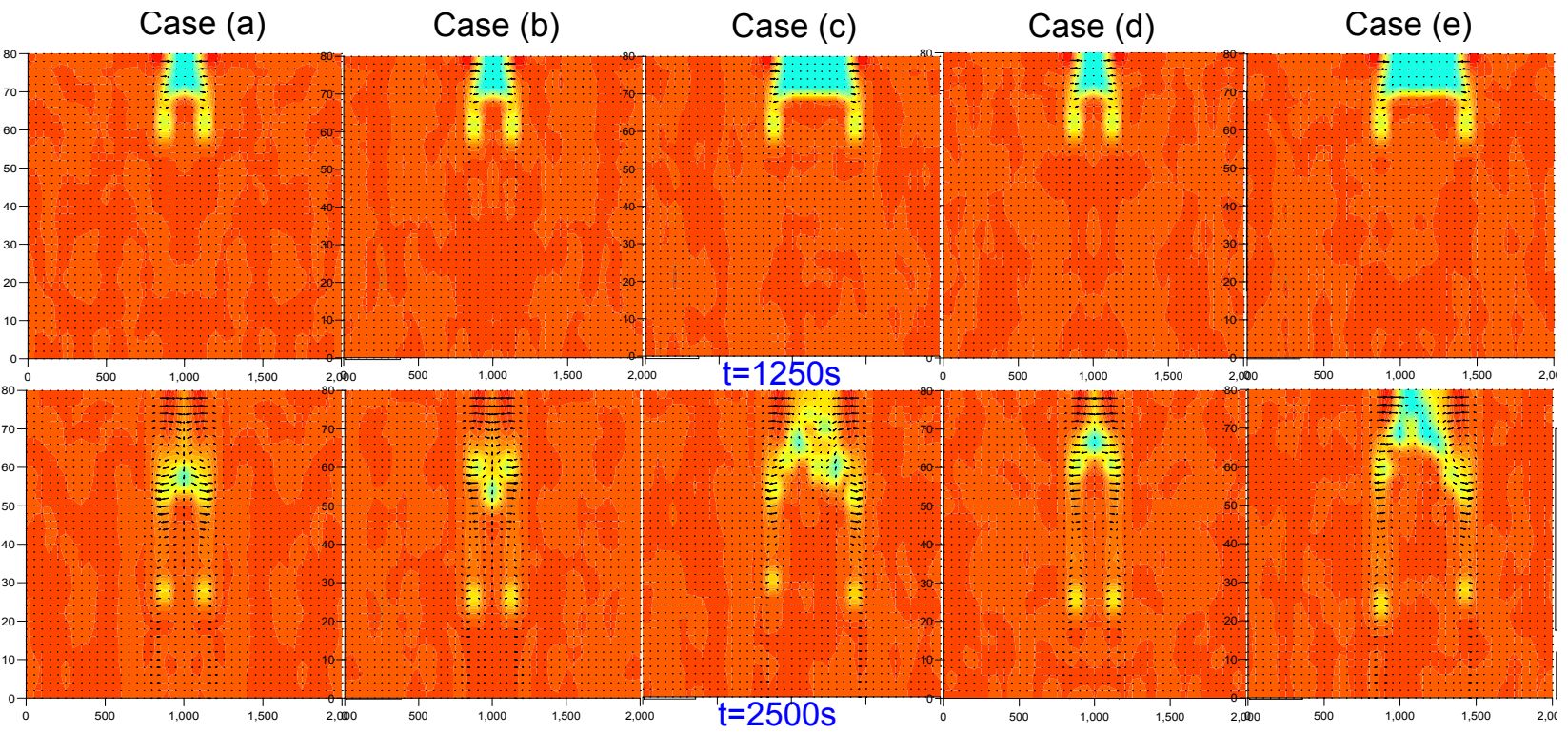
Figure 3.23: Positions of cold sites at different times and neighboring patterns. The velocity and temperature scales are not shown because of space limitations but are the same as those in figure [3.22]

After modeling of important flow features, simulations were carried-out using six (6) water surface cooling rates, Q_{00}, in order to gain understanding of the effect of magnitude of Q_{00} in the cooling process. The parameter Q_{00} may represent surface processes caused by various climatic factors. The information from these numerical experiments were crucially included for comparison with stochastic model approach (discussed in next chapter).

Statistical analysis of thermal cooling was done with a focus on cold sites as representative process through cooled bodies falling from the water surface. From the analysis, global density of cold sites grew with increase in magnitude of water surface cooling rate. Similar trend was observed with local density. Variation of averaged cluster size with water surface cooling rate did not show conclusive trend at lower discriminats while grew at small values at relatively larger discriminat values. The variation of averaged cluster size, global and local densities taken at different depths were not conclusively following any particular trend, with the difference not being significantly large. In general, global density was larger than local density meaning there was n't a strong pairing properties between cold sites.

Cluster size analysis indicated a power law relation between cluster size and its number of occurrence. Smaller values of criterion used in cells categorization allowed more cells to qualify as cold sites, hence larger number and sizes of cluster to be formed, and thus the power law property clearly observable. Power law property is an indication of scale-free property which can be an indication of presence of fractal structure. Study of fractal structure as one of the phenomenon of thermal cooling lake is open for further investigation.

IV

Considerations of Numerical Results of Thermal Convection by Means of Stochastic Model

4.1 Background

In Chapter [III], § [3.5] the influence on dynamics of a cold cell entity from its neighbors was presented. It was pointed-out that the likelihood of a cold site to undergo transition increases proportionally with the number of hot sites in its neighborhood. Various researchers in ecology reported similar property in forests regarding influence on a canopy site from its neighboring gap sites. It was observed that the chance of a canopy site to undergo transition and becoming a gap site increases with the number of gap sites in its neighborhood. Following these characteristics reported to occur in real forests various researches have been initiated to study the dynamics of forests.

Forests have been assumed to be composed of regular uniform cells in a manner similar to lattice's surface and each site assigned a cell value similar to magnetic spins in electromagnetism. With such similarity, lattice forest dynamics models with sites' interactions derived from the conceptualized framework of the Ising model (*Ising*, 1925), have been applied bearing some extension to respective forests conditions. Generally, few decades ago several researches were done in bio-ecological studies such as dynamics of colon pop-

ulations as well as forests dynamics with or without using formulation of Ising model. *Schlicht and Iwasa* (2004), *Harada and Iwasa* (1994), *Kizaki and Katori* (1999), *Katori et al.* (1998) and *Kubo et al.* (1996) are among the names of researchers who worked on the forest gap dynamics' frontiers.

The latter introduced a Markov-like stochastic model with its mean-field theory and paired approximations. A conclusive remark of the model, also collectively named as *KIF model*, after the initials of their authors, testified that the model was promising in explaining some aspects of gap-recovery dynamics, but ultimately, the model was not capable of predicting the existence of large-sized clusters of gap sites.

In this chapter, a stochastic model based on the work of *Kubo et al.* (1996) is described. The adapted model is applied in consideration of behavior of thermally stratified lake which undergoes thermal cooling. Two theoretical approximations of the stochastic model, namely the mean-field approximation and paired-approximation are discussed. A modified form of mean-field theory is suggested in consideration of results from 3-D numerical model. A computer simulation of the stochastic model was presented and the results were compared with those from the two theories. Finally the aspects of the stochastic model prediction are compared with those from 3-D numerical model in the prospect of prediction of the main characteristics of the thermally cooling lake.

4.2 Model's Overview

In the formulation of Markov chain-like stochastic model by *Kubo et al.* (1996) in prediction of dynamics of gap-recovery in forests, a forest is considered as regular lattice of particular spatial dimensions. Similar approach was also discussed in the work of *Harada and Iwasa* (1994). Forests are assumed to consist of regular sites of uniform size, in most cases preferred as squares. Two kinds of cell (or *sites* - we will use the two terms interchangeably throughout the thesis) were identified to compose the forest, namely, non-gaps (or canopy) and gaps. Canopy trees when disturbed fall down and the site become a gap site, in similar manner gap sites under favorable conditions may develop seedlings or seeds and become matured canopy in the process known as gap recovery. It was reported

by several researchers that the canopy trees suffer more disturbances when they are surrounded with more number of gap sites.i.e the likelihood of transition of canopy into gap sites is proportional to the number of surrounding gaps sites.

Gaps were assumed to be created at a constant rate, b, while the transition from nongaps to gaps were represented as $d + (\delta/z)n(0)$, where d is the death rate and the term $(\delta/z)n(0)$ is the disturbances on a canopy site caused by its neighbors. As postulated earlier this term is a function of number of gap sites surrounding a canopy site. n is the number of gap sites in the neighborhood, z is the total number of neighbors in the neighborhood and δ is a non-dimensional parameter.

4.2.1 Lake's Cooling Process as Analogous System

Based on formulation by *Kubo et al.* (1996) we develop in similar manner a stochastic model in consideration of thermal convection of a lake.

Lake's thermal convection process takes place involving real movement of its water particles. The dominant and most important positional change is a vertical movement which is driven by gravitational pull as well as temperature gradient within the water column. Temperature gradient between particles causes flux due to density difference as the heavier waters having acquired lower temperatures stabilize themselves by occupying lower vicinities while the less denser and relatively hotter particles are displaced and raise upwards. Mass conservation ensures that the waters in the lake are compensated, and hence, the lake's waters attain their energy stability through this basic properties interchange attained by real movements of water particles.

By assuming continuum fluid-flow hypothesis the water particles contained in hypothetical cells behave as the macro fluid itself. Cells are therefore assumed to possess the averaged properties of the waters they contain and while they move they interact and exchange properties with their neighboring cells. This kind of motion and exchange in the real lake, can be viewed as particles exchanges in many-body system, and hence fairly attracting interest of applicability of the laws which are suggestive to offer solution to that family of science. Thermal convection process can be viewed as a lattice model's problem

and the water's cells as sub-domains (similar to electromagnetic *spins*). Computational domain with regular uniform grids occupied by fluid can be considered as a lattice. During thermal cooling actual movement occurs in a water column. If we consider dynamics of the process in a horizontal plane, sites are changing their states in similar way as in forests.

4.2.2 Definitions, Terms and Parameters

Stochastic model which is proposed in this chapter considers a system composed of *cells*, with each cell categorized with *cell value* or *spin*. The cells are interchangeably referred to as *sites*. Only two kinds of cell values are allowed to represent the dynamics of the process.

We identify two types of cells occupying a thermally stratified lake's horizontal plane; termed as *hot* and *cold* with spins '0' and '1' respectively, as already denoted in Chapter [III] under § [3.4.2]. Hot site is assumed to be unstable with high possibility of stabilizing itself by undergoing a vertically upward positional change due to its lesser density. In contrast a cold site is postulated to be stable and more likely to undergo a vertically-downward motion as it posses higher density.

The definitions of spatial variables such as densities and clusters are similar to those defined in Chapter [III], § [3.4.2] taking the same form of denotation. Global and local densities of cold sites are denoted as ρ_0 and $q_{0/0}$ respectively, while those of hot sites are referred as ρ_+ and $q_{+/+}$ respectively. Furthermore, we present local densities of "0+" and "+0" pairs as $q_{0/+}$ and $q_{+/0}$ respectively. Sites' neighborhood definition follow Neumann's neighborhood definition already explained in previous chapter and represented in brief as per figure [3.13] in page [51].

4.3 Mean-field Theory and the Modified Form

The stochastic model predict the evolution of a system under the dynamics of the natural process, in this context, thermal cooling phenomenon. Mean-field theory is one of the theoretical approximation of the stochastic model. Equation [4.1] is the adapted generalized theoretical representation of the stochastic model after *Kubo et al.* (1996).

$$\frac{d\rho_0}{dt} = b\rho_+ - (d + \delta q_{+/0})\rho_0 \qquad (4.1)$$

The equation describe the rate of change of global density of cold sites as they are being created and destroyed from a given surface.

The first term in the RHS represents the positive transition which favors cold spins, as their number grow instantaneously from their opposite counterparts at a constant rate, *b*. The second in the RHS show the negative growth of cold sites, the transition which depends on a constant death rate, *d*, as well as influence from its neighboring sites. The weight offered by this influence is assumed to be directly proportional to the number of neighbors of opposite spins, that is, a cold site will have a higher probability of undergoing transition into a hot site if it has higher number of neighboring hot sites. It is important to be noted the 'neighbor' follows the Neumann neighborhood. The transition can be illustrated well using figure [4.1]. The basis of neighborhood influence on a cold site due to neighboring hot sites was already introduced in Chapter [III], § [3.5].

Mean-field approximation theory ignores the difference between global and local densities, and as a result the local density $q_{+/0}$ can be replaced with global density ρ_+, and thus equation [4.1] is rewritten as [4.2].

$$\frac{d\rho_0}{dt} = b\rho_+ - (d + \delta\rho_+)\rho_0 \qquad (4.2)$$

4.3.1   The Modified Form

Equation [4.1] is a simple model proposed for dynamics of a sinking (cold) sites in a cooling lake following the stochastic model. From the numerical model results it was revealed that the values of global density had a smaller spectrum of values which is much different from the characteristics shown in the original dynamics from *Kubo et al.* (1996) where the full range of between $0 - 1$ was a possibility. Naturally, extreme values of 0 and 1 are not achievable in a cooling process at any point in time. Lake evolves towards
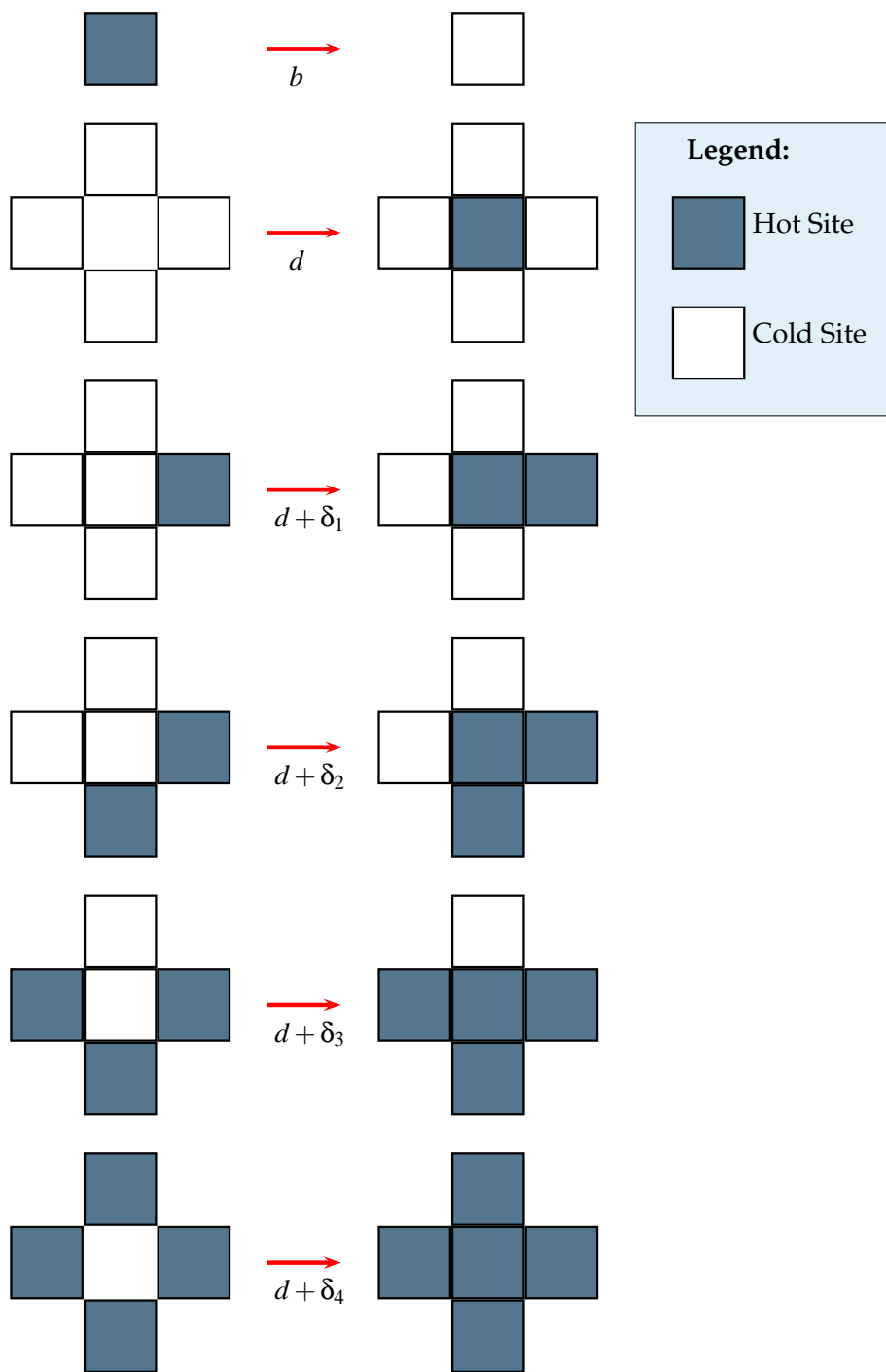
Figure 4.1: Possible transition showing influence from neighboring sites.

stability it does so with real movement of fluid particles, full one-directional *all-cell* or *no-cell* movement is surreal scenario, a violation of mass conservation.

A broader form of the model was therefore proposed, with a family of equations (eqn. 4.3) with limited coefficients to study the behavior of a cooling system, by modifying equation [4.1]. The model was formulated with eight sub-models or equations. This modified form was meant to offer flexibility in limiting the possible estimation of densities.

$$\frac{d\rho_0}{dt} = \underbrace{b(\rho_+)^n}_{Growth} - \underbrace{\frac{\{d + \delta(q_{+/0})^m\}}{(1 - \epsilon\rho_0)^p}\rho_0}_{Decay} \tag{4.3}$$

As before, mean-field approximation theory treats global and local densities as equal, and as a result, local density $q_{+/0}$ can be substituted with global density ρ_+ and this enables equation [4.3] to be rewritten as equation [4.4].

$$\frac{d\rho_0}{dt} = b(\rho_+)^n - \frac{\{d + \delta(\rho_+)^m\}}{(1 - \epsilon\rho_0)^p}\rho_0 \tag{4.4}$$

Table [4.1] show the parameters related to each of the sub-model in the family of the modified form of mean-field theory. The extra parameters in the proposed model ie. *m,n* and *p* are added to those already existed in the previous model. These parameters show the importance of growth's and decay's orders in the dynamics of the system. At $n = 1$, $m = 1$ and $p = 0$ the equation is a simple Mean-field Approximation Theory, and hence the previous model is a subset of the newer and larger family of modified mean-field approximations.

As in the previous model, the first term in the RHS represents the growth of sinking cells from non-sinking portion i.e. (ρ_+) whilst the second term shows the negative growth of cold sites from hot ones. The effect of neighborhood to towards decay transition assumes a linear dependence associated with parameter, δ.

Table 4.1: Sub-models considered in the modified mean-field theory

| Sub-model	Parameters		
ID's	m	n	p
A	1	1	1
B	1	1	0
C	1	2	0
D	1	2	1
E	2	1	0
F	2	2	0
G	2	1	1
H	2	2	1

4.3.2 Characteristics

Equilibrium global density of cold (sinking) cells predicted by the modified form of mean-field theory shows that the density decreases with the increase of δ, the parameter which represent disturbance to a cell from its neighbors in the transition from a cold to hot site. In contrast, the equilibrium density of cold sites was directly proportional to b. Both of these relations were expected as both b and δ are responsible for growth and decay of cold sites, respectively. Figure [4.2] is made from *sub-model A* and *B*, though similar trend can be confirmed in all of the remaining sub-models. From the figure, the influence of denominator part in the variation of densities and parameters b and δ can be observed. Sub-model A, for example has a denominator term in the second term of RHS (ref. eqn 4.4), contrary with *sub-model B* with none. Under identical choice of parameters, variation of ρ_0 with b show that *sub-model A* gives smaller estimation than *sub-model B*. Results from 3-D numerical model indicated the density values (both local and global) were recorded to in smaller range of 0.50 under the chosen discriminants and therefore a theoretical approximation obtained from modified form of mean-field theory shows the importance modifying the original model to fit the numerical results. The denominator term with ε is a limiting parameter for approximation of densities.

Increase in fraction of number of cold sites in a two-dimensional domain with parameter b is an indication that the model could be comparable with numerical results from fluid's conservation laws. In general, fraction of sinking cells in numerical results, shown
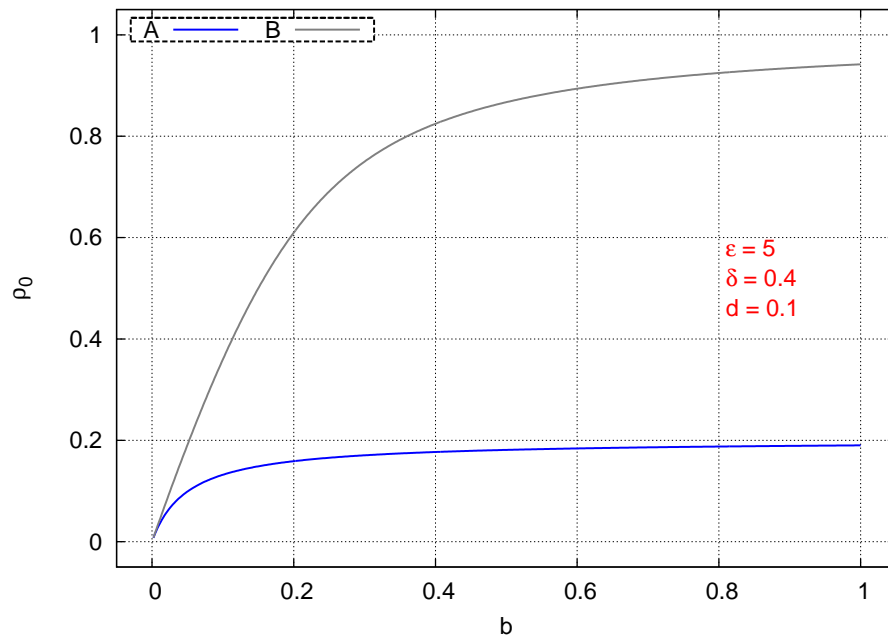
(a)
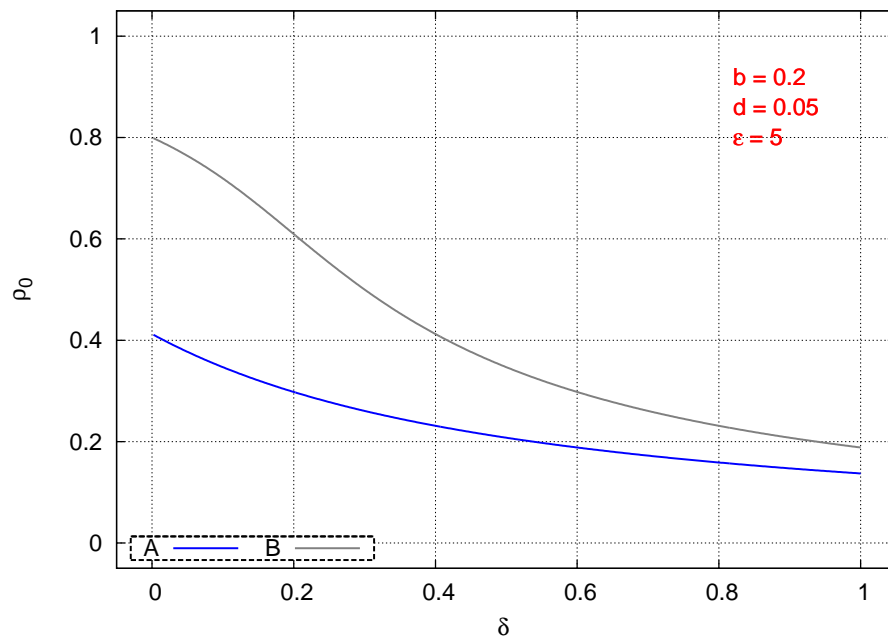
(b)

Figure 4.2: Equilibrium density variation by modified mean-field approximation. Introduction of factors reduces the estimated densities as demonstrated by *Case A*.

to grow as the value of Q_{00} were increased. The main aspect of correspondence is between parameter b from Stochastic model with water surface cooling rate, Q_{00} from 3-D numerical model.

Modified mean-field approximation prediction of equilibrium spatial densities suggests existence of asymptotes. Considering equation [4.5] below, equilibrium density of ρ_0 are computed as its rate of change ceases to exist, ie.

$$\frac{d\rho_0}{dt} = 0$$

$$\frac{d\rho_0}{dt} = b(1-\rho_0)^n + \frac{\{d+\delta(1-\rho_0)^m\}}{(1-\varepsilon\rho_0)^p}\rho_0 \qquad (4.5)$$

With rates substitution at steady state, equation [4.5] then simplifies into [4.6]

$$\frac{1}{b} = -\frac{(1-\rho_0)^n(1-\varepsilon\rho_0)^p}{\{d+\delta(1-\rho_0)^m\}\rho_0} \qquad (4.6)$$

As the value of b grow infinitively large, its reciprocal tend to zero.ie.

$$\lim_{b\to\infty} \frac{1}{b} = 0$$

As a result, equation [4.6] simplifies into equation [4.7].

$$0 = -\frac{(1-\rho_0)^n(1-\varepsilon\rho_0)^p}{\{d+\delta(1-\rho_0)^m\}\rho_0} \qquad (4.7)$$

The resulting relation can only be true if the term in the numerator in RHS is zero:

$$0 = -(1-\rho_0)^n(1-\varepsilon\rho_0)^p \qquad (4.8)$$

In our consideration, the value ρ_0 is in the range between 0 and 1, hence, the term $(1-\rho_0)^n$ is non-zero, this leaves the possibility of having zero on the term $-(1-\varepsilon\rho_0)^p$.ie.

$$0 = -(1-\varepsilon\rho_0)^p \qquad (4.9)$$

Equation [4.9] simplifies further into :

$$\rho_0 = 1/\varepsilon \qquad (4.10)$$

Equation [4.10] show the dependence of the equilibrium asymptotic values of the global densities of hot sites (or ρ_0^∞) in variation with parameter ε as the value of parameter b is infinitively large.

From the equation the following instances can be deduced easily :

if $\varepsilon = 1.25$, $\rho_0^\infty = 0.80$

if $\varepsilon = 2.50$, $\rho_0^\infty = 0.40$

if $\varepsilon = 4.00$, $\rho_0^\infty = 0.25$

etc.,

The above theoretical consideration can be supported from numerical solution of some of model combinations from modified mean-field theory's family. Shown in the figure [4.3] below is the numerical results from *sub-model A*, whereby the x - axis is in logarithmic scale. The asymptotic values for the above given examples are clearly observable when the value of parameter b becomes infinitively large. The results from 3-D numerical model of variation of global density of cold sites, ρ_0 with water surface cooling rate, Q_{00}, the rate of change decreases with increase in Q_{00} indicating possibility of asymptotic values of ρ_0 at infinitively large values of Q_{00}.

4.4 Computer Simulator

Based on abstract of dynamics explained by equation [4.1], a simple computer model based on random number generator was proposed to consider the equilibrium dynamics of the process.
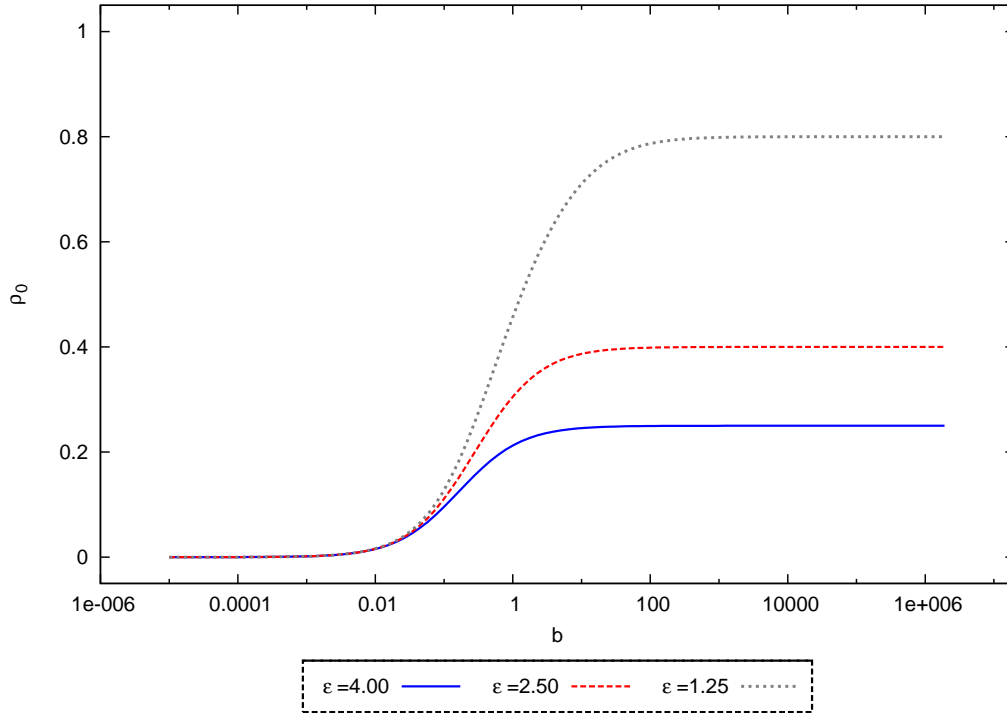
Figure 4.3: Asymptotes of ρ_0 as a function of ε (Sub-model A)

A two-dimensional surface with 51 x 51 quadrats is used to define the cooling surface, whereby the transition between the two states occur randomly after several probabilistic sampling. Dimensioning of such quadrats is meaningless and inapplicable in this context. The use of probabilistic sampling based on random number generator is the basis of Monte Carlo Experiments; therefore, this method can be viewed as the Monte Carlo Model for this purpose. The equilibrium surface's properties such as global densities as well as local densities can then be computed and compared with the equilibrium values predicted by theoretical equilibrium equations. All comparisons between theoretical models' and computer simulator's results are essentially done after some of the corresponding parameters are fixed in order to allow other important properties to be studied with ease.

The neighborhood definition between sites follows Neumman neighborhood definition. In the definition the neighbor of a site only counts when it is sharing a boundary and adjacently positioned; that means diagonally-placed sites and other sites beyond the vicinities are not considered as neighbors. Based on this neighborhood definition, cluster size of either spin is counted not beyond neighborhood.

4.4.1 Simulator Setup

The simulator assumes the process takes place in a plane, and therefore a two-dimensional computational domain is sufficient. A rectangular shaped domain with 51 x 51 cells is adopted. The sites' neighborhood follows Neumann neighborhood definition. In order to ensure stability of the simulation, periodicity is introduced for the corner sites along the boundaries. The random number generated is compared with the transition in every experimental count with either of the transition being a function of this comparison and current state (or spin) of a particular site in question. A 1000 experimental count has proved to be sufficient for process' dynamics to equilibrate. However other criteria such as introducing an allowable error in value of densities could also be used. In this criterion, the process is assumed to be in equilibrium when the changes in densities are smaller than a chosen before-hand value of allowable error.

4.4.2 Verification

The usefulness of the simulator needs to be predetermined from proven results in order to be of any merit to our proposed extended theory. Before proceeding into further use of the simulator, it is subjected to some results from *Kubo et al.* (1996) as part of efficacy-testing. Simulator was set to simulate forest dynamics described by *Kubo et al.* (1996) and his research associates, whereby the general dynamics of the stochastic model were summarized by equation [4.11] below,

$$\frac{d\rho_0}{dt} = -b\rho_0 + (d + \delta q_{0/+})\rho_+ \tag{4.11}$$

whereby, *in this context*:

ρ_0, ρ_+ are the global density of gaps and canopies sites respectively,

b, d are the birth and decay rates of canopies and gaps sites respectively,

δ is the parameter associated with contribution of neighboring sites in canopies' transition and

$q_{0/+}$ is the local density of the gap-canopy pairing

Mean-field assumes that local and global densities for both kinds of spins are the same, while the paired approximation assumes that the two kinds of densities are different. The equilibrium values of these densities i.e. $\rho_0^M (= q_{0/0}^M)$, ρ_0^P and $q_{0/0}^P$ can be found by setting the rate of change of the particular quantity to zero. The superscription C, M and P denote for Computer Simulator, Mean-field and Paired Approximation approaches, respectively.

The top sub-figure in figure [4.4] shows the results from *Kubo et al.* (1996, §4.2, figure 2(b)). The results from their computer simulator are shown symbolically with *circles*, *squares* and *triangles*. *Solid* and *empty circles* were used to represent ρ_0^c and ρ_+^c respectively, while *triangles* and *squares* represent $q_{0/0}^c$ and $q_{+/+}^c$ respectively.

The results are matched well with those from our computer simulator (bottom sub-figure in figure [4.4]) , whereby ρ_0^c and ρ_+^c are represented by *red* and *blue solid circles*, while $q_{0/0}$ and $q_{+/+}$ are denoted using *triangles* and *squares*, respectively.

Individual global and local densities from our results are shown more clearly in figures [4.5] and [4.6]. The results from paired approximations were closer to those from computer simulator in variation of both, local and global densities with parameter δ. Prediction of ρ_0 from mean-field approximation overshoot the estimates from the other two approaches, while its ρ_+ undershoots the estimates from other two approaches. Mean-field prediction underestimated the values of $q_{+/+}$ compared to other two approaches, while also underestimating the values of $q_{0/0}$, especially at smaller values of δ. All these trends are clearly shown in the results by *Kubo et al.* (1996), and hence the trends verify the accuracy and practicality of our computer simulator.

4.4.3   Comparison - Modified Mean-field Theory (MMFT)

Eight cases were identified in the proposed extension of Mean-field prediction (ref. Table 4.1). Computer simulator is set to follow these eight cases' dynamics. To have a common reference ground, some of the parameters are fixed while other variables are allowed to vary. For the purpose of this research we fix parameters as shown in table [4.2]. Variable ρ_0 is allowed to vary with changes in the value of parameter *b*.
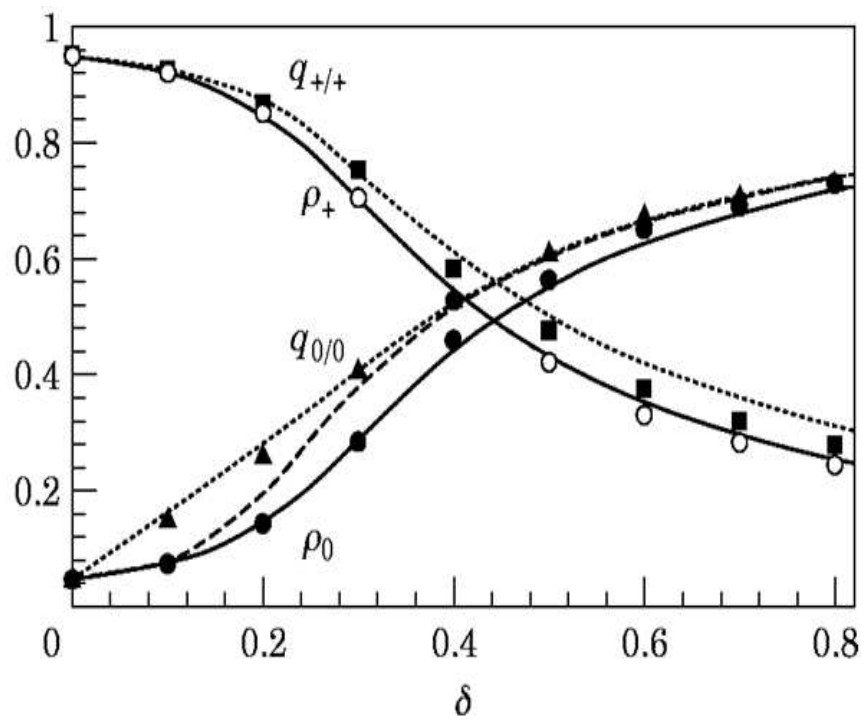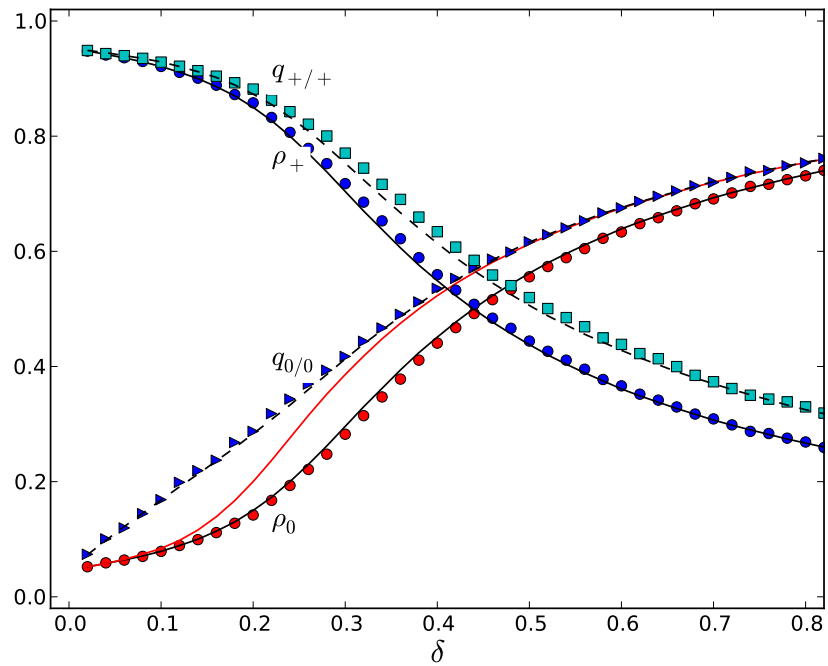
(a) After

Figure 4.4: Verification of Computer Simulator [$b = 0.2$, $d = 0.01$]. The top and bottom figures are results from *Kubo et al.* (1996) and Computer Simulator, respectively.
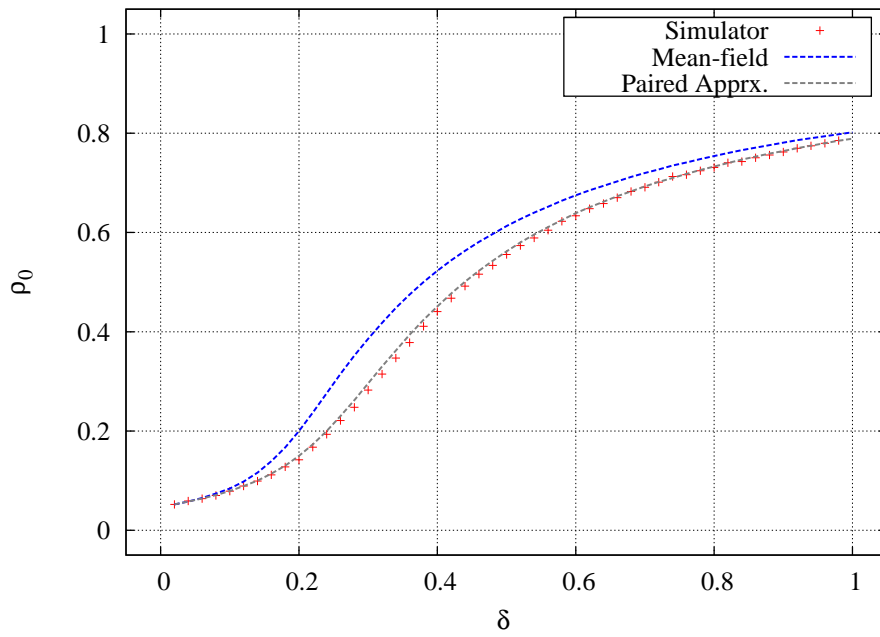
(a) ρ_0 equilibrium values
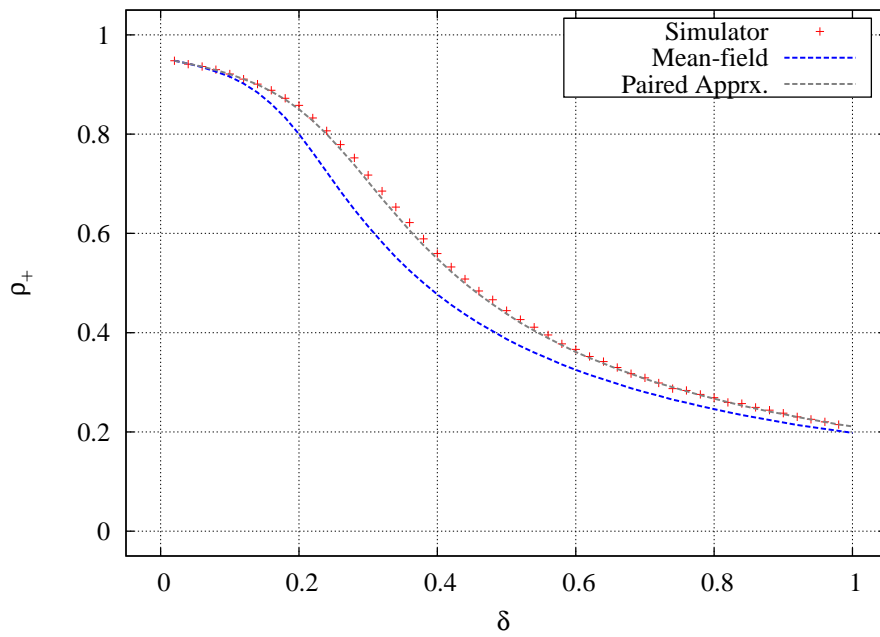
(b) ρ_+ equilibrium values

Figure 4.5: Variation of global densities [$b = 0.2$, $d = 0.01$]
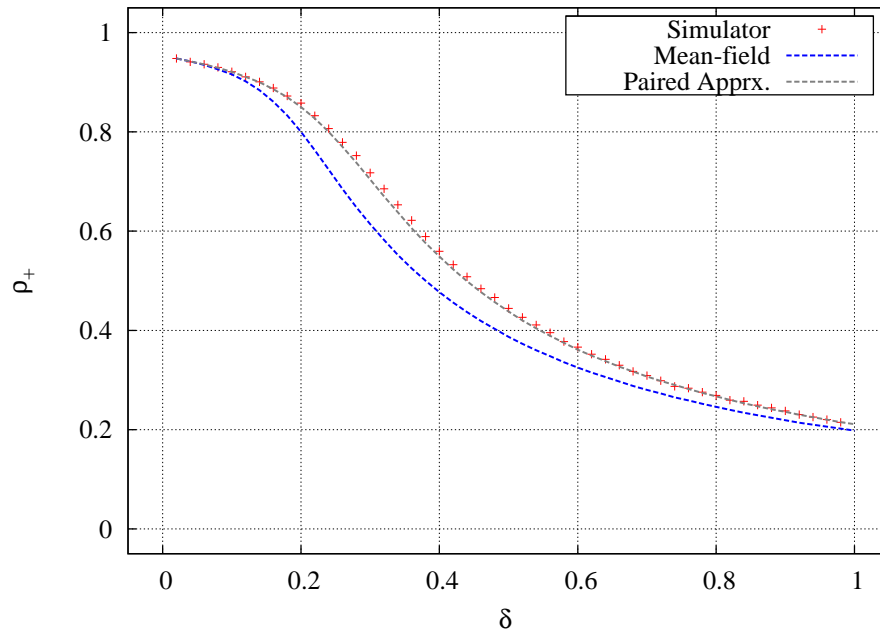
(a) $q_{0/0}$ equilibrium values
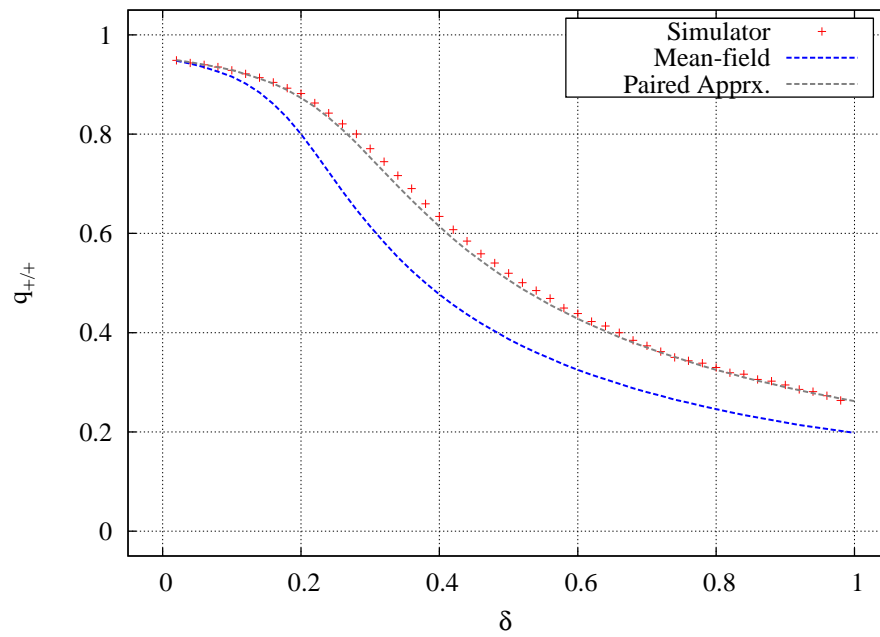
(b) $q_{+/+}$ equilibrium values

Figure 4.6: Variation of local densities [$b = 0.2$, $d = 0.01$]
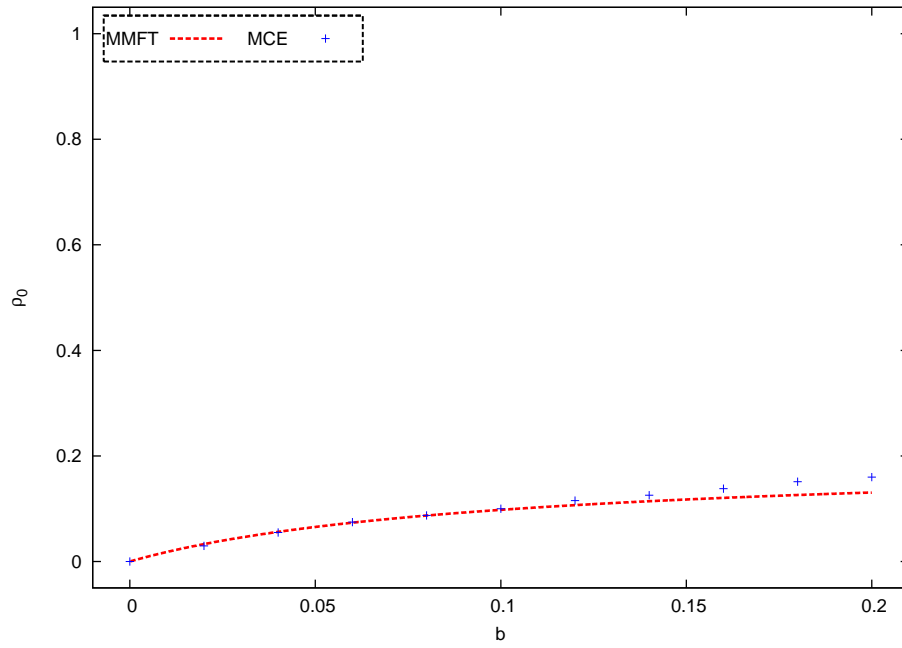
(a) Case **A**
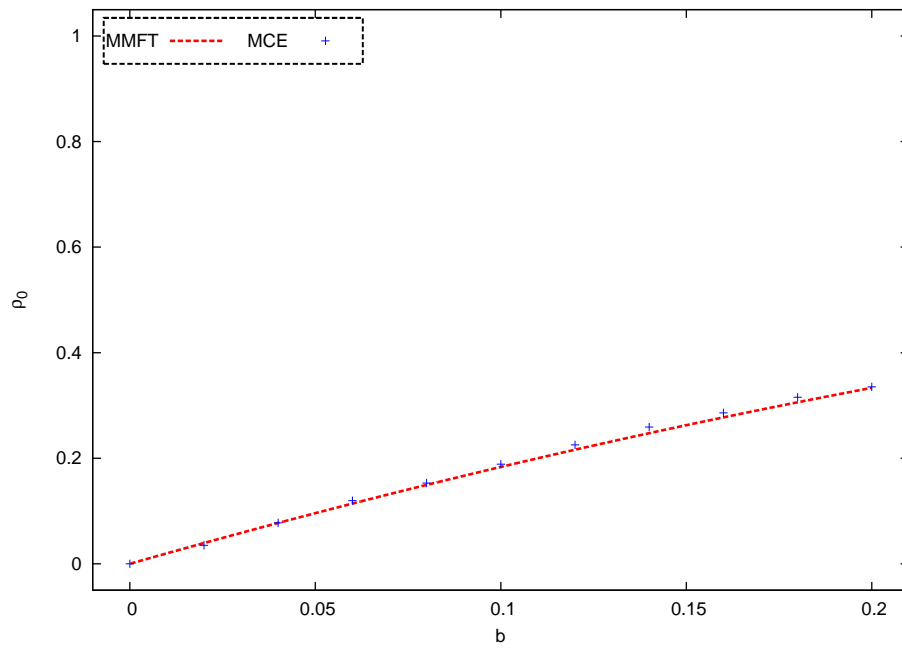
(b) Case **B**

Figure 4.7: Cases A and B : variation of ρ_0 with b from MMFT and MCE
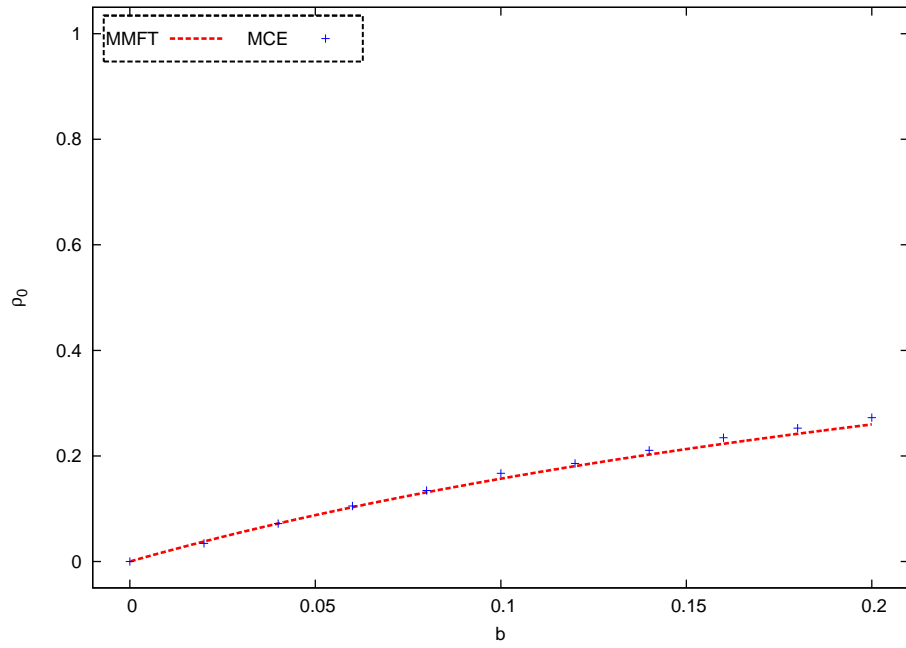
(a) Case **C**
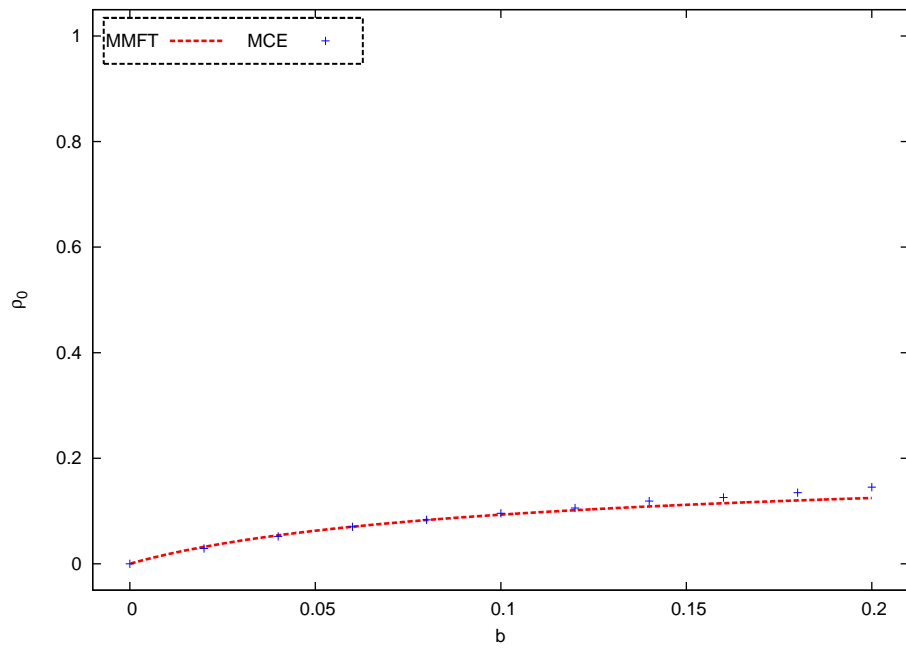
(b) Case **D**

Figure 4.8: Cases C and D : variation of ρ_0 with b from MMFT and MCE
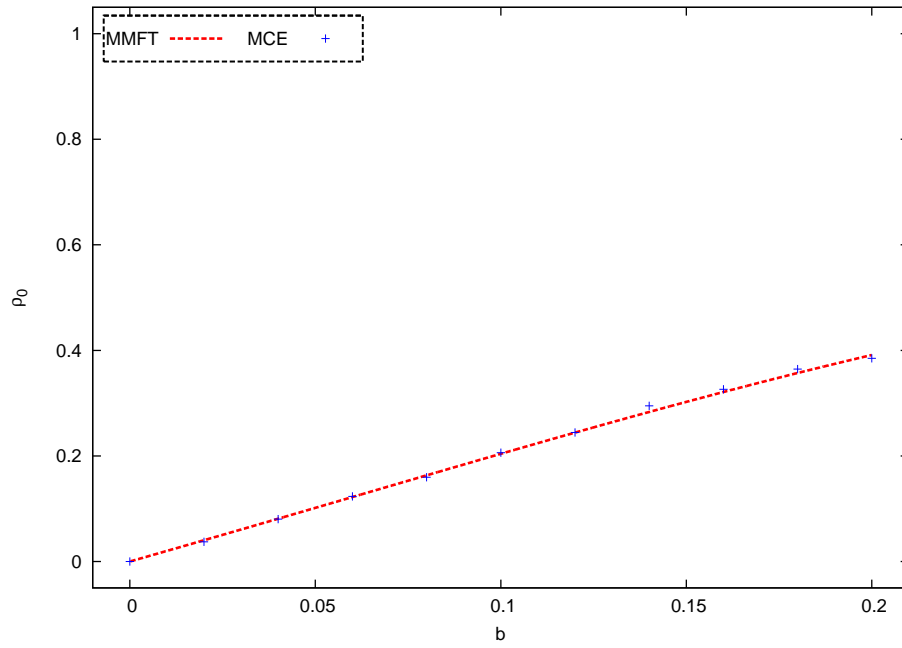
(a) Case **E**
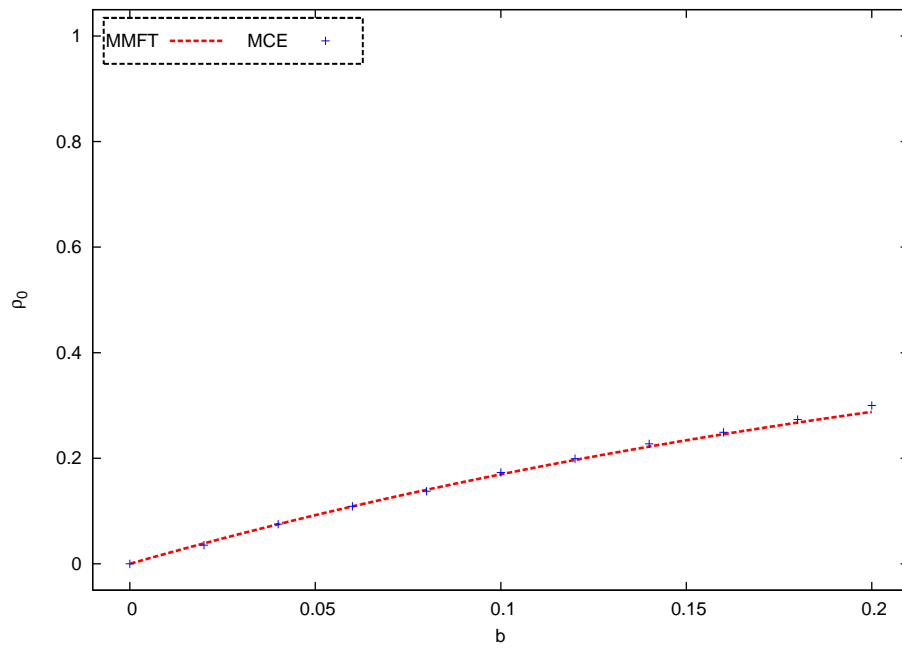
(b) Case **F**

Figure 4.9: Cases E and F : variation of ρ_0 with b from MMFT and MCE
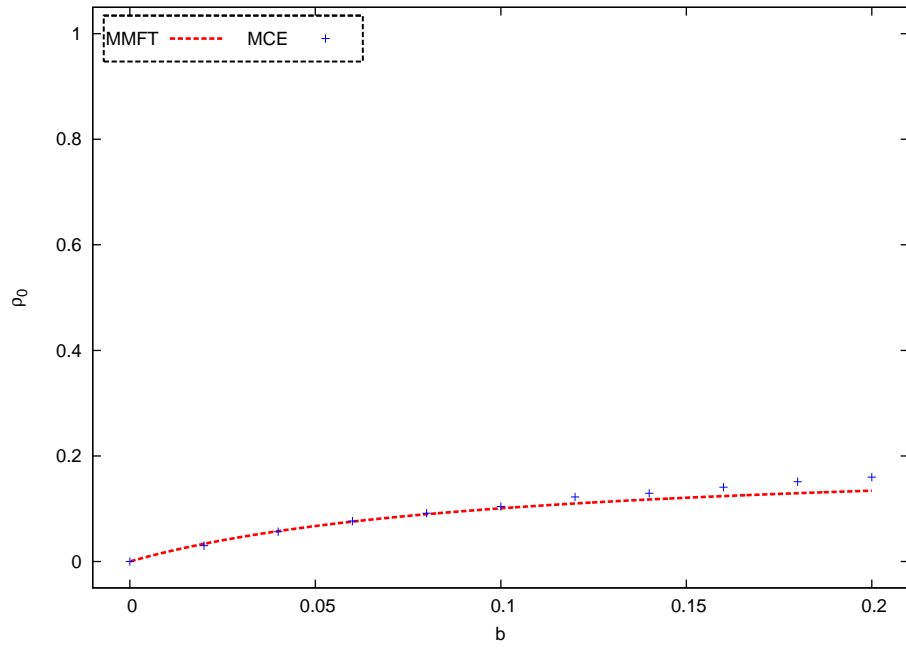
(a) Case **G**
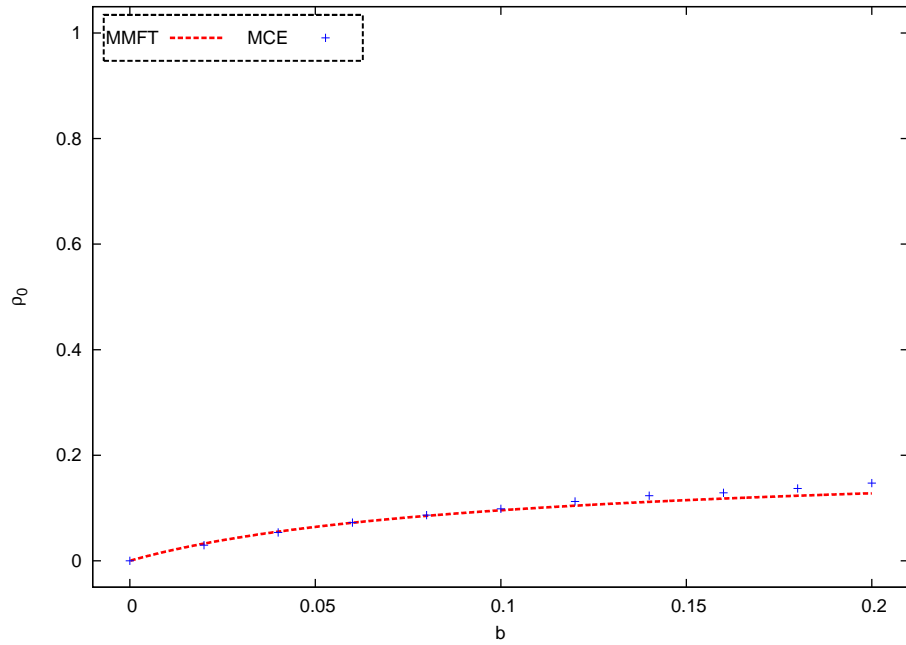
(b) Case **H**

Figure 4.10: Cases G and H : variation of ρ_0 with b from MMFT and MCE

Table 4.2: Parameters used in modified mean-field theory

Parameter	Value
d	0.2
δ	0.3
ε	5

Results from figures [4.7] to [4.10] summarizes the Monte Carlo experimental results to the results from modified mean-field theory. Abbreviation *MCE* used in the figures stands for Monte-Carlo Experiments. The estimates from the simulator are satisfactorily close to those obtained from the theoretical approach. The closeness of the two results are confirming that the computer simulator could also be useful in prediction of spatial patterns of sites at equilibrium; the information which can not be retrieved from a mere theoretical equations, which are only capable of prediction of global densities.

4.4.4 Comparison - Paired Approximation

Both, Paired Approximation and Mean-field Theory, are useful into spatial densities' prediction of spins which describe a natural process, in this particular context, a lake's thermal cooling mechanism. Unlike mean-field approximation theory, it assumes that the global density of the sites of a particular spin differs with its local density, which ultimately, depends on the states of its neighbors. That is:

$$\rho_0 \neq q_{0/0} \tag{4.12}$$

and,

$$\rho_+ \neq q_{+/+} \tag{4.13}$$

After equation [4.3], a case (sub-model B) is chosen whereby $p = 0$ while m and n values are kept at 1. With substation of these coefficients, [4.14] is the resulting equation.

$$\frac{d\rho_0}{dt} = b\rho_+ - (d + \delta q_{+/0})\rho_0 \tag{4.14}$$

Derivation of equilibrium equations for paired approximation theory considers the doublet density termed as the probability of any particular pair of two cold sites,i.e. '00' pair to undergo transition into a hot site. This quantity is related with $q_{0/0}$ and ρ_0 by equation [4.15].

$$q_{0/0} = \frac{\rho_{00}}{\rho_0} \tag{4.15}$$

Simple time differentiation of equation [4.15] yield a new relation, equation [4.16].

$$\frac{q_{0/0}}{dt} = -\frac{q_{0/0}}{\rho_0}\frac{d\rho_0}{dt} + \frac{1}{\rho_0}\frac{d\rho_{00}}{dt} \tag{4.16}$$

Equilibrium conditions can be applied to equation [4.14]; the resulting expression relating ρ_0 and $q_{0/0}$, in combination of equation [4.16] above and the expression portraying dynamics of ρ_{00} are necessary to obtain equilibrium values of $q_{0/0}$.

4.4.4.1 Global density variation, ρ_0

Parameter b is responsible growth of cold sites as it favors transition of non-sinking (hot) sites into sinking (cold) sites. As expected, figure [4.11(a)] reveals that increase of value of b is directly proportional to increment of equilibrium values of ρ_0. The resulting trend which shows that parameter b encourages the growth of sinking sites, is the basis of the hypothetical correspondence between b and coefficient of water surface cooling rate, Q_{00}, in 3-D numerical model.

In contrast, parameter δ increases with the decrease in ρ_0, as revealed by figure [4.11(b)].

4.4.4.2 Local density variation, $q_{0/0}$

The variation of the local density shows similarity with the trend evinced by the global density counterparts. Figure [4.12] shows the variation of $q_{0/0}$ with both δ and b whereby decay was supported with increased value of δ whilst growth was in line with increase in value of b.
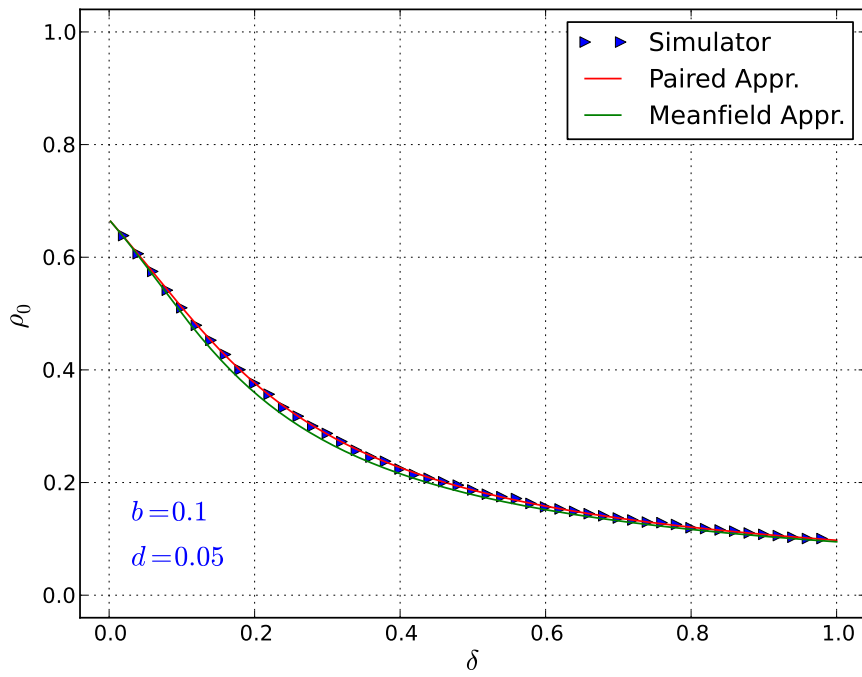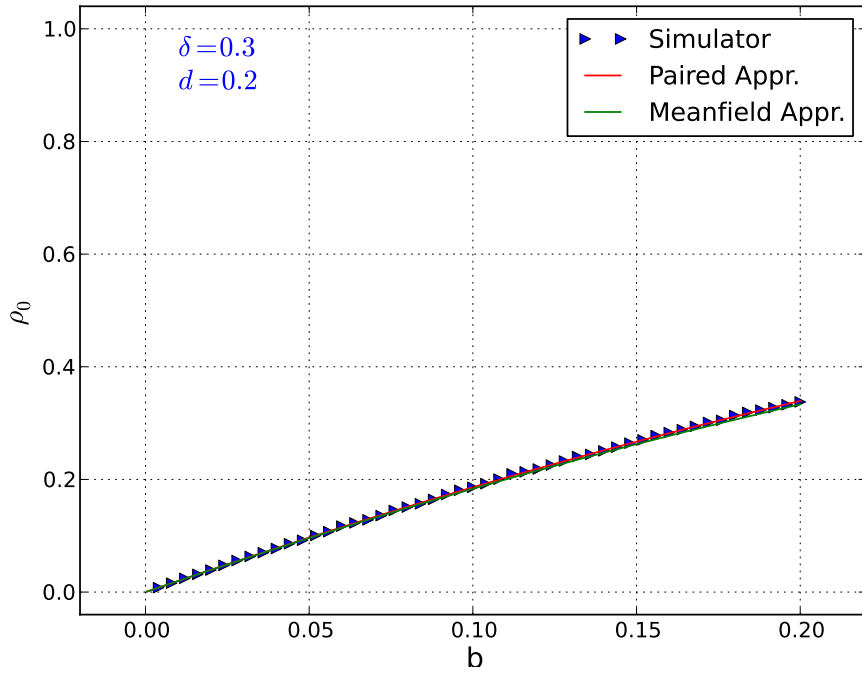
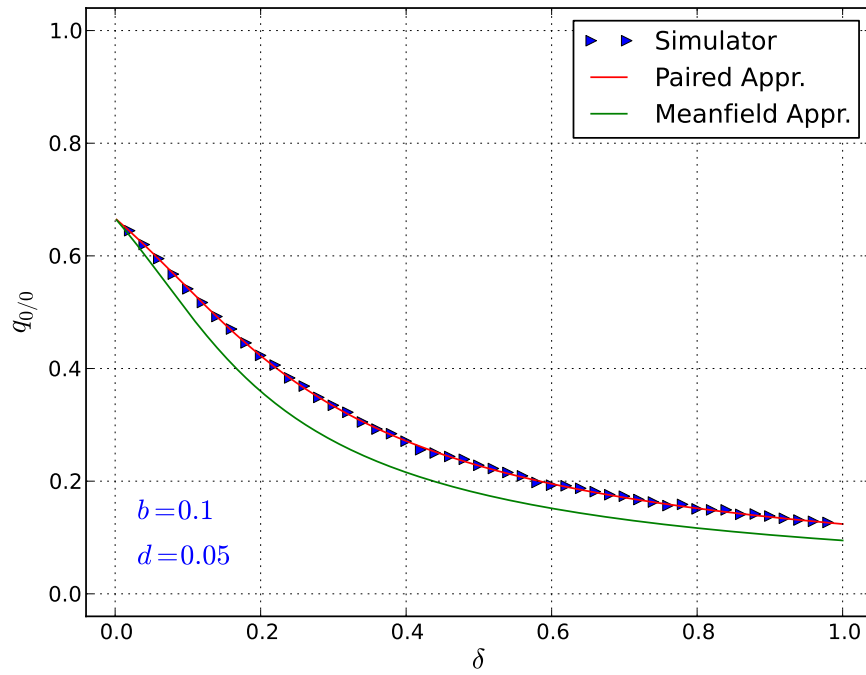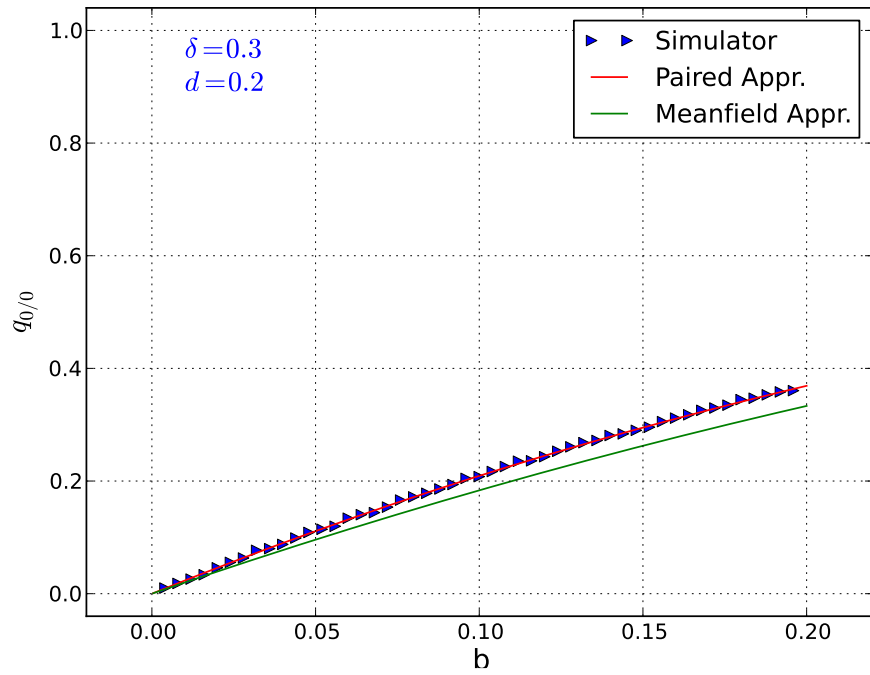Figure 4.11: Computer Simulation compared to Paired Approximation: ρ_0

Figure 4.12: Computer Simulation compared to Paired Approximation: $q_{0/0}$

Table 4.3: Power law regression of cluster sizes from Stochastic Model

Case IDs	Regression coefficients	
	β	R^2
A	1.36	0.966
B	0.90	0.925
C	1.51	0.997
D	1.71	0.998
E	0.65	0.751
F	1.35	0.964
G	1.02	0.966
H	1.59	0.997

4.5 Clusters Analysis

One of the use of Monte Carlo Simulations is to enable scientists to study some aspects of the theoretical models which might not be possible under normal circumstances with use of other scientific methods; that is, theoretical and experimental methods. Intractability of the theoretical models, thus, can be eased in given particular conditions whereby Monte Carlo simulations are applicable and attractive.

In context of our model, we now get a window of opportunity to analyze cluster size distribution of sinking cold cells from our computer simulator, the information which might not be available from theoretical equations per se. After acceptable degree of agreement between some of the quantities tested from theoretical model and its Monte Carlo formulation, it is compelling to rely on the cluster sizes information obtained from Monte Carlo experiments.

Clusters of cold sites formed after conducting Monte Carlo Experiments of the stochastic model are analyzed. For the purpose of this thesis we chose instances based on the previous section by fixing parameters as shown in table [4.2]. Furthermore, parameter *b* is fixed as 0.3, which allows the simulator to simulate a process under these conditions and give equilibrium surfaces for each case in the family of the proposed extension.

Figure [4.13] shows cluster size distribution, from two selected cases, cases D and H. In general, the number of occurrence of small-sized clusters is larger than larger-sized ones. In the figures, a power law regression curve is displayed in red color, alongside with
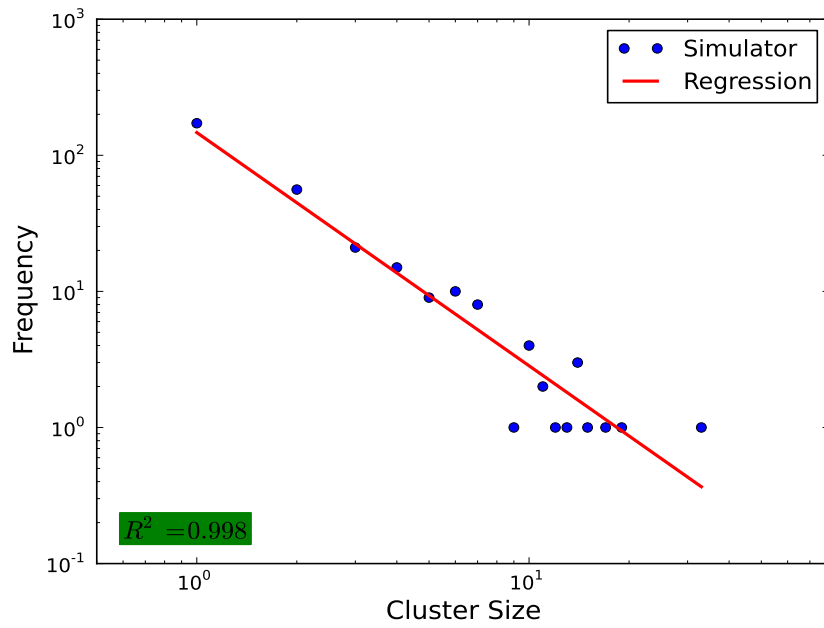
(a) Case D
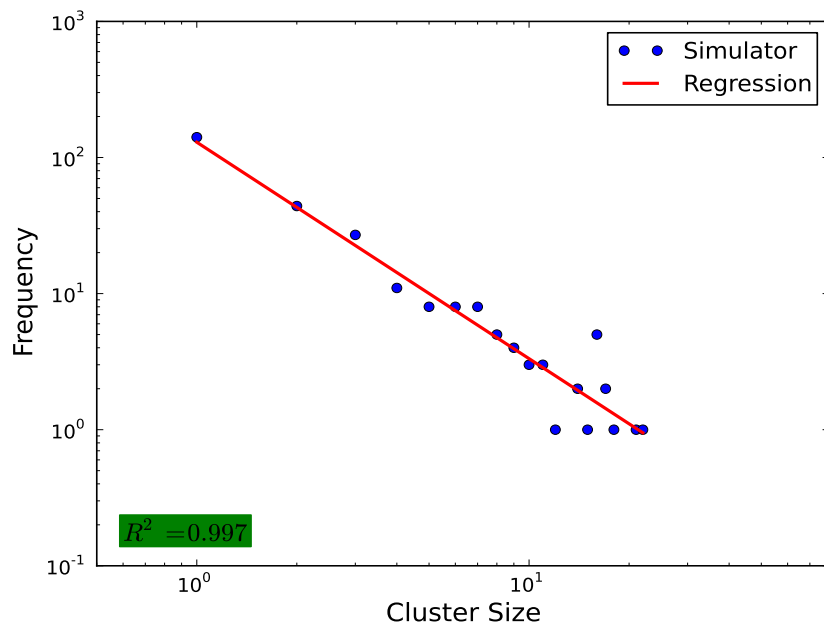
(b) Case H

Figure 4.13: Relation of cluster sizes and frequencies from Stochastic Model's results plotted in log-log. Power law property is observable for these two variables.

results from the simulator, marked as solid blue circles. The regression line is obtained after minimization of *Chi-squared distribution*. In general, by establishing a power regression line, data from all cases responded well with high value of *coefficient of determination*, R^2. The best value being around 0.998 and the lowest being 0.751.

The power indices obtained from power law regression ranges from 0.65 to 1.71. This range corresponds to a range observed in spatial analysis of numerical results. The rest of the results are summarized in table [4.3].

The results and a good regression fit indicate that cluster sizes are *scale-independent* from their number of occurrences.The *scale-free* property was also observed in the spatial analysis of numerical results. The similarity of the shared behavior between the two modelling approaches is interesting and suggests the stochastic model could explain some of the features predicted by the numerical model.

4.6 Similarities between Stochastic and 3-D Numerical Models

Numerical solution of Navier-Stokes equations simulating lake's flow under condition of thermal convection was introduced in §[3.3]. This model was used in study of cold cells dynamics under different temperature conditions of its neighbors in understanding the influence of disturbance caused by neighboring sites. Five patterns were identified as explained in §[3.5]. The results showed the importance of number of hot sites in influencing the dynamics of a cold site. The dependence between the dynamics of the cold sites and number of neighboring hot sites is evident as it was shown that the cold site seemed to move deeper in the patterns where the number of neighboring hot sites is relatively large. This result enabled us to make use of a stochastic model discussed in Chapter [IV] in consideration of the thermal convection in a thermally stratified lake. The dynamics of stochastic model by *Kubo et al.* (1996) in forests dynamics, assumed that the rate of transition of non-gaps sites into gaps is dependent on the number of neighboring gap sites. With the simulated results of dynamics of cold site under different neighborhood configurations, similar conditions were noted and hence the use of the stochastic model is quiet

similar in the those dynamics from gap-recovery in forests.

Spatial analysis of 3-D model results under various conditions of Ω showed that ρ_0 and $q_{0/0}$ increases as the value of Q_{00} increases. Similar observation was observed from stochastic model whereby the densities were varied with parameter b. The growth curve of densities from the 3-D showed consistent decrease in growth of density as the value of Q_{00} was increased, suggesting that at larger value of Q_{00} the densities are at asymptotic limit. This property could be shown mathematically from the stochastic model (§[4.3] part [4.3.2]).

Analysis of clusters of cold sites from both models showed that there is a power law relation between clusters sizes and their respective number of occurrences. Power law relation shows the scale-free property of the process.

In general, the two models can be said that they are corresponding to each other as showed by the statistical behavior of the cold sites, which are important elements in representing thermal cooling process.

4.7 Summary

In this chapter a stochastic model was proposed to consider thermal convection process in a lake. Due to lack of required observation data from lake, the aspects of the model were tested against the results from the 3-D numerical results explained in chapter [III]. The inception of this stochastic model in consideration of lake's flow during thermal convection was motivated from formulation by (*Kubo et al.*, 1996) in modelling of forest gap-recovery. Lake's flow was analyzed based on horizontal planes. Only two kinds of spins were allowed in a plane in similar way as forests gap-canopy dynamics.

The stochastic model was further extended to include shape factors in order to resemble some results from numerical model. Mean-field theory approximation of the stochastic model was introduced. Mean-field approximation was used to predict equilibrium densities of the sinking portion of the computational domain which is considered to be occupied by relatively colder cells. These colder cells have a higher density and therefore more chance to move vertically downwards. Two types of the densities were identified to

describe the process, the local density which is computed in consideration of the condition of the states found in the neighborhood and global density, computed as the arithmetic mean of the cold sites found in the computational plane. The equilibrium densities increased with the increase with parameter, b, which is the instantaneous birth rate of cold sites. Conversely, the equilibrium densities decreased with the increase with parameter δ, the decay rate of cold sites.

The computer simulator was introduced to based on the theoretical formulations. The resulting density variation with growth and decay rates matched well from results obtained from theoretical approximations. Cluster sizes from the simulator were analyzed and the power law regression fitted well the distribution of clusters with their respective number of occurrences; with values of coefficient of determination (R^2)with 0.75 being the worst estimate.

The stochastic model showed the prowess to predict some aspects also observed from the numerical model in numerical experiments of lake's flow during thermal convection. Some of the aspects include variation of parameter b, the growth rate of cold sites with densities of cold sites; which resembles the relation between water surface cooling rate and densities of cold sites from numerical model's results. Also the possibility of asymptotic variation of global density with b and Q_{00} was revealed. The cluster size analysis revealed power law relation between cluster sizes of cold sizes with their respective number of occurences.

Conclusively, the stochastic model showed some potential in explaining typical results thermal convection by means of numerical model. Movement and resulting statistical information embedded in clusters of cold sites were linked with thermal convection process. The model though, could be refined to consider 3-D movement of cold sites; while also introduction of the third spin-type could explain more the cell types which lack strong character of neither cold (undergoing downward movement) nor hot(undergoing upwards movement) sites.

V

Density Currents Induced by Thermal Convection over Slope

5.1 Background

In this chapter, investigation of lake's flow due to thermal convection during cooling period was done focusing on shore part of the lake. In general, flow characteristics around the shores is expected to be influenced by geometry and other factors around the shores. Figure [5.1] is a sketch showing the shore part of the lake, littoral zone of a typical lake, the part which is the focus area of numerical simulations described in this chapter. The flow investigation is based entirely on geometrical influence alone, without considering other physical, chemical or biological factors around the area. Influence on a flow at these areas could explain distribution of water properties, some of which such as temperature and dissolved oxygen can be observed from regular lake's water quality monitoring. Snapshot dissolved oxygen and temperature records from Lake Biwa taken near the lake's bed will be used in comparing the flow phenomenon which closely could be the source of similar observations.

Flow simulations are conducted based on the 3-D numerical model already described in chapter [III]. In this 3-D model, Navier-Stokes equations are solved numerically without considering the turbulent terms. This formulation is capable of simulating to some extent
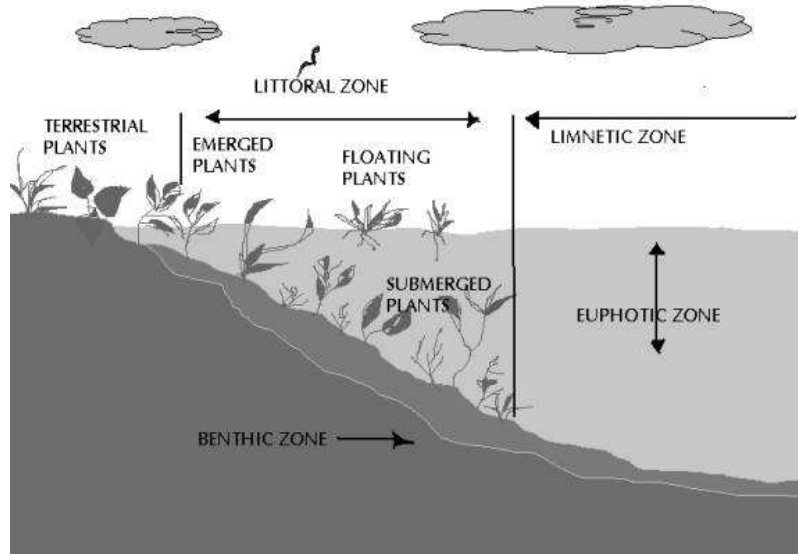
Figure 5.1: Sketch showing coastal or shore region of a lake. (Source: http://gowanusseedsproject.wordpress.com/)

the turbulent flows as partial *direct numerical simulation* (DNS) although the computational mesh is infinitively large compared to the typical turbulent scales in turbulent flows. To fit-out the physical nature of the flow near lake's shores, the computational domain is modified to include a slanting edge as one of the vertical side-walls to reflect a slope on lake's shore.

5.2 Model's Application

The 3-D numerical simulations use the numerical model already described in chapter [III] with the changed geometry of the computational domain. All other computational conditions and assumptions regarding simulations are kept unchanged. Conditions of variables arrangement, numerical scheme, time-integration method, solution's algorithm for coupled velocity and pressure fields and conservations equations are all unchanged.

Following the geometrical shape of the lake around shores, an idealized computation domain assumes shape of a 'Right Trapezoidal Prism'. To replicate the thermal layers in the water column at the onset of cooling period, uniform temperature is assigned as shown in figure [5.2]. The figure shows the plan and side-views of the computational domain as well as the initial temperature conditions. L assumes values of 1 Km and 4 Km, making

two corresponding simulation cases with slopes 8 % and 2 %, respectively. Temperature in the upper layer ($20\ m \leq y \leq 80\ m$) was kept at 9 ^0C while in the lower thermal layer ($0\ m \leq y < 20\ m$) 7 ^0C temperature was assumed.

Total number of cells in two of the spatial dimensions is maintained at 40. These are axes Y-Y and Z-Z. Number of cells in the third spatial dimension decreases from 40 to 20 (X-X axis). A dark spot in the plan view (Fig. 5.2) shows the cold water cells included to instigate the flow. The cold site entity includes a square of 6 × 6 cells in plan view extending by 5 cells in the vertical direction.

Water surface is assumed to undergo cooling at a constant rate of 50. $\times 10^4\ cal/cm^2/sec$ during the entire simulation time.

5.3 Flow Mechanism

In general, the results show that the model was capable of reproducing some basic features of thermal convection in the lake during cooling period. Comparison with respect to time showed that as the time progresses the entire water column loses heat energy as the lake cools on its surface at constant rate and thermocline moving downwards towards the lake's bed. Cooled water particles from near the surfaces vicinities having cooled and become denser, sink downwards and in turn the hotter and less dense particles replace them in completion of mass conservation.

The simulation with 2 %-slope seemed to cool relatively faster compared to the 8 % -slope simulation, as the simulation with milder slope has a larger area exposed at the surface enhancing relatively larger amount of heat energy to be lost. Figure [5.3] in page [101] and figure [5.4] in page [101] show the side views from both simulations cases after 186 hours and 399 hours simulation time whereby it can be shown that milder slope case is relatively cooler than the steeper slope case.

Figure [5.5] in page [104] show plan views of the simulated flow from the simulation case with 8 % slope. The data were taken from a layer of cells adjacent to the lake's bed. During the early stages of the simulation, temperatures at the slopes were recorded to be higher than the remaining portion of the computational domain. After a period of time
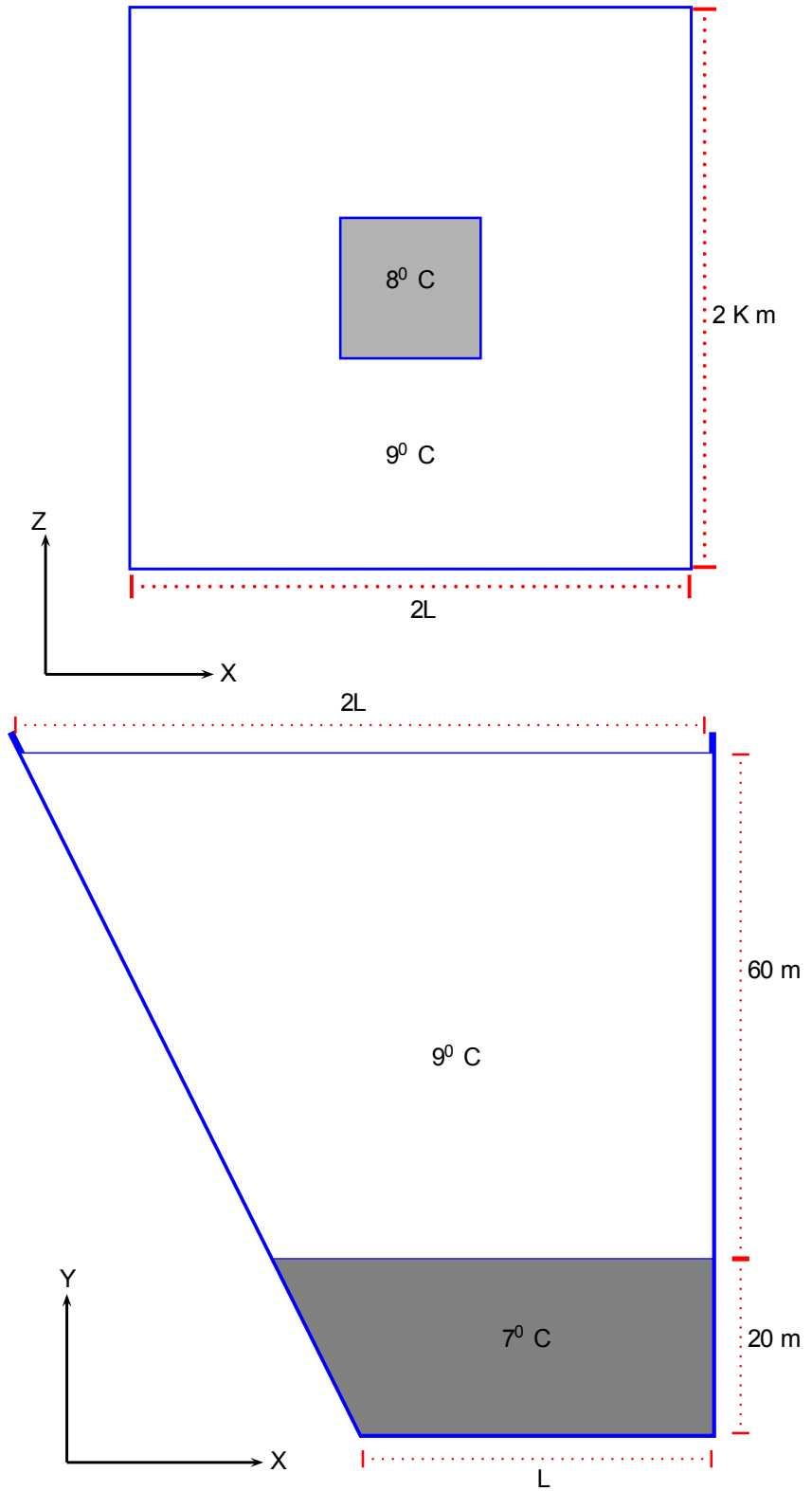
Figure 5.2: Plan-view (top) and side-view (bottom) of the computational domain with initial temperature conditions
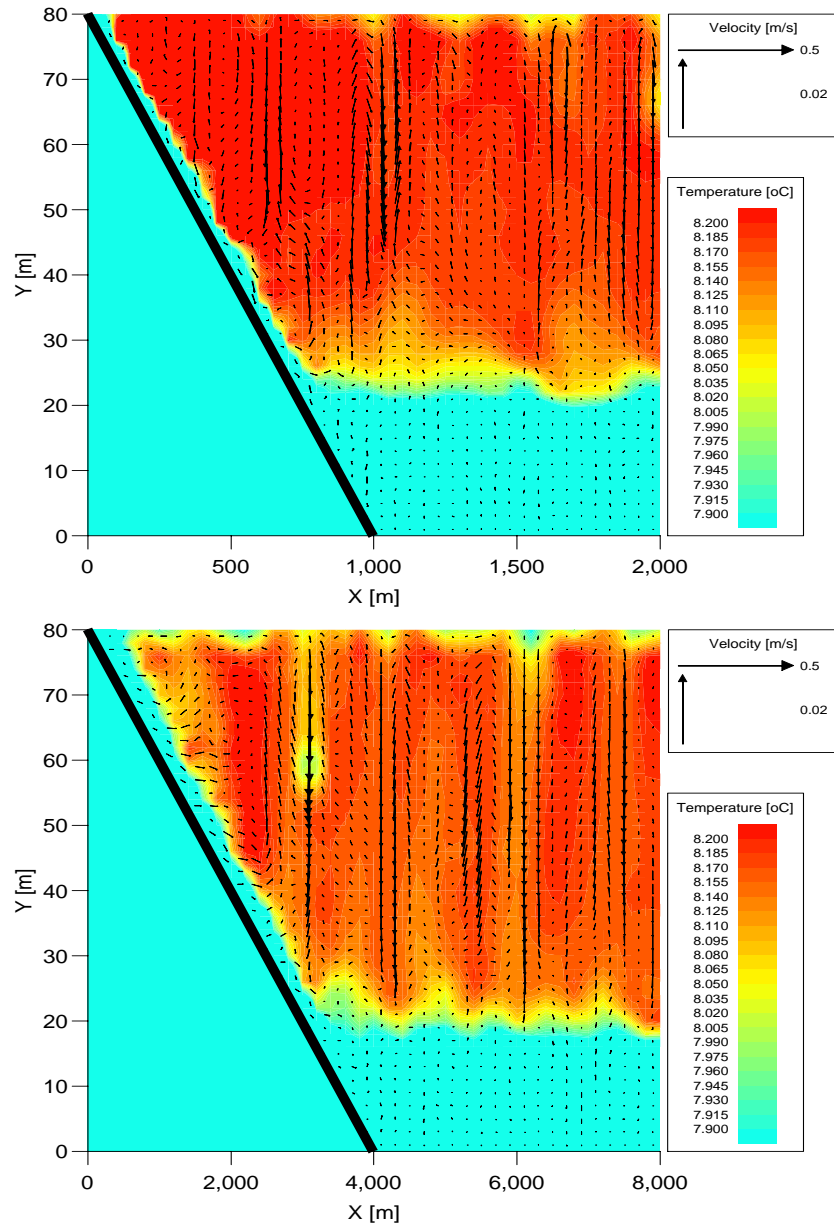
Figure 5.3: Side views after 186 hrs from simulation with 8% slope (top) and 2% slope (bottom)
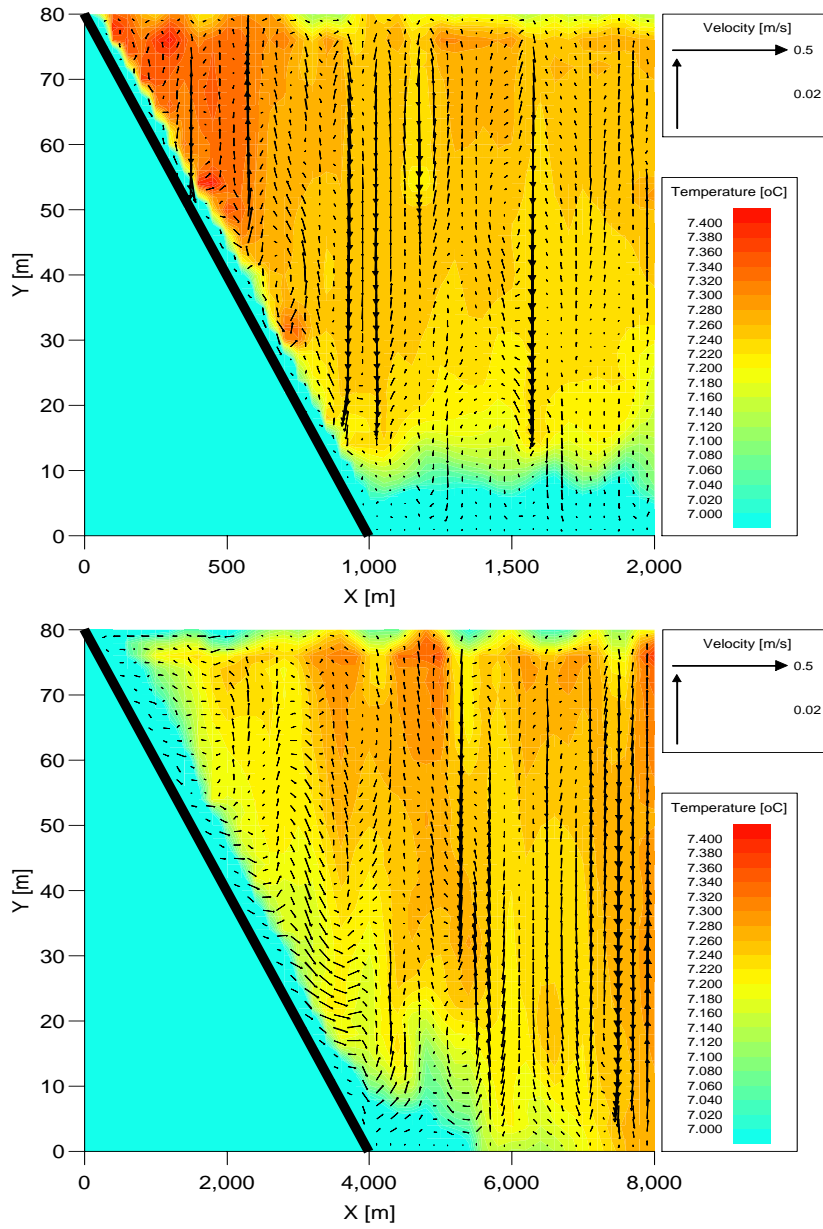
Figure 5.4: Side views after 399 hrs from simulation with 8% slope (top) and 2% slope (bottom)

the temperature conditions were reversed with those at the slopes being lower than other parts of the domain, indicating that the water column was losing heat from the surface down to lake's bed with the lowering of thermocline. Similar results can be seen from figure [5.6] in page [105] taken from a simulation with 2 % slope. The results describe the overall dropping of temperature and lowering of thermocline as time elapsed.

Circulation or distorted circulations could be noticed at times around the slope close to the surface. The simulation case with milder slope seem to show more clearly these circulations. Figure [5.7] in page [106] taken from simulation with 2 % slope shows the side view of the simulated flow with circulations along the slope near the surface.

5.4   Simulated Temperature Time-series

Simulated temperature time-series data were sampled at different depths. The overall variation shows the decrease in temperature as simulation time progresses, which is basic concept of thermal cooling. The information about the temperature variation is also an indicator of flow properties around these areas. The temperature time-series is capable of being retrieved and could give the information about the flow. In general, the simulated temperature were recorded to be systematically decreasing at the upper thermal layer indicating the overall temperature decrease.

Figure [5.8] in page [107] shows the simulated data from numerical experiment with 2 % slope. Temperature is decreasing monotonously which could be easily approximated into a straight line. Similar results can be viewed from numerical experiment with 8 % slope represented by figure [5.9] in page [108].

The simulated temperature were recorded to be fluctuating at different magnitudes when sampled from points at the lower thermal layer. Figures [5.10 & 5.11] in pages [109 & 110] respectively show some simulated data sampled at several points at the location near the lake's bed from both of the numerical experiments. Sharp highs and low could be observed, the variation which can be traced from the water particles' interaction at lower vicinities of the lake.

Side-views of the simulated flow revealed the existence of internal waves around the

Figure 5.5: Plan view showing simulated flow from simulation with 8 % slope. Data are taken from cells adjacent to lake's bed or slope
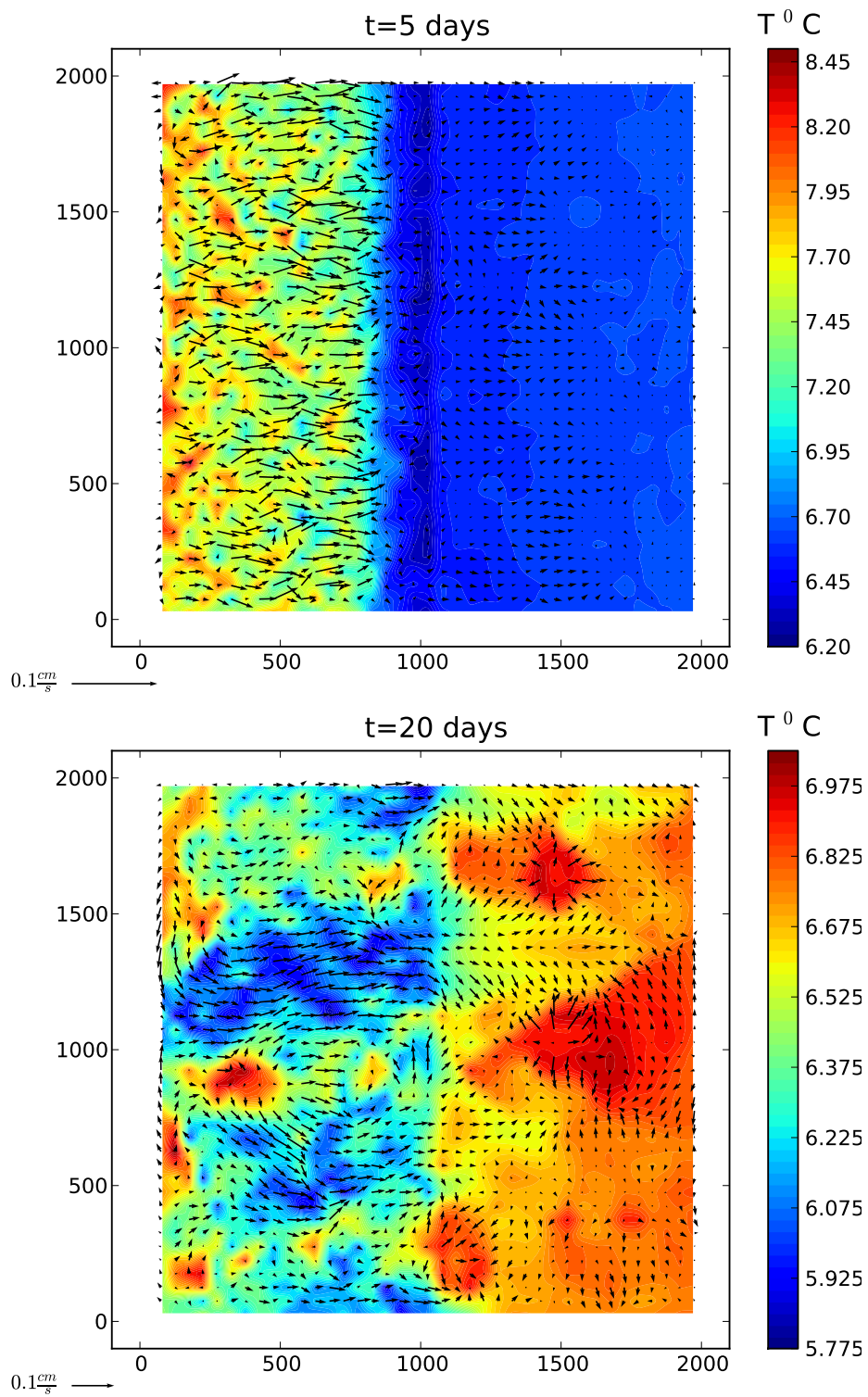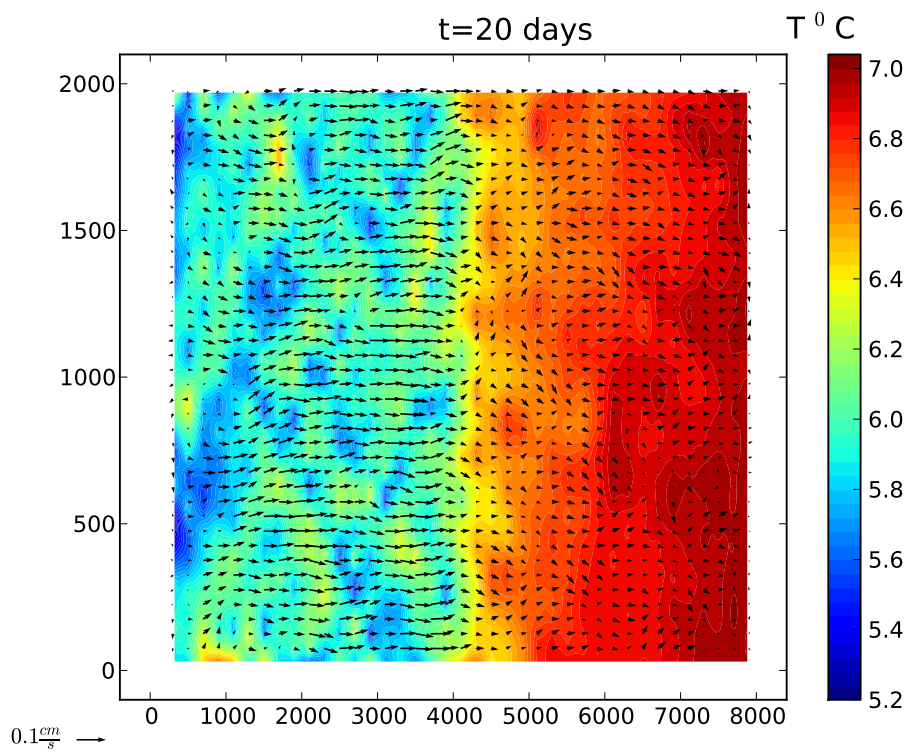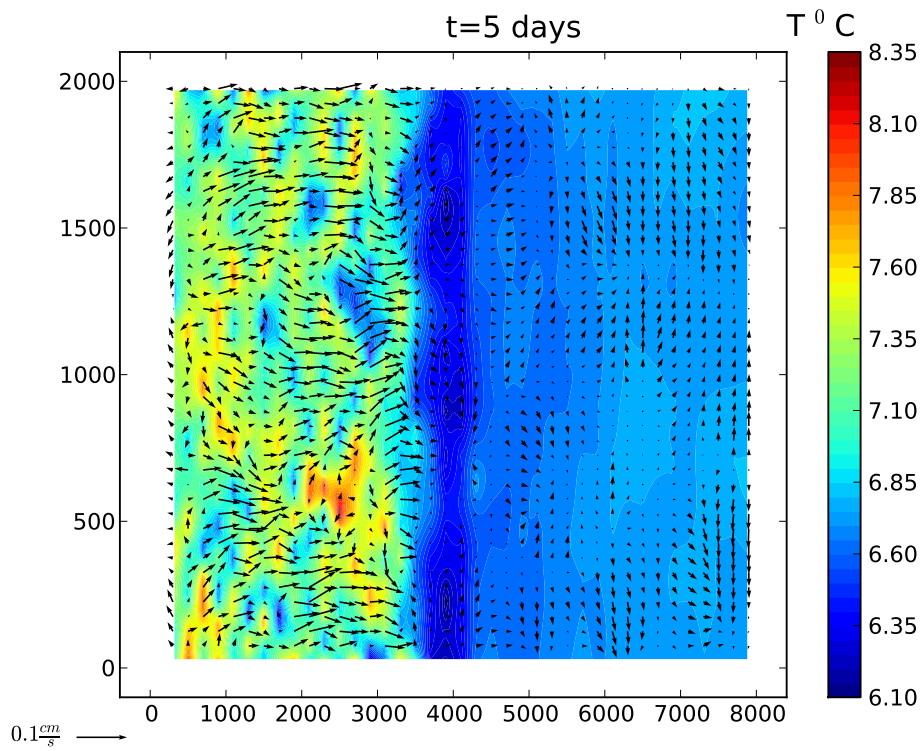
Figure 5.6: Plan view showing simulated flow from simulation with 2 % slope. Data are taken from cells adjacent to lake's bed or slope
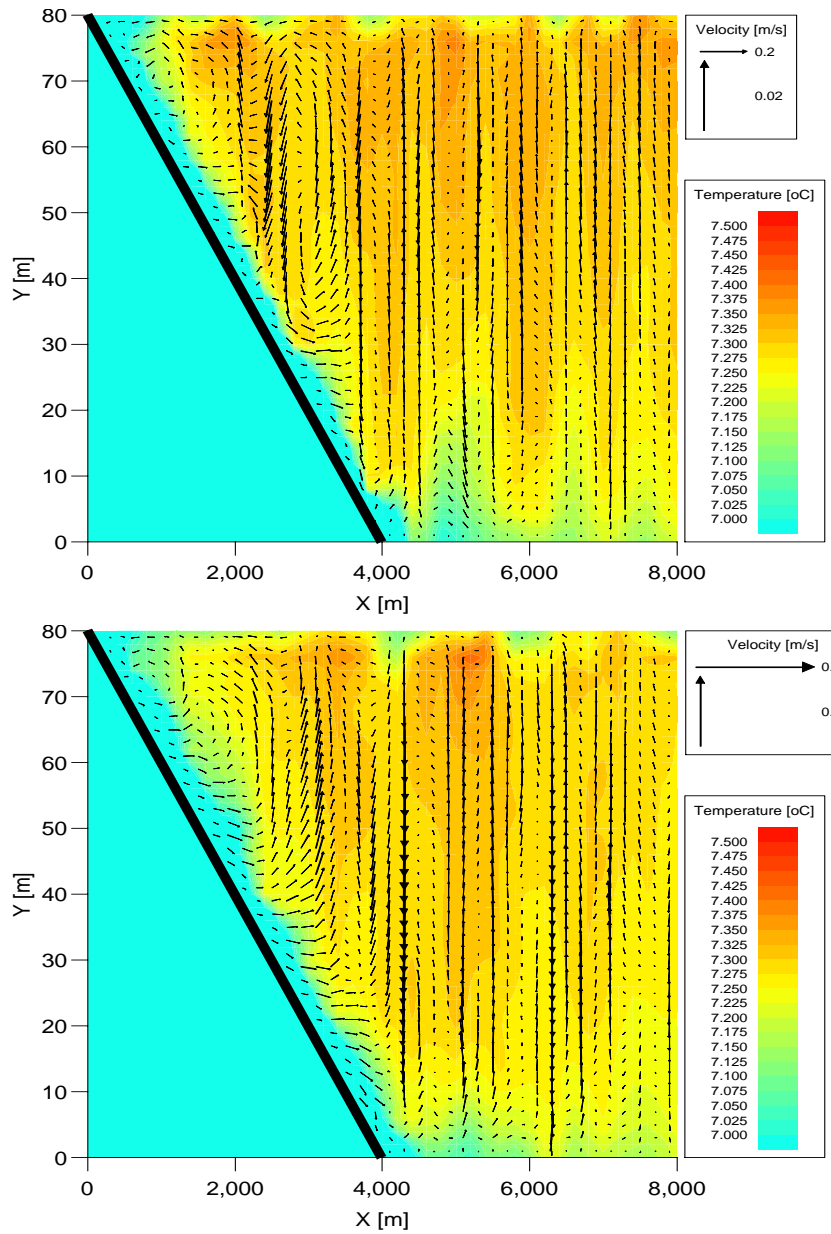
Figure 5.7: Side view of simulated flow from simulation with 2 % slope at t= 383 hrs(top) and 386 hours (bottom) respectively. Circulations are formed along the slope near the surface.
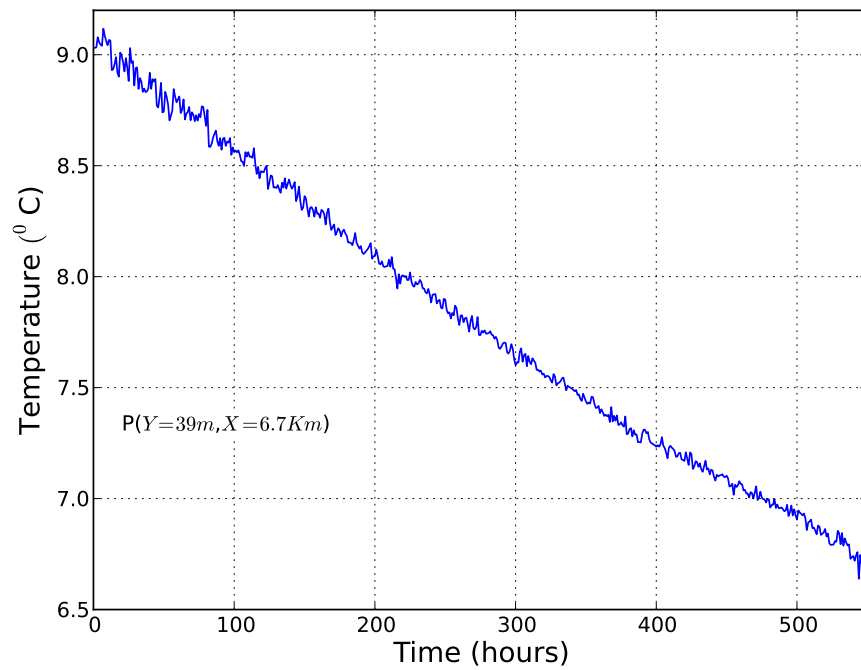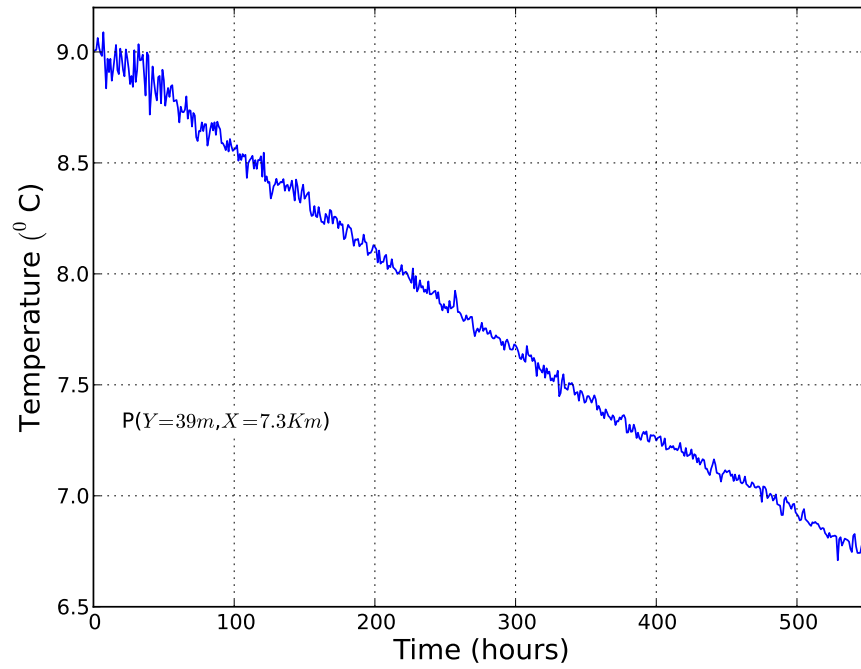
Figure 5.8: Simulated temperature time-series from simulation with 2 % slope taken at upper thermal layer.
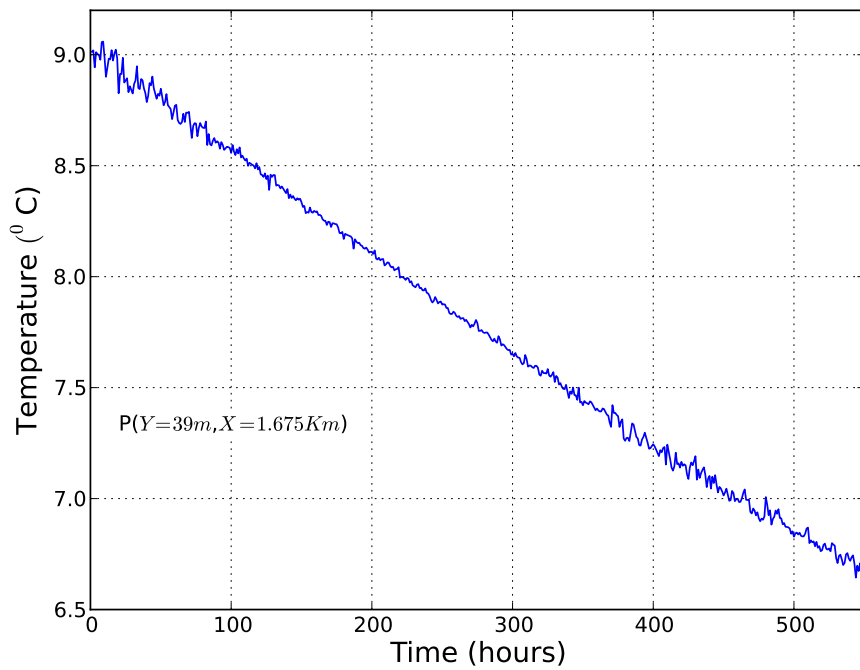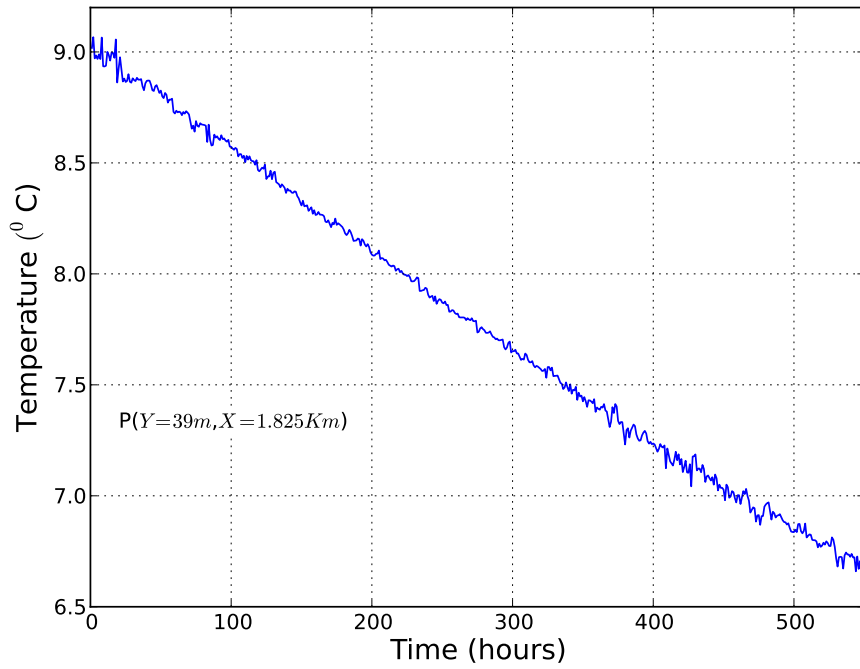
Figure 5.9: Simulated temperature time-series from simulation with 8 % slope taken at upper thermal layer.

Figure 5.10: Simulated temperature time-series from simulation with 8 % slope.

Figure 5.11: Simulated temperature time-series from simulation with 2 % slope.

separating layer of the two thermal layers. The internal waves are believed to be caused partly by flow induced by the density currents on the slope as well as the impact of falling cooled water bodies as the results of thermal convection. Water particles after been cooled at the surface they are relatively heavier and therefore fall down into the lake's bed. When reaching there cause impact du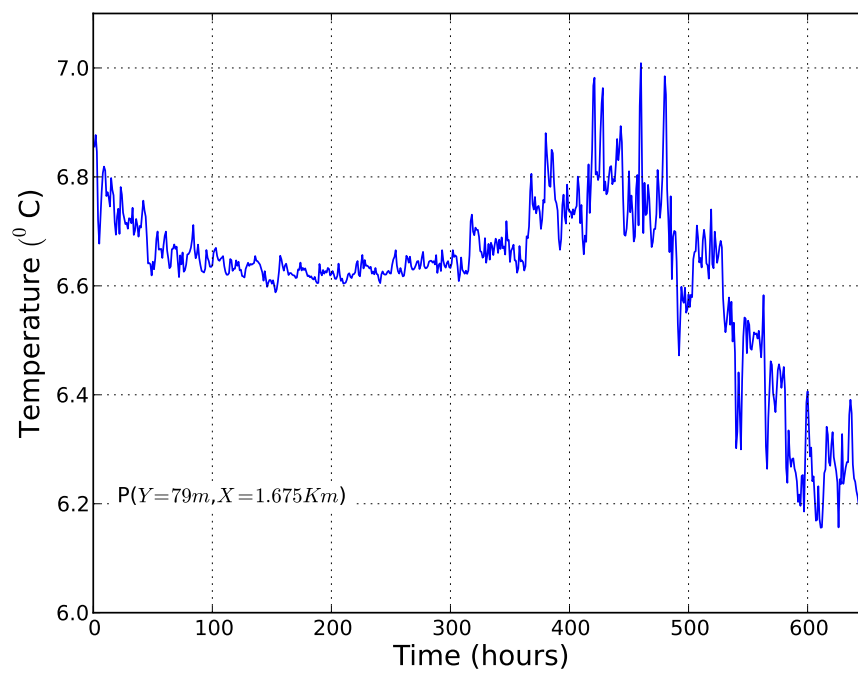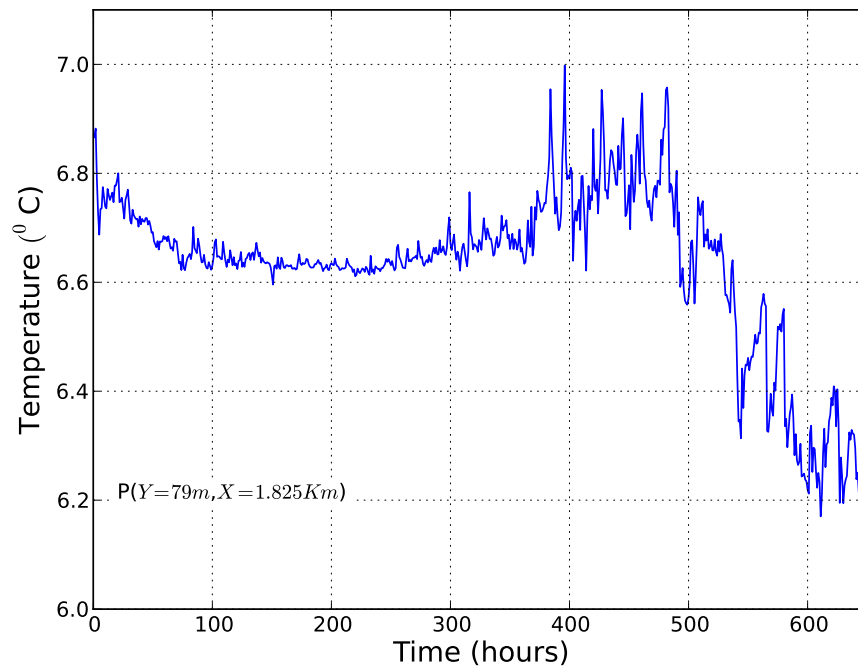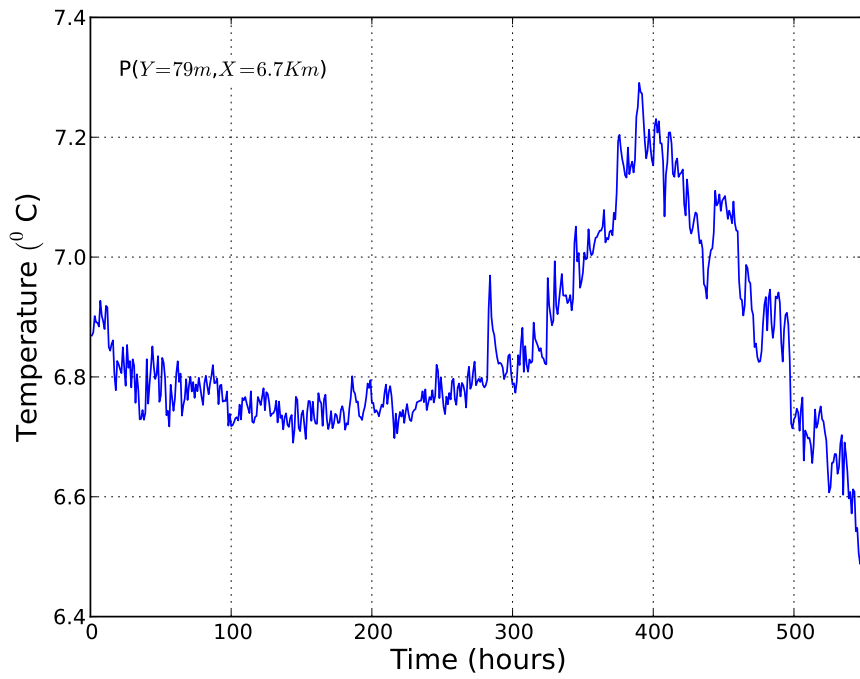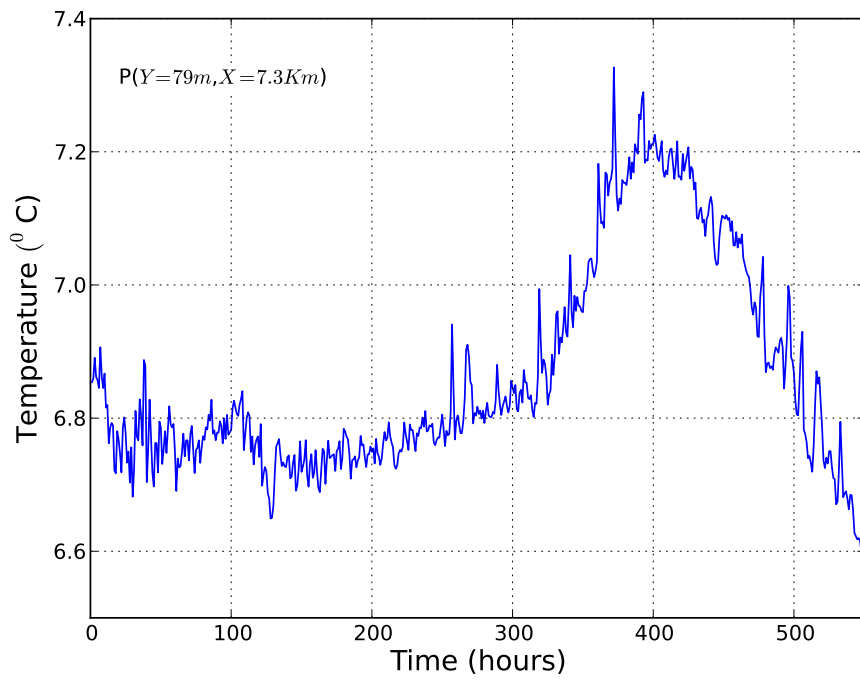e to colision and the effect spread as a ripple. Falling cooled water particles were spotted to land on the slopes causing interruption on the flow induced by density currents which looked steady before. The flow induced by density currents down the slope cause impact at the foot of the slope and partly influence the internal wave in the X-X direction. Internal waves occurred in both X-X and Z-Z directions as the falling cooled water bodies also contributed to Z-Z motion.

Internal waves had irregular shape, causing rapid movement of water particles while incidentally trapping them in. Non-uniform periodicity of the internal wave can traced from irregular intervals of falling cooled water bodies. The wave's movement can explain the rapid variation of temperature time-series data recorded from the simulated flow. Sharp changes in temperature and dissolved oxygen reported by Lake Biwa Research Institute (LBRI) (Fig. [5.12]) can be explained by these internal wave motions. Dissolved oxygen influx at lower depths is mainly through flow induced by density currents and cooled water at the surface falling due to thermal convection. Waters from the surface are richer in dissolved oxygen concentration.

Figures [5.13] - [5.15] are included to demonstrate the effect of internal wave motion in relation to sharp temperature changes at location near the lake's bed. The focus area is the point around $X = 1.500\ Km$ and $Y = 79m$ (Y referenced from the water surface). The side-views were taken at mid-point in the Z-Z direction. At $t = 383\ \&\ 384$ hours as shown in figure [5.13] in page [113], the focus area is occupied with hot water. At $t = 385$ hours (Fig. [5.14] (top), page [114]) the area is occupied with cold water with peak amplitude occuring around the focus area. At $t = 386$ hours (Fig. [5.14] (bottom), page [114]) the section seem to contain more of cold water than the previous time-step, meaning that there has been internal wave movement towards this section from the Z-Z direction. Figure [5.15] in page [115] demonstrates temperature time-series variation around the focus area. The
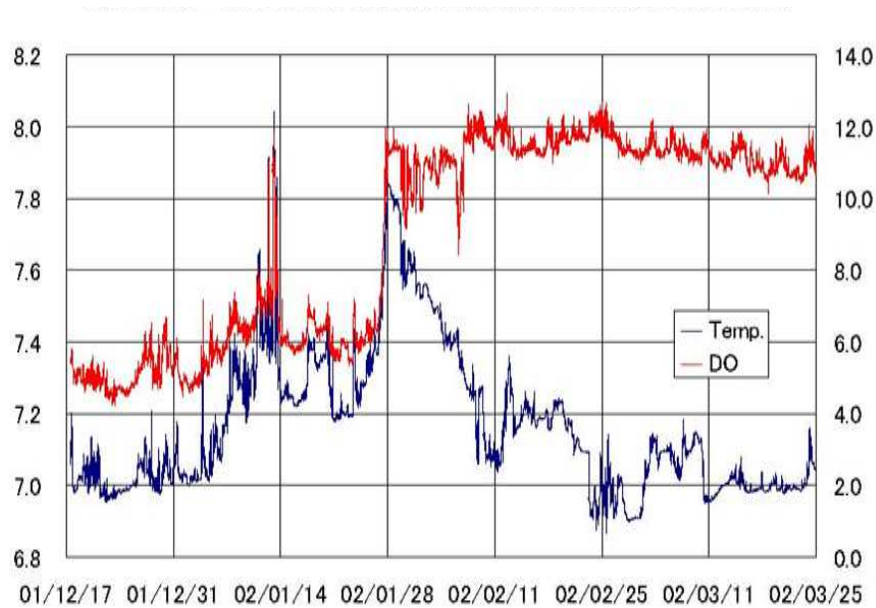
Figure 5.12: Observed DO and temperature time-series data from Lake Biwa. Data were taken near Imazu observation station near the deepest point of the lake (Source: LBRI)

temperature variation can be viewed at the interval between 383 to 386 hours.

5.5 Summary

In this chapter, investigation of lake's flow due to thermal convection during cooling period was done. The investigation focused on part of the lake on the shore.

Numerical simulations were done using the 3-D model already introduced in chapter III. Due to the physical nature of part of the lake near the shores, the computational domain assumed a shape of a right-trapezoidal prism with a slanting edge in one of the vertical walls. To understand the flow under different slopes, two numerical experiments were done with slopes 2 % and 8 %.

In general, the model could simulate some basic features of a cooling lake undergoing thermal cooling. Cooled water particles near the surface vicinities could be seen falling into bottom layers. Overall temperature in the computational domain was reduced as the simulation progressed, while the thermocline was also moving down towards the lake's bottom.

The simulation involving a milder slope appeared to cool relatively faster than the
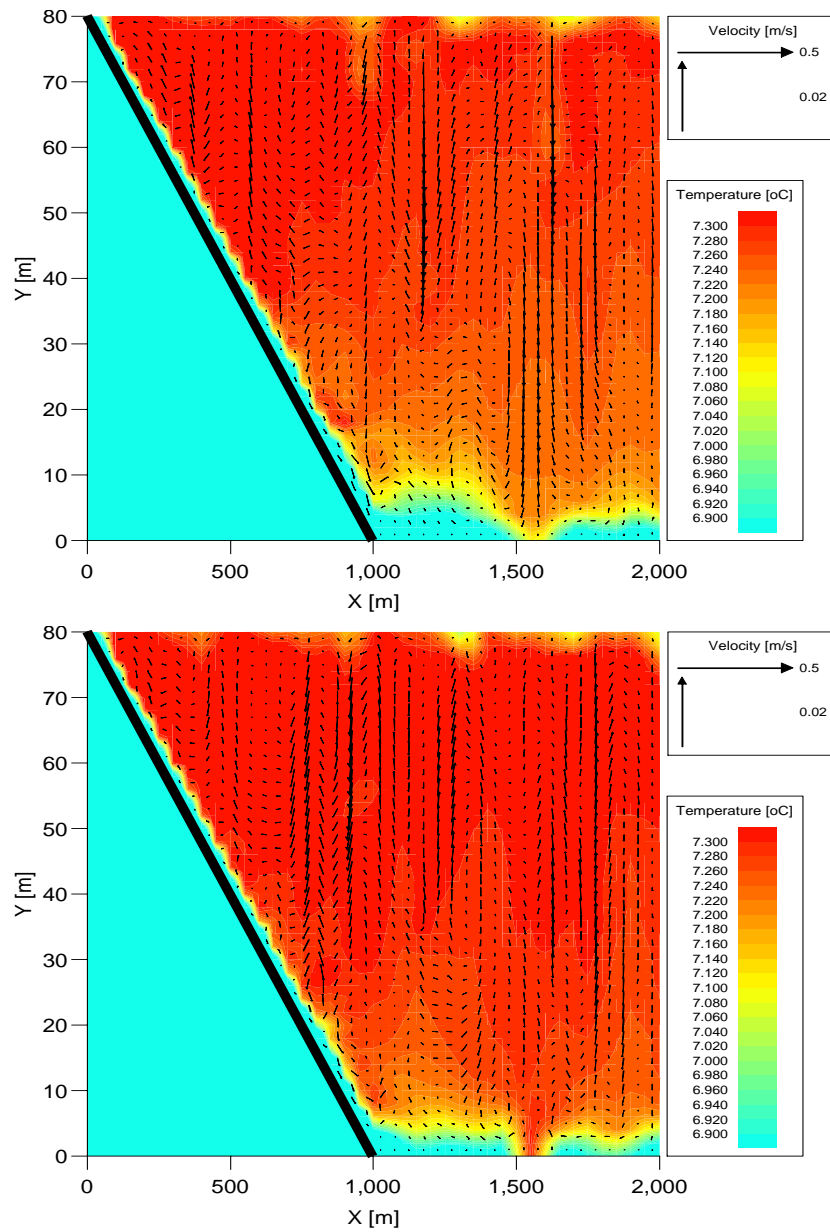
Figure 5.13: Side views showing simulated flow from a case with 8 % slope after 383 (top) and 384 hours (bottom)
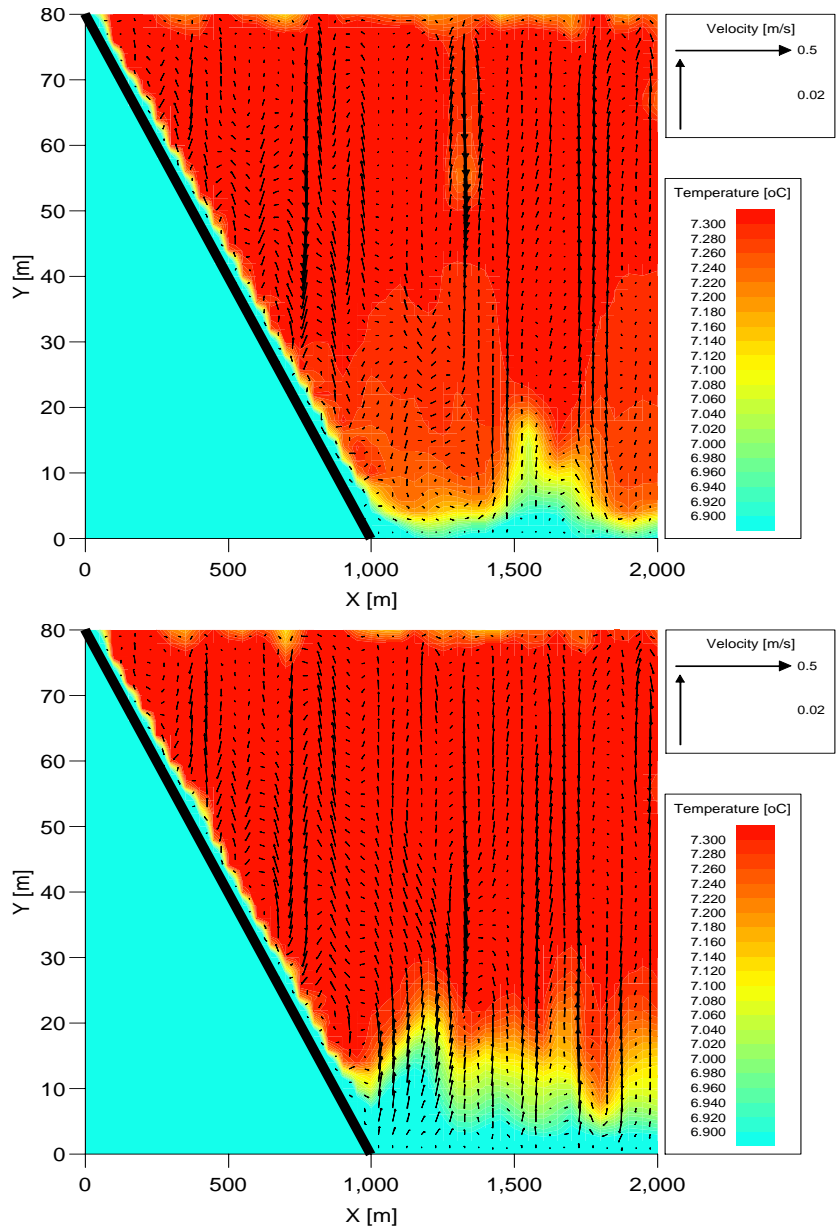
Figure 5.14: Side views showing simulated flow from a case with 8 % slope after 385 (top) and 386 hours (bottom)
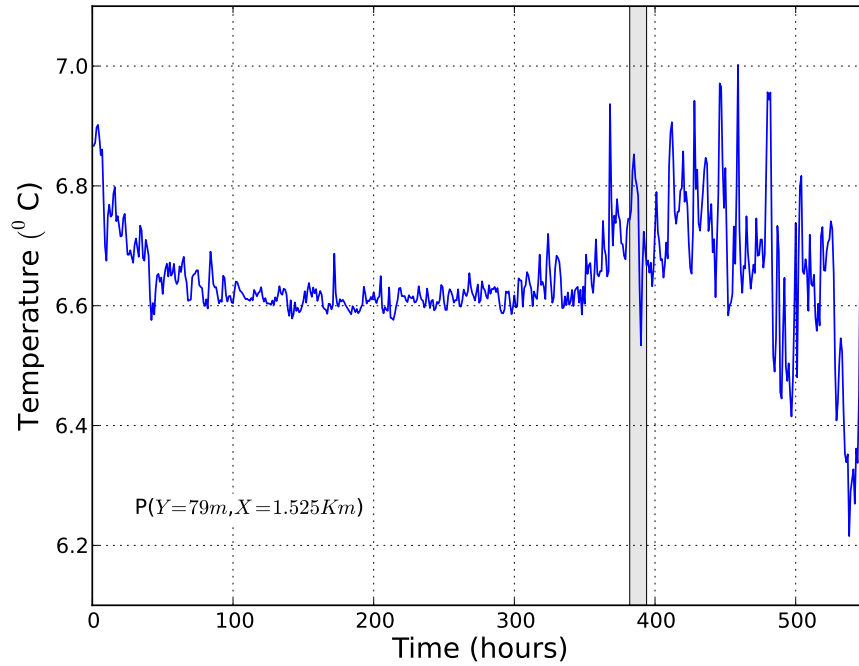
Figure 5.15: Temperature time-series showing sharp changes corresponding to figures [5.14] & [5.14]

other case with steeper slope. It is reasoned that the difference in cooling is due to the fact that in the milder slope case, a relatively larger area is exposed at the water surface and hence more heat is likely to be lost from this simulation case.

Internal waves were spotted around the interface of thermal layers. The waves were exacted to be a results of flow induced by density currents on the slope and falling of cooled water from the vicinities near the surface. Flow induced by density currents on the slope collide with the waters at the foot of the slope and momentous impact could cause a wave moving away from the foot of the slope and towards it after bouncing over the wall on the other side of the computational domain or barrier. The falling water bodies after being cooled at the surface cause impact resulting into formation of a ripple which give further strength to the waves. The irregular shape of the internal waves could be traced from the irregular time interval of falling cooled water bodies from the water surface.

Conclusively, this 3-D numerical experiments could simulate the flow resulting into some similar temperature time-series observations from Lake Biwa, despite the theoretical simplicity and lumping of environmental inputs. The numerical model could be refined to

include modelling of turbulent terms, turbulent effect at the surface due to wind and finer mesh of the computational domain near the slope in order to capture much more details of the flow. Consideration of other factors such as resistance to flow due plants near the shore might also be useful.

VI

Conclusions

6.1 General

In this chapter, a brief summary is provided explaining the value of the reserach's methodology and results described in the previous chapters. Some few suggestions are included for further extension in the future regarding some aspects of this research.

6.2 Summary

6.2.1 1-D Modeling DO Generation

Modeling of water quality indices using 1-D model under unsteady conditions based on formulation by *Hosoda and Hosomi* (2004) was presented. The momentum and mass conservation equations were solved numerically and the turbulent terms were modelled using standard $k - \varepsilon$ approximation. The obtained results were compared with observed data from Lake Biwa, a case study of this research. Computed distributions of temperature and DO profiles and other selected water qualities indices showed a qualitative resemblance with recorded data from the lake. Overall, the model could be used to predict the long-term effects of global warming.

The predicted results of dissolved oxygen components were then used in mathematical formulation of a simple 1-D dissolved oxygen generation model; these are diffusion

coefficient and consumption and production distributions with depth. The results from DO generation model suggested existence of two kinds of DO distributions, DO decreasing distribution with a minimum value at the thermocline, and the second distribution in which DO decreases monotonously with depth throughout the water column. The model pointed-out the importance of limitation on diffusive terms at depths near the thermocline on the stability of the vertical DO distribution. The results suggests that the local minimum in DO values at this layer can be broken by overcoming the deficiency between productive and consumption agents and hence allowing dissolved oxygen to diffuse easily along the thermocline. Supply of DO at this layer through mechanical or any other means could therefore enhance a stable DO distribution and ensuring more DO is supplied at lower layer near the lake's bed.

6.2.2   3-D numerical mode for thermal convection

The 3-D numerical model was capable of simulating the main characteristics of the process such as velocity field which represented the interaction between the fluid particles. The temperature profile variation with time was a good indication of thermal energy contained in various depths within a water column during thermal cooling. The model have shown the effect of variation of surface warming, represented in the model by water surface cooling rate. Simulations involving these various theoretical values of water surface cooling rate showed differing temperature profiles; with higher values causing relatively quicker cooling.

6.2.3   Stochastic model

Stochastic model was proposed to simulate some aspects of thermal convection process in the lake. Influence of neighborhood to a cold site was studied using the 3-D model and showed the position of centroid of the cold cells are proportional to the number of its neighborhood hot sites. This relation was similar to the dynamics in forest gap recovery, as a result, the stochastic model formulation by *Kubo et al.* (1996) was adapted. Meanfield and paired approximation approaches were used in approximations of some of the

spatial properties of the model. Results from paired approximation was closely agreed with the results from the Monte Carlo simulation. The spatial analysis from Monte-Carlo simulation showed the power law dependence between clusters of cold sites and their respective number of occurrences, the property which could also be seen from clusters behavior from the 3-D numerical model's results.

6.3 Open Ends

With the current initiative described in this thesis, we present potential window of opportunity which might prove worth it in improving the overall or some aspects of this work in the future. We highlight some of them in the next few subsections.

6.3.1 1-D Numerical Model

Refinement of 1-D Hydrodynamic Model Mathematical formulation of this model by (*Hosoda and Hosomi*, 2004) can be revisited in order to improve the estimated distribution of water quality indicators by reconsideration of some water quality sub-models.

1-D DO Generation Model 1-D DO generation model can be expanded further to ascertain which distributions are more practical to offer the background mechanism of the DO production in the water column.

6.3.2 3-D Numerical Model

Modelling of Convective terms: In the work described herein, modelling of convective terms has been done using QUICK scheme. Use of other conservative schemes have not been tested.

Effects of Grid Size: In the current initiative in studying external climate change effects on the lake, lake's flow near the shores and study of neighborhood interaction, we did consider only one type of grid size when setting such simulations. Further study can be done by extending the simulations using several other grid sizes.

Surface Discrimination Criterion In spatial analysis of the 3-D model results, the spins of the sites were determined by applying a threshold value on vertical velocity for a given surface. Other methods might be applied in delineating these spins such as temperature of the sites, or criterion imposed as a function combining temperature, simulation time, depth reference point, surface conditions and velocity vertical component of a cell. i.e.

$$\Omega = f(T, t, y, Q_{00}, v_{i,j,k})$$

.

Consideration of turbulent terms Numerical experiments of lake's thermal convection process using two geometrical configurations, cuboidal and right-trapezoidal prism, as described in chapters [III] and [V], the Navier-Stokes equations were solved numerically without considering turbulent terms. It is attractive to reconsider these numerical experiments where modelling of turbulent terms is considered.

6.3.3 Stochastic Model

Model's Spatial Dimensionality: Stochastic model can be reconsidered to include three spatial dimensional dynamics in the pursue of describing the cooling process in real lakes. The current formulation considers only spatial domain representing dynamics in a horizontal plane with no connectivity or interaction from its adjacent neighbors on bottom or top of it. It is desirable to extend the model into three-dimensionality while relating dynamics from one layer with its neighboring adjacent layers.

Spins: The model can be extended by considering more than two types of state (spins). Modeling of thermal convection process by means of 3-D numerical model showed that some of the cells undergo upwards or downward movement, reflected by their strong component of vertical velocities, but there are also cells which are not characterized with such relatively large magnitudes of vertical velocity component, these cells would need a 'special' category of their own in the dynamics of the stochastic model consideration. A refinement therefore, could be imposed in which the third

kind of spin type be introduced in describing the mechanism.

APPENDICES

1-D Water Quality Submodels

[Chlorophyll-a in Phytoplankton]

$$\frac{\partial P}{\partial t} = (G_P - D_P).P - \frac{\partial w_O P}{\partial z} + + D\frac{\partial^2 P}{\partial z^2}, \tag{A.1a}$$

$$G_P = S_P.R_{Rh}.\theta_{Rh}^{(T-20)}\frac{I_\gamma}{I_S}exp(1 - \frac{I_\gamma}{I_S}).\frac{C_{IN}}{K_{IN} + C_{IN}}.\frac{C_{IP}}{K_{IP} + C_{IP}}, \tag{A.1b}$$

$$D_P = R_{CP}.\theta_{CP}^{(T-20)} + C_g.\frac{K_{PP}}{K_{PP} + P}.Z \tag{A.1c}$$

[Carbon in Zooplankton]

$$\frac{\partial Z}{\partial t} = (G_Z - D_Z).Z + D\frac{\partial^2 Z}{\partial z^2}, \tag{A.2a}$$

$$G_Z = \alpha.a_Z.C_g.\frac{K_{PP}}{K_{PP} + P}.P, \tag{A.2b}$$

$$D_Z = R_Z.\theta_Z^{(T-20)} \tag{A.2c}$$

[Inorganic Nitrogen]

$$\frac{\partial C_{IN}}{\partial t} = \quad -\beta_N.G_p.P + \beta_N(1-a_Z).C_g.\frac{K_{PP}}{K_{PP}+P}.P.Z$$

$$+R_N.\theta_N^{(T-20)}.(C_{ON}-\beta_N.P-\gamma_N.Z)$$

$$+E_{IN}.\theta_{EIN}^{(T-20)}/\Delta Z$$

$$+D\frac{\partial^2 C_{IN}}{\partial z^2} \tag{A.3}$$

[Organic Nitrogen]

$$\frac{\partial C_{ON}}{\partial t} = \quad \beta_N.G_p.P - \beta_N(1-a_Z).C_g.\frac{K_{PP}}{K_{PP}+P}.P.Z$$

$$-R_N.\theta_N^{(T-20)}.(C_{ON}-\beta_N.P-\gamma_N.Z)$$

$$-\frac{\partial(w_N(C_{ON}-\gamma_N.Z))}{\partial z}$$

$$+D\frac{\partial^2(C_{ON}-\gamma_N.Z)}{\partial z^2} \tag{A.4}$$

[Inorganic Phosphorus]

$$\frac{\partial C_{IP}}{\partial t} = \quad -\beta_p.G_p.P + \beta_P(1-a_Z).C_g.\frac{K_{PP}}{K_{PP}+P}.P.Z$$

$$+R_p.\theta_P^{(T-20)}.(C_{OP}-\beta_P.Z-\gamma_p.Z)$$

$$+E_{IP}.\theta_{EIP}^{(T-20)}/\Delta Z$$

$$+D\frac{\partial^2 C_{IP}}{\partial z^2} \tag{A.5}$$

[Organic Phosphorus]

$$\frac{\partial C_{OP}}{\partial t} = \quad \beta_p.G_p.P - \beta_P(1 - a_Z).C_g.\frac{K_{PP}}{K_{PP} + P}.P.Z$$

$$- R_p.\theta_P^{(T-20)}.(C_{OP} - \beta_P.P - \gamma_p.Z)$$

$$- \frac{\partial(w_P(C_{OP} - \gamma_P.Z))}{\partial z}$$

$$+ D\frac{\partial^2(C_{OP} - \gamma_P.Z)}{\partial z^2} \tag{A.6}$$

[Dissolved Oxygen]

$$\frac{\partial DO}{\partial t} = \quad K_{DO1}(DO_{sat} - DO)$$

$$+ K_{DO2}(G_p - R_{cp}.\theta_{cp}^{(T-20)})P$$

$$- K_{DO3}.\theta_{DO}^{(T-20)}.COD$$

$$- E_{DO}.\theta_{DO}^{(T-20)}/\Delta Z$$

$$+ D\frac{\partial^2 DO}{\partial z^2} \tag{A.7}$$

$$K_{DO3}COD \cong K_{DO4}(C_{ON} - \beta_N.P - \beta_N.Z) \tag{A.8}$$

where:

$P(\mu g_{chla}/l)$; chlorophyll-a in phytoplankton,

$Z(mg_{-C}/l)$; carbon in zooplankton,

$C_{IN}(\mu g_{-N}/l)$; inorganic nitrogen,

$C_{IP}(\mu g_{-P}/l)$; inorganic phosphorus,

$C_{ON}(\mu g_{-N}/l)$; organic nitrogen,

$C_{OP}(\mu g_{-P}/l)$; organic phosphorus,

$DO(mg/l)$; dissolved oxygen,

$\mu_s = 0.00385$; space effect function for primary production,

R_{Ph} ($1/sec$) ; growth rate of phytoplankton at $20^0 C$ ($= 2/(24*60*60)$),

D ; turbulennt diffusion coefficient,

$I_\gamma = Q_z$; light intensity at z,

D_z ; mortality of zooplankton,

G_z ; grazing term of zooplakton,

K_{PP}($\mu g/l$) ; saturation constant of grazing ($=60$),

C_g($l/mg_{-c}/sec$) ; grazing rate of phytoplankton by zooplankton ($= 0.25/(24*60*60)$),

K_{IN}($\mu g/l$) ; half saturation constant ($= 25$),

K_{IP}($\mu g/l$) ; half saturation constant ($= 2$),

R_{CP} ($1/sec$) ; respiration and mortality rate of phytoplankton ($= 0.01/(24*60*60)$),

θ_{CP} ; temperature coefficient on respiration of phytoplankton ($= 1.05$),

θ_{Ph} ; temperature coefficient on primary production of phytoplankton ($= 1.05$),

α ($mg_{-C}/\mu g_{-chla}$) ; rate of carbon to chlorophyll-a in phytoplankton ($= 0.05$),

a_z ; assimilation rate of carbon in phytoplankton ($= 0.6$),

R_Z ($1/sec$) ; mortality rate of zooplankton ($= 0.02/(24*60*60)$),

θ_z ; temperature coefficient on mortality rate of zooplankton ($= 1.05$),

β_N ($\mu g{-}N/\mu g_{-chla}$) ; N/Chl.a in phytoplankton ($= 10$),

R_N ($1/sec$) ; mineralization rate of organic N ($= 0.027/(24*60*60)$),

θ_N ; temperature coefficient on mineralization rate of N ($= 1.05$),

γ_N ($\mu g_{-N}/mg_{-C}$) ; N/C in zooplankton ($= 200$),

E_{IN} **($\mu g/m^2/sec$)** ; release rate of inorganic N at bottom ($= 30/(24*60*60)$),

θ_{EIN} ; temperature coefficient on release rate of IN ($= 1.12$)

$|w_N|$ **(m/sec)** ; settling velocity of organic N ($= 0.1$),

β_P **($\mu g_{-P}/\mu g_{-Chla}$)** ; P/Chlain in phytoplankton ($= 1$),

R_P **($1/sec$)** ; mineralization rate of organic P ($= 0.2/(24*60*60)$),

θ_P ; temperature coefficient on mineralization rate of P ($= 1.05$),

γ_P **($\mu g_{-P}/mg_{-C}$)** ; P/Chla in zooplankton ($= 26$),

E_{IP} **($\mu g/m^2/sec$)** ; release rate of inorganic P at bottom ($= 0.0/(24*60*60)$),

θ_{EIP} ; temperature coefficient on release rate of IP ($= 1.12$),

$|w_P|$ **(m/sec)** ; settling velocity of organic P ($= 0.1$),

DO_{sat} **(mg/l)** ; saturated dissolved oxygen concentration,

$K_{DO1}, K_{DO2}, K_{DO3}$; constants ($= 0.000035,\ 0.06,\ 0.00000002$),

θ_{DO} ; temperature coefficient on mineralization of COD ($= 1.05$),

E_{DO} **($mg/m^2/sec$)** ; consumption rate of DO at bottom ($= 15/(24*60*60)$),

θ_{EDO} ; temperature coefficient on consumption rate of DO ($= 1.12$)

BIBLIOGRAPHY

BIBLIOGRAPHY

Adrian, R., et al. (2009), Lakes as sentinels of climate change, *Journal of Limnology and Oceanography*, *54*(6(Part 2)), 2283 – 2297.

Anderson,, J. J. (1995), *Computational Fluid Dynamics - The Basics with Applications*, International ed., McGraw-Hill International, Singapore.

Bell, V., D. George, R. Moore, and J. Parker (2006), Using a 1-D mixing model to simulate the vertical flux of heat and oxygen in a lake subject to episodic mixing, *Ecological Modelling*, *190*(1-2), 41 – 54, doi:DOI:10.1016/j.ecolmodel.2005.02.025.

Carr, G., and J. Neary (2008), *Water Quality for Ecosystem and Human Health*, 2nd ed., UNEP Global Environment Monitoring System / Water Programme, Burlington, Ontario, L7R 4A6 Canada.

Elçi, S. (2008), Effects of thermal stratification and mixing on reservoir water quality, *Limnology*, *9*, 135–142, 10.1007/s10201-008-0240-x.

Ferziger, J., and M. Peric (2002), *Computational Methods for Fluid Dynamics*, third ed., Springer-Verlag, Berlin, Germany.

Hamilton, D. P., and S. G. Schladow (1997), Prediction of water quality in lakes and reservoirs. Part I – Model description, *Ecological Modelling*, *96*(1-3), 91 – 110, doi: DOI:10.1016/S0304-3800(96)00062-2.

Harada, Y., and Y. Iwasa (1994), Lattice population dynamics for plants with dispersing seeds and vegetative propagation, *Researches on Population Ecology*, *36*(2), 237 – 249, doi: 10.1007/BF02514940.

Harlow, F. H., and J. E. Welch (1966), The MAC method: A computing technique for solving viscous, incompressible, transient fluid flow problems involving free surfaces, *Los Alamos Scientific Laboratory report*, *LA-3425*.

Hirt, C., and J. Cook (1972), Calculating three-dimensional flows around structures and over rough terrain, *Journal of Computational Physics*, *10*(2), 324–340, cited By (since 1996) 130.

Hosoda, T., and T. Hosomi (2004), A simplified model for long term prediction on vertical distributions of water qualities in lake biwal, in *Sustainable Development of Energy, Water and Environment Systems*, edited by N.Afgan, Z.Bogdan, and N.Duic, pp. 357 –365, A.A. Balkema Publishers.

Hosoda, T., and F. Malembeka (2010), Generation mechanism of typical vertical distributions of dissolved oxygen in the northern part of Lake Biwa, in *Proceedings of 6th International Symposium on Environmental Hydraulics, Athens, Greece, 23-24 June 2010*, vol. 1, edited by G. Christodoulou and A. Stamou, pp. 385–390, Taylor & Francis Group, London.

Ising, E. (1925), Beitrag zur theorie des ferromagnetismus, *Zeitschrift Physik*, *31*, 253–258.

Jacimovic, N., M. Ivetic, and T.Hosoda (2011), Modeling of dissolved oxygen vertical distribution changes in lakes: Case study of the lake zavoj in serbia, in *Proceedings of 4th International Perspective on Water Resources & the Environment*, 00564, National University of Singapore.

Katori, M., S. Kizaki, Y. Terui, and T. Kubo (1998), Forest dynamics with canopy gap expansion and stochastic Ising Model, *Fractals*, *6*(1), 81 – 86.

Kizaki, S., and M. Katori (1999), Analysis of canopy-gap structures of forests by ising-gibbs states - equilibrium and scaling property of real forests, *Journal of the Physical Society of Japan*, *68*(8), 2553–2560.

Kubo, T., Y. Iwasa, and N. Furumoto (1996), Forest spatial dynamics with gap expansion: Total gap area and gap size distribution, *Journal of Theoretical Biology*, *180*(3), 229 – 246, doi:10.1006/jtbi.1996.0099.

Kundu, P., and I. Cohen (2002), *Fluid Dynamics*, second ed., Academic Press, Orlando, Florida, U.S.

Leonard, B. (1979), A stable and accurate convective modelling procedure based on quadratic upstream interpolation, *Computer Methods in Applied Mechanics and Engineering*, *19*(1), 59–98, cited By (since 1996) 1328.

Morinishi, Y., T. S. Lund, O. V. Vasilyev, and P. Moin (1998), Fully conservative higher order finite difference schemes for incompressible flow, *Journal of Computational Physics*, *143*(1), 90 – 124, doi:10.1006/jcph.1998.5962.

Schlicht, R., and Y. Iwasa (2004), Forest gap dynamics and the ising model, *Journal of Theoretical Biology*, *230*(1), 65 – 75, doi:DOI:10.1016/j.jtbi.2004.04.027.

Yoshimizu, C., K. Yoshiyama, I. Tayasu, T. Koitabashi, and T. Nagata (2010), Vulnerability of a large monomictic lake (Lake Biwa) to warm winter event, *Limnology*, *11*, 233–239, 10.1007/s10201-009-0307-3.